Research and Development Technical Report

DELET-TR-79-0282-2

HIGH CONTRAST CRT FACEPLATE.

T. G. Maple
I. D. Liu
Lockheed Missiles & Space Co., Inc.
1111 Lockheed Way
Sunnyvale, California 94086

Dec[redacted]1980
Second Interim Report, for the period 19 Jan[redacted] 18 May 1980,

DISTRIBUTION STATEMENT
Approved for public release, distribution unlimited

Prepared for:

ELECTRONICS TECHNOLOGY AND DEVICES LABORATORY

ERADCOM
US ARMY ELECTRONICS RESEARCH AND DEVELOPMENT COMMAND
FORT MONMOUTH, NEW JERSEY 07703

HISA-FM 195-78

NOTICES

Disclaimers

The citation of trade names and names of manufacturers in this report is not to be construed as official Government indorsement or approval of commercial products or services referenced herein.

Disposition

Destroy this report when it is no longer needed. Do not return it to the originator.

(Unclassified)

SECURITY CLASSIFICATION OF THIS PAGE (When Data Entered)

REPORT DOCUMENTATION PAGE

READ INSTRUCTIONS BEFORE COMPLETING FORM

1. REPORT NUMBER: DELET-TR-79-0282-2	2. GOVT ACCESSION NO.: AD-A098091
3. RECIPIENT'S CATALOG NUMBER:	
4. TITLE (and Subtitle): HIGH CONTRAST CRT FACEPLATE	5. TYPE OF REPORT & PERIOD COVERED: Interim Technical Report, 19 January - 18 May 1980
6. PERFORMING ORG. REPORT NUMBER:	
7. AUTHOR(s): T. G. Maple; I. D. Liu	8. CONTRACT OR GRANT NUMBER(s): DAAK 20-79-C-0282
9. PERFORMING ORGANIZATION NAME AND ADDRESS: Advanced Systems Division, LOCKHEED MISSILES & SPACE CO., INC., 1111 Lockheed Way, Sunnyvale, Ca. 94086	10. PROGRAM ELEMENT, PROJECT, TASK AREA & WORK UNIT NUMBERS: 1L162705AH94 03 01
11. CONTROLLING OFFICE NAME AND ADDRESS: U.S. Army Electronics Research and Development Command, Attn: DELET-BD, Fort Monmouth, N.J. 07703	12. REPORT DATE: December, 1980
	13. NUMBER OF PAGES: 155
14. MONITORING AGENCY NAME & ADDRESS (if different from Controlling Office)	15. SECURITY CLASS (of this report): UNCLASSIFIED
	15a. DECLASSIFICATION/DOWNGRADING SCHEDULE

16. DISTRIBUTION STATEMENT (of this Report)

Approved for public release;
Distribution unlimited

17. DISTRIBUTION STATEMENT (of the abstract entered in Block 20, if different from Report)

18. SUPPLEMENTARY NOTES

19. KEY WORDS (Continue on reverse side if necessary and identify by block number)

3-inch CRT
Two-Color CRT
Thin Film Phosphor
Color Penetration Tube
High Contrast Displays

20. ABSTRACT (Continue on reverse side if necessary and identify by block number)

The objective of this program is the development of a high contrast, two color CRT faceplate employing evaporated thin film phosphors and nonreflective backing, utilizing 1710 glass and also sapphire substrates. Results of the Eu optimization study show that La_2O_2S:6.5a/o Eu meets the technical requirements for IPL red. Faceplates Lots #1 and #2 were delivered to ERADCOM. Distortion has been eliminated by an increase of preheat time prior to the $H_2 + SO_2$ treatment.

DD FORM 1 JAN 73 1473 EDITION OF 1 NOV 65 IS OBSOLETE

SECURITY CLASSIFICATION OF THIS PAGE (When Data Entered)

TABLE OF CONTENTS

1.0 CONFERENCE

1.1 26-27 February 1980 at LMSC

Report of conference held at LMSC, Mountain View, California, 26 and 27 February 1980 with ERADCOM to review progress on Contract DAAK20-79-C-0282, High Contrast CRT Faceplates.

Personnel Present

ET&D Lab - ERADCOM

E. Schlam

P. F. Krzyzkowski

LMSC, Inc.

R. A. Buchanan

T. G. Maple

I. D. Liu

The purpose of the meeting was to review and discuss progress under the current contract.

1.1.1 Contract Documentation

P. Krzyzkowski is reviewing the draft of the first interim report.

1.1.2 Phosphor Characteristics

LMSC reported results of the europium optimization study. Cathodoluminescence brightness measured as a function of europium concentration definitely shows a peak in the red at 6.5 a/o Eu. The results are completely analogous to those which have been published for Y_2O_2S:Eu, except the red peak of the latter occurs at 3.5 a/o. The chromaticity coordinate measurements indicate that the requirements of the Technical Guideline for IPL red as defined in MIL-C-25050A are satisfied by La_2O_2S:6.5 a/o Eu films treated at 1050°C on sapphire. Due to the lower treatment temperature of the 1710/1720 faceplates, these may not have the same coordinate values.

P. Krzyzkowski pointed out that measurements at Watkins-Johnson Co. (W-J) and also ERADCOM show an apparent saturation at about 10 F-L for high current densities (200 - 500 μA), whereas the LMSC measurements show cathodoluminescence brightness (CL) an order of magnitude greater at only 5 μA, and the same anode potential (10 Kv). The LMSC raster size and duty cycle differ significantly from that used at W-J and ERADCOM. The LMSC measuring system appears to be limited to a maximum screen current of 13 μA. The LMSC measuring system should be modified to permit measurements similar to those at ERADCOM.

1.1.3 Faceplate Processing

1.1.3.1 Sulfur Contamination

Poisoning of the cathode occurred on only three of the CRTs assembled at W-J. The LMSC study showed that the amount of elemental sulfur present on faceplates following the $H_2 + SO_2$ treatment to be only one-half microgram. The amount of sulfur which is sufficient to poison a dispenser-type cathode as used by W-J is not known at present. The sulfur can be eliminated by a vacuum bake. It can also be removed by dissolving in hot trichloroethylene (TCE). Only one faceplate can be vacuum baked at a time, while an entire lot can be treated with TCE at one time. LMSC proposes to use 3 changes of hot TCE.

1.1.3.2 Distortion

At present, the faceplates must be polished to remove the distortion occurring during the $H_2 + SO_2$ treatment. This reduces the faceplate thickness to 0.110 in. Some flexing of the thinned faceplates has been observed when CRTs are evacuated. This stresses the frit seal and may impair the seal. ERADCOM had suggested that the starting thickness of the faceplates be increased. The sheets from which the faceplates are cut is only 0.160 in. in thickness. They are then polished to a thickness of 0.125 - 0.130 in. by United Lens, Inc. This allows only 0.030 in. of material to be removed during grinding and polishing. An increase of thickness does not appear practicable because the allowance for grinding and polishing would be too small.

P. F. Krzyzkowski noted that during $H_2 + SO_2$ treatment, the faceplates are below the centerline of the furnace tube. He pointed out that the quartz rod which had been tacked on one edge of the support plate could produce asymmetric heating. It was suggested that additional carbon platens be used to raise the faceplate to the tube centerline.

1.1.3.3 Aluminum Conducting Layer

P. F. Krzyzkowski noted that an 800Å aluminum layer was added to Lot #1 after deposition of the black NR layer. As an aluminum layer will be added after the faceplates are assembled to the CRT funnel in order to effect the required internal connection, the first layer is not needed and unnecessarily reduces the beam energy available for phosphor excitation. It was agreed that the aluminum layer would be omitted from Lot #2.

1.1.4 Black Layer Degradation

P. F. Krzyzkowski presented results of the ERADCOM Auger analysis study of the LMSC NR films. There appears to be oxygen present in the metallic portion of the film. Also, nitrogen was unexpectedly found to be present. These results are interesting, but it is not clear that there is any relation to possible degradation of the black layer.

1.1.5 Measurements

1.1.5.1 Cathodoluminescence (CL)

The results of previous measurements at a writing speed of 5,000 in./sec. made at Watkins-Johnson were discussed. The measurements were reportedly made at screen currents of about 300 to 500 microamperes; the results appeared to suggest a saturation of the phosphor at about 10 ft-L. On the other hand, the LMSC measurements using a TV raster at 5 microamperes screen current gave cathodoluminescence values as high as 1000 ft-L, with no evidence of saturation. Dr. Buchanan pointed out that other LMSC measurements have shown the oxysulfide phosphor capable of CL at 40,000 ft-L without saturation. Unfortunately, the LMSC CL measurement system is presently limited to screen currents much lower than used in the Watkins-Johnson measurements. It would be desirable to duplicate the Watkins-Johnson measurement conditions, since there is a question whether the apparent saturation may have been due to an artifact in the measurements.

1.1.5.2 Optical Reflection

The results of optical reflectance measurements on Lot #1 were discussed. The plots of relative intensity vs. position of the detector with respect to the specular angle of reflectance show a broad maximum instead of the expected sharp peak. The cause appears to be poor collimation of the light beam. P. F. Krzyzkowski suggested that better collimation should be obtained by increasing the source to sample and sample to detector distances.

1.1.6 Miscellaneous

A possible modification of the present contract was discussed.

MAIN TEXT OF REPORT

2.0 INTRODUCTION

2.1 Background

This program is a continuation of previous work at LMSC as a subcontractor to the Watkins-Johnson Company under Contract No. DAAB-07-77-C-2639 (see Research and Development Technical Reports ECOM-77-2639-1, Jan. 1978; ECO-77-2639-2, May, 1978; DELET-TR-77-2639-3, Aug. 1979; DELET-TR-77-2639-4, Aug. 1979; DELET-TR-2639-5, Aug. 1979; and DELET-TR-77-2639-F, Feb. 1980).

The progress under the present contract during the period 19 September 1979 - 18 January 1980 has been described in the First Interim Report, DELET-TR-79-0282-1, April, 1980.

This Second Interim Report describes the progress during the period 19 January 1980 - 18 May 1980.

The faceplates to be fabricated under this program are an essential component of the proposed high contrast multicolor CRT.

2.2 Statement of the Problem

The basic problem addressed by this program is the ability to display information generated by various electronic systems with suitable high resolution in two colors with its legibility maintained under ambient illumination ranging from 10^{4} to 10^{-3} fc.

Existing color tubes cannot satisfy the above requirement. Such tubes which employ aperture masks are severely limited in brightness and resolution by the aperture mask. Their brightness is limited because the aperture mask transmission is only 15 to 20 percent, therefore wasting 80 to 85 percent of the current. The wide spacing between holes degrades the resolution below that required in most military systems. Furthermore, the color purity of such tubes is influenced by their position with respect to the earth's magnetic field, and it is therefore impractical to incorporate them in airborne systems.

The use of color penetration phosphors overcomes some of the problems of mask type tubes. The color purity is no longer affected by the tube orientation and the resolution is higher than that which can be achieved with a mask type tube. Conventional color penetration tubes which employ powdered phosphors cannot be used for daylight (high brightness) viewing because of their high

reflectivity and low brightness, particularly in red, which produces a washed-out low contrast display. The reflectivity of the phosphor is high because of its particulate nature. The brightness of the red is low because most of the light generated by the red phosphor is scattered by the green phosphor before it reaches the faceplate of the CRT.

3.0 TECHNICAL APPROACH

The technical guidelines for the program and the technical approach developed to achieve the objectives of the program have been described in the First Interim Report, DELET-TR-79-0282-1, April, 1980. Results to date have not indicated any need for modification of the technical approach.

4.0 PROGRESS DURING REPORT PERIOD

4.1 Materials and Supplies Procurement

4.1.1 Sapphire Substrates

The initial shipment of 6 of the 3-in. dia. sapphire substrates was not received from Crystal Systems, Inc., on March 1 as promised. As any further delay in receipt of these substrates threatened to impede the program, ERADCOM was advised of the problem. The supplier was contacted by ERADCOM personnel and as a result, all 20 sapphire substrates were received on March 18. One of the substrates was found to have a small edge chip. In view of the prolonged delay in delivery of the substrate, it was felt that a replacement for the chipped substrate would probably not be obtained within sufficient time to be fabricated into a faceplate during the term of the contract, and that this substrate could still be useful as a test specimen in developing the sapphire sealing technique. The shipped substrate was therefore retained for fabrication into a faceplate.

4.2 Europium Optimization Study

This study has now been completed. The cathodoluminescent brightness measured as a function of europium concentration definitely shows a peak in the red at 6.5 a/o (atomic percent) replacement of La by Eu (see Table 1, and Figure 1 attached). The results are completely analogous to those which have been published for Y_2O_2S:Eu, except the red peak of the latter occurs at 3.5 a/o Eu (Refs. 1, 2, 3).

The results of the chromaticity coordinate measurements are shown in Table 2 and in the chromaticity diagram of Figure 2. The measured coordinates for the 6.5 a/o Eu composition saitsfy the Technical Guideline requirement for IPL red as defined in MIL-C-25050A,

y is not greater than 0.306

z is not greater than 0.001

from which it can be determined by calculation that

x is greater than 0.693.

The samples were prepared at 1050°C. Because the faceplates on 1710 glass are treated at 850°C, it would be of interest to repeat the measurements on samples

prepared at 850°C. It is planned to do this in the future, time permitting.

Table 1

Cathodoluminescence vs. Eu Concentration

Sample No.	a/o Eu	Foot-Lamberts
53	La_2O_2S:Tb Std.	252.5
7	1	220
11	1.5	74
12	2.5	46.5
17	3.5	85.2
20	5.0	177.5
27	6.5	240
43	8.0	200
46	10.0	137.5
50	15.0	10

Table 2

Chromaticity Coordinates Measured for La_2O_2S:Eu

Sample No.	% Eu	Chromaticity Coordinates x	y	z
7	1	.6124	.3866	.0010
11	1.5	.6126	.3850	.0024
12	2.5	.5998	.3991	.0011
17	3.5	.6043	.3863	.0095
20	5.0	.6633	.3361	.0006
27	6.5	.6991	.3004	.0005
43	8.0	.6968	.3026	.0006
46	10.0	.6835	.3110	.0047
50	15.0	.7130	.2845	.0026

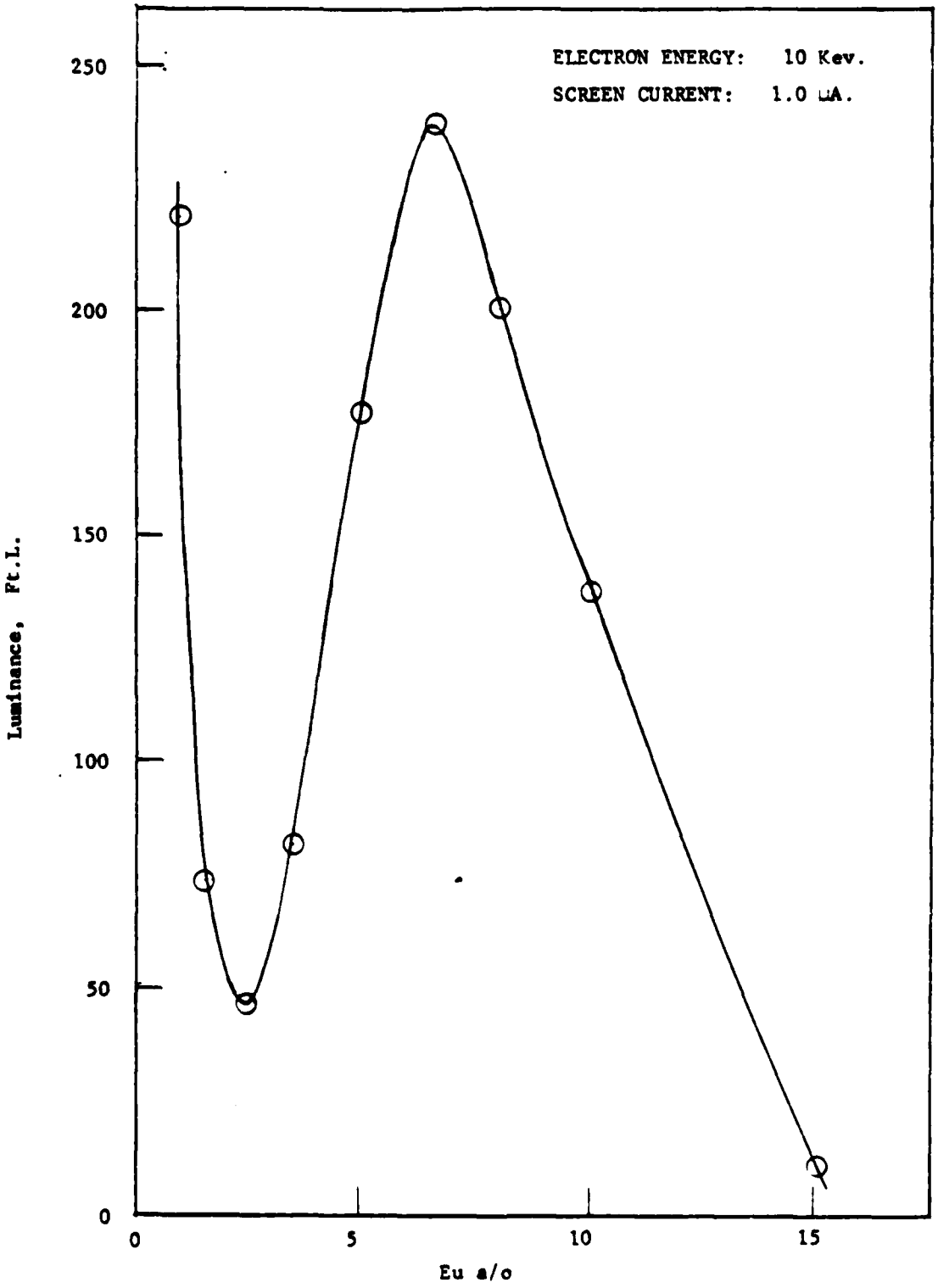

Fig. 1 Cathodoluminescence of La_2O_2S:Eu

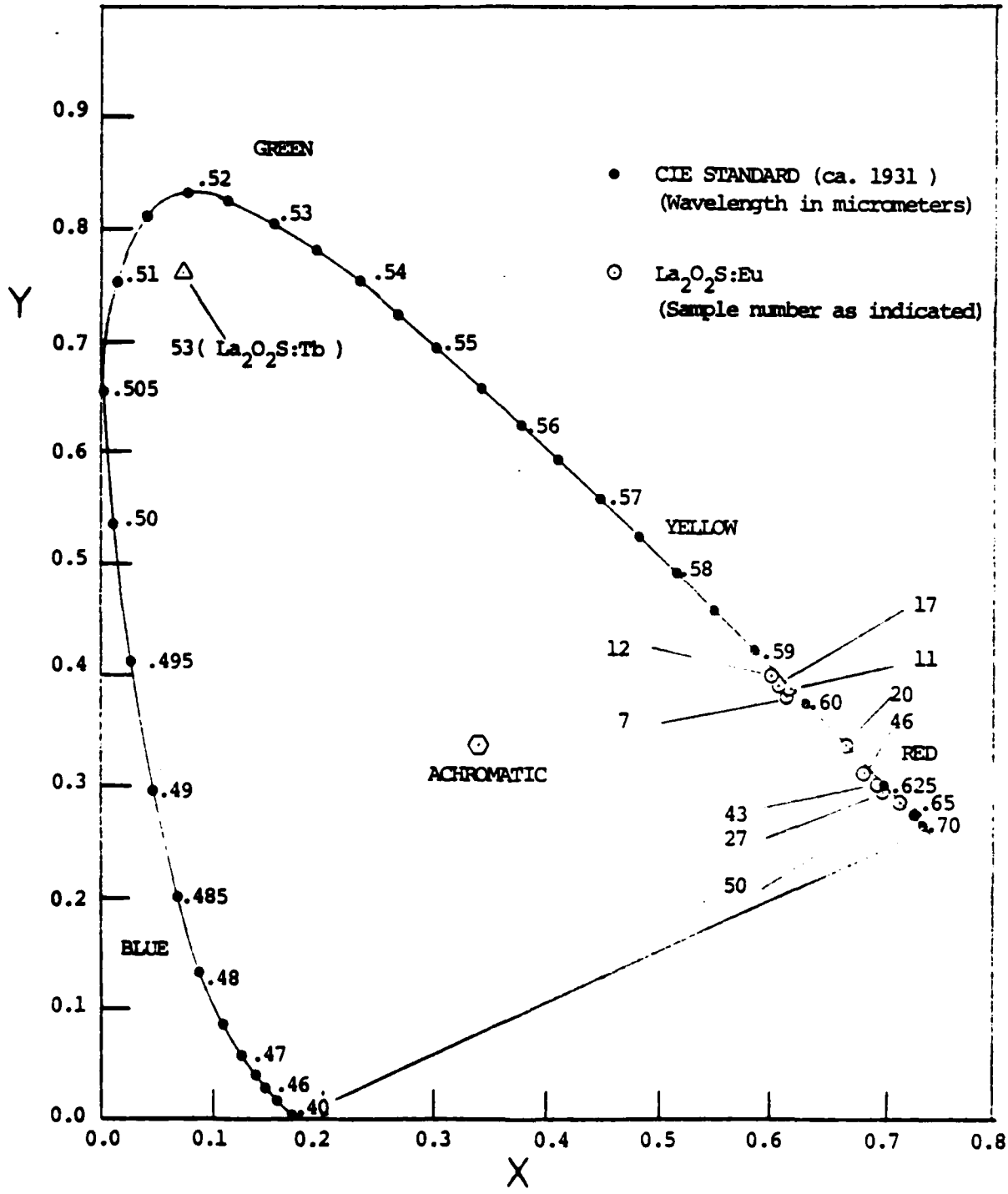

Fig. 2 Chromaticity Diagram of La_2O_2S:Eu Cathodoluminescence

4.3 Fabrication of Faceplates

4.3.1 Numbering of Faceplates

In order to provide a complete record of fabrication, each substrate was numbered consecutively. To allow for loss during fabrication, the number of substrates for each lot was generally greater than the number required for delivery. For various reasons, some faceplates were damaged or otherwise rejected during fabrication and therefore some faceplate numbers do not appear in the list of faceplates delivered as a given lot. Where practicable, measurements were made on the rejected faceplates, and are reported here for the sake of completeness.

4.3.1.1 Lot #1

The substrate selected for fabrication of Lot #1 were numbers 38-50 inclusively. The fabrication of Lot #1 is summarized in Table 3. Faceplates 39, 43, 47, 49, and 50 were rejected for the reasons indicated under "remarks" in the table.

The reflectance measurements on Lot #1 were completed and the 8 faceplates shipped via Federal Air Express to ERADCOM on February 6.

4.3.1.2 Lot #2

The substrates for Lot #2 were numbers 51-63 inclusive. Fabrication is summarized in Table 4. Faceplates 51 and 57 were broken during optical polishing to remove glass distortion occurring during the $H_2 + SO_2$ treatment. Faceplate 61 was rejected on account of the frosty appearance of the phosphor film after the $H_2 + SO_2$ treatment, and 63 on account of numerous pinholes.

The 1710 glass was annealed at 750°C prior to phosphor deposition in hope that this would eliminate distortion during sulfurization treatment. This is somewhat greater than the published annealing temperature for the glass so any frozen-in stress should have been relieved. The annealing did not, however, eliminate the distortion.

Table 3

Lot #1 Faceplate Fabrication Summary

F.P. No.	Glass Type	Anneal °C	La_2O_2S:Tb Run No.	Min.	La_2O_2S:Eu Run No.	Min.	$H_2 + SO_2$ °C	Min.	Vac. °C	Bake Min.	NR(V) Run No.	Al Å	Remarks
38	1720	No	20-79	120	4-79	55	830	60	350	60	11-80	800	
39	1720	No	21-79	124	5-79	55	850	74	350	60	12-80	800	Chipped
40	1720	870	22-79	120	6-79	55	850	60	350	60	13-80	850	
41	1720	870	23-79	121	7-79	55	850	60	350	60	14-80	800	
42	1720	870	24-79	122	8-79	55	850	60	350	60	15-80	800	
43	1720	870	25-79	130	9-79	55	850	60	350	60	16-80	830	Deep pits
44	1720	870	26-79	124	10-79	55	850	60	350	60	17-80	800	
45	1720	870	27-79	120	11-79	55	850	60	350	60	18-80	800	
46	1720	870	28-79	120	12-79	55	850	60	350	60	19-80	800	
47	1720	844	29-79	120	13-79	55	850	60	350	60	-	-	Frosty
48	1720	No	30-79	120	14-79	55	850	60	350	60	20-80	800(?)	
49	1710	No	31-79	120	15-79	55	870	60	350	60	-	-	Frosty
50	1710	750	32-79	125	16-79	55	870	60	-	-	-	-	Frosty

(?) Monitor Defect

Table 4

Lot #2 Faceplate Fabrication Summary

F.P. No.	Glass Type	Anneal °C	La_2O_2S:Tb Run No.	Min.	La_2O_2S:Eu Run No.	Min.	H_2O+SO_2 °C	Min.	NR(V) Run No.	Al Å			Remarks
51	1710	750	2-80	120	4-80	55	850	60	-	None			Broken
52	1710	750	3-80	120	1-80	59	850	60	2180	none			
53	1710	750	4-80	120	2-80	55	850	64	2280	None			
54	1710	750	5-80	120	3-80	55	850	60	23-80	None			
55	1710	750	6-80	122	5-80	50	850	60	24-80	None			
56	1710	750	7-80	120	6-80	50	850	60	25-80	None			
57	1710	750	8-80	129	7-80	50	850	60	-	None			Broken
58	1710	750	9-80	120	8-80	55	850	60	26-80	None			
59	1710	750	10-80	120	13-80	50	850	60	27-80	None			
60	1710	750	11-80	120	9-80	50	850	73	28-80	None			
61	1710	750	12-80	120	10-80	50	850	60	-	None			Frosty
62	1710	750	13-80	120	11-80	50	850	64	29-80	None			
63	1710	750	14-80	121	14-80	52	850	62	30-80	None			

Deposition of the final 800Å aluminum film was omitted at the request of ERADCOM because a simular aluminum film must be deposited after assembly of the faceplate to the CRT funnel in order to provide an electrical connection for removal of charge that would otherwise accumulate on the faceplate; the presence of two aluminum films would increase the voltage required for electron penetration to the phosphor film, and since the maximum screen potential of the intended application is limited to 20 milovolts, the potential available for phosphor excitation would consequently be reduced.

Follwoing optical reflectance and cathodoluminescence measurements, the remaining nine faceplates were shipped via Federal Air Express to ERADCOM.

4.3.1.3 Lot #3

The substrates for Lot #3 were numbers 64-74 inclusively. Fabrication is summarized in Table 5.

4.3.2 Faceplate Distortion

The phosphor films as deposited have very low luminescence. There appears to be an unavoidable loss of a small amount of sulfur during deposition. The deposit is therefore not truly stoichiometric and contains vacancies which produce quenching of the luminescence. By treating the film in $H_2 + SO_2$ at elevated temperature, the stoichiometric deficiency is corrected and the luminescence greatly increased. The optimum temperature for treatment is 1050°C. The softening point of Corning 1710 and 1720 aluminosilicate glasses is, however, 915°C. To avoid extensive distortion of the glass during the $H_2 + SO_2$ treatment, a temperature for treatment of 850°C has been chosen, at the price of some reduction in luminescent brightness of the faceplate. Tests have shown that no distortion of uncoated 1710 or 1720 glass disks occurs when exposed to the $H_2 + SO_2$ atmosphere at 850°C for periods in excess of 1 hour. The thermal coefficient of expansion of the aluminosilicate glass is $41 \times 10^{-7}/°C$ and that of lanthanum oxysulfide about $80 \times 10^{-7}/°C$. As a result of the mismatch in coefficients, considerable distortion of the glass and some warpage of the phosphor film has been experienced when the coated glass disks are treated at 850°C. Although this could likely be eliminated

Table 5
Lot #3 Faceplate Fabrication Summary

F. P. No.	Glass Type	Anneal °C	La_2O_2S:Tb Run No.	Min.	La_2O_2S:Eu Run No.	Min.	$H_2 + SO_2$ °C	Min.	NR(V) Run No.	Al Å°			Remarks
64	1710	750	15-80	127	15-80	45	850	60	38-80				
65	1710	750	16-80	120	12-80	50	850	60	37-80				Bent
66	1710	No	17-80	125	16-80	56	850	60	39-80				
67	1710	No	18-80	120	17-80	55	850	90	40-80				
68	1710	No	19-80	120	18-80	55	850	60	41-80				
69	1710	No	20-80	120	19-80	55	850	72	42-80				
70	1710	No	21-80	120	20-80	55	850	60	43-80				
71	1710	750	22-80	120	21-80	58	850	72	44-80				
72	1710	750	23-80	120	22-80	56	850	60	45-80				
73	1710	750	24-80	120	23-80	55	850	65	46-80				
74	1710	750	25-80	120	24-80	55	850	90	47-80				

by further lowering the treatment temperature, the luminescent brightness would be reduced to an unacceptable level.

To remove the distortion from the glass following the $H_2 + SO_2$ treatment, optical grinding and re-polishing has been employed. A similar means for removing the film warpage cannot be used because the phosphor film would be destroyed in the process.

During a visit to the laboratory on February 26-27, P. F. Krzyzkowski of ERADCOM noted that the faceplates were positioned somewhat below the centerline of the furnace tube while undergoing the $H_2 + SO_2$ treatment. He suggested that this might result in nonsymmetric heating of the faceplate, and that tests be made with faceplates raised to the centerline of the tube to ascertain the effect on distortion.

Accordingly, some tests were made during treatment of the Lot #2 faceplates. The faceplates were raised to the centerline by adding various combinations of added quartz plates and carbon plates to the usual support consisting of one vitreous carbon plate and one quartz plate. No significant reduction of distortion was found, although the region of distortion was generally better centered on the faceplate.

The normal treatment procedure is to place the faceplate on the support plates within that part of the furnace tube which projects outside of the furnace. The tube is capped, then flushed for 20 minutes with argon gas before introducing the treatment gases. During the flushing period, the faceplate is positioned just outside the furnace proper. After the $H_2 + SO_2$ gas flow is established, the faceplate is pushed to the center of the tube by means of a quartz rod passing through an O-ring seal on the tube cap, at a rate of 2 in/min.

During one of the tests, the operator was called to the phone after positioning the faceplate just within the end of the furnace proper, where it remained for some 15 or 20 minutes. Upon return, the operator proceeded with the usual treatment schedule. Upon removal from the furnace, the faceplate was found free of distortion. This result was reproduced in subsequent tests in which

it was found that a preheat period of 10 minutes minimum with the faceplate just within the furnace proper completely eliminates distortion.

A subsequent optical polishing of the glass side of the faceplate is still required; however, because under the pressure of its own weight, the faceplate acquires a reproduction of the grain pattern of the carbon support plate surface. Less than 0.010 in. need be removed to eliminate the grain pattern.

This preheat procedure was followed during treatment of Lot #3. No distortion occurred, except on Faceplate #66 which was supported on the vitreous carbon plate, whereas the other faceplates were supported on a densified carbon plate. This result suggests that the vitreous carbon plate has nonsymmetrical thermal conductivity properties which contribute toward distortion.

The results with Lot #3 indicate that distortion is caused by a thermal gradient across the faceplates produced by insufficient preheating and that proper preheating completely eliminates the problem.

It would be desirable to eliminate the necessity of post-treatment optical polishing. In principle, this could be accomplished by supporting the faceplate during treatment upon an optically polished surface. The support material would need to be inert toward H_2+ SO_2, as well as the aluminosilicate glass. Polished quarts or alumina cannot be used as it has been found that the aluminosilicate faceplates fuse to these at the treatment temperature. A polished gold plate appears to be a possible solution. Budget considerations however, preclude acquisition of a gold plate at present.

4.4 Cathodoluminescence Brightness Measurements

The cathodoluminescence study of the faceplates was made on a modified demountable electron beam system whose original design has been described elsewhere. ("Demountable Excitation Unit for Cathodoluminescent Spectroscopy", E. E. Anderson and J. L. Weaver, Applied Spectroscopy, 24, 90 (1970)). It consists mainly of a conventional high vacuum system, except the glass bell jar is replaced by a vertical 5-in. dia. aluminum tube with four 1-1/2 in. dia. horizontal side access ports. As shown in the accompanying Figure 3, the electron gun assembly using a Superior Electronics Type SE-3K15U, or

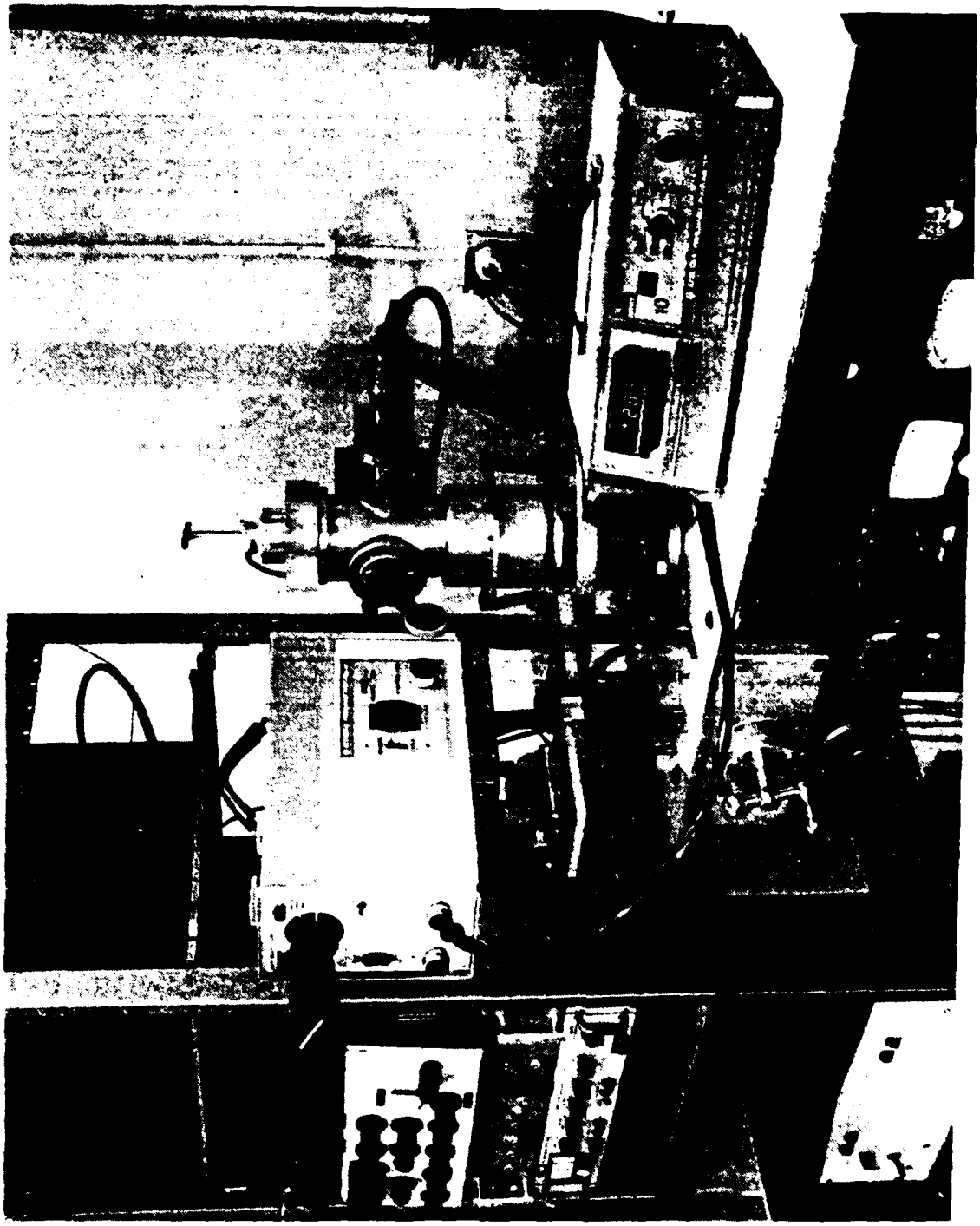

Figure 3 Demountable Electron Beam System

5UP1, electron gun is mounted on the rear port. Directly opposite and perpendicular to it are ports with slight glasses for viewing the transmitted luminance of the excited high contrast screen and the reflected luminance of the luminescent solids. The remaining fourth port consists of a high voltage feed-through leading through a flexible insulated cable to the sample holder for post-acceleration of the electron beam. Standard O-ring seals are used for vacuum, and the system can be evacuated to pressures below 10^{-6} Torr within 30 minutes with a 4-in. diffusion pump.

After the system has been pumped down to below 10^{-6} Torr, the electron gun is activated by gradually increasing the heater voltage first to about 6V, then to about 8V after the anode high voltage is turned on. After the screen current has been adjusted to and stabilized at 5.0 μA by varying the grid voltage, the luminance of the sample, excited by an electron beam having energies from 8-18 KeV is measured. Since the original design of the demountable system was for the purpose of spectroscopic studies of solid luminescent materials, its capability to produce a sizeable and well defined raster scan has been neglected. In fact, the small diameter aluminum enclosure of the electron gun appears to give rise to a proximity ground potential that practically disabled the deflection of the beam completely. Attempts to correct this by imposing a grid potential surrounding the beam or using a glass enclosure have not been satisfactory.

The luminance of the faceplates was measured using a Pritchard Model 1980-PL photometer with a 4-in. fixed focus Spectar 1962-PD lens and an aperture of 20 minutes to cover a field of 0.98 mm within the 0.1 x 0.1 cm^2 TV raster.

Methods for improving the focusing of the electron beam of the demountable system that had been suggested by P. Krzyzkowski of ERADCOM were tried. Some improvement was found, but considerably less than required for the program.

First, a short ring electrode at anode potential was inserted in the aluminum side arm just before the beam entered the main chamber in the hope that the beam could be refocused. No significant improvement of the focusing was observed. But, because of insufficient insulation, electronic breakdown from this ring to ground occurred even at anode voltage below about 10 Kv. This

ring was then removed and a 10 cm long cylinder fashioned from copper foil was slipped over the gun structure. It was hoped that when the cylinder was at grid potential, the electron beam would be shielded from the ground, i.e., the aluminum side arm, which was thought to be the source of problems affecting good focusing and deflection. Again, this latter arrangement made the deflection worse.

As an interim measure, the cathodoluminescence of the Lot #1 faceplate was measured following previous procedures: that is, by first producing a small 1mm x 1mm raster and then slightly defocusing the raster so as to form an apparently uniform spot of 2.5mm diameter. Nine faceplates were measured this way.

A maximum deflection of 0.1 cm, poor spot definition, and maximum screen current of about 5 microamperes have been serious limitations of the demountable cathodoluminescence system.

A test was made of the present 5UP1 type gun, using a 10 in. dia. glass cylinder in place of the present small dia. metal chamber and gun sleeve. The gun was inserted through a plexiglass plate with O-ring seal to the top of the glass cylinder. The upper three-fourths of the cylinder had a metal film to simulate the opaque coating of a typical CRT. The film was electrically connected to the screen potential. Screen to gun spacing was about twice that of the usual setup. A well-defined raster as large as 1-1/2 x 1-1/2 inch was readily obtained. It was also found possible to focus the beam to a rather well-defined spot with a minimum dia. of about 3/32 in. Screen currents as large as 180 μA were also obtained. These results indicated the limitations of the original demountable system were due to severe compression of the no drift region potential lines, and that a change to a glass system should remove the limitations.

An all-glass system was therefore assembled as shown in Figure 4. A deflection capability of better than 1 inch was observed, a great improvement. Screen currents as large as 120 microamperes were obtained. Spot size was not appreciably improved, although with defocusing, a line width of 0.030 in. was attainable.

The CL measurements on Lot #2 were made at TV rate, 5 microamperes screen current, and a raster size of a 1 cm x 0.1 cm. Results are presented in Table 6 and Figures 5 through 14. In addition, the CL electronics were modified to permit a single line scan of 1 in. at a writing speed of 5,000 in./sec. and a 60 Hz refresh rate.

Measurements at the 5,000 in. per sec. writing speed were made on several faceplates of Lot #2 at screen currents up to 120 microamperes. Results, as shown in Figure 15 were linear within the measured range. Comparison with the previous W-J measurements at the same writing speed could not be made because screen currents of 350-500 microamperes would be required. Figure 16 also shows results of measurements at a writing speed of 250 in./sec. made on two faceplates of Lot #2.

CL measurements were also made on Lot #3, Table 7, at TV rate, 5 microamperes and a small raster of 0.5 x 0.5 cm. This raster was the smallest practical with the modified, all-glass system, but larger than the 0.1 x 0.1 cm raster with the metal system used for Lot #2. Thus, when comparing the results for Lot #2 with those for Lot #2, allowance must be made for the reduced power density of the Lot #3 measurements approximately one-fifth of that for Lot #2. Results for Lot #3 are shown in Figures 17 through 27.

Writing speed measurements on Lot #3 were not made due to failure of the beam blank-off. In view of the fact that the 5UP1 gun does now allow writing speed measurements at the high current densities of the Watkins-Johnson measurements, it was decided to replace the 5UP1 gun with a magnetic deflected, electrostatic focused gun capable of 500 milliampere beam current, rather than spend time trying to push the 5UP1 into a region for which it was never intended. The necessary components have been obtained and construction of the deflection amplifiers is in progress.

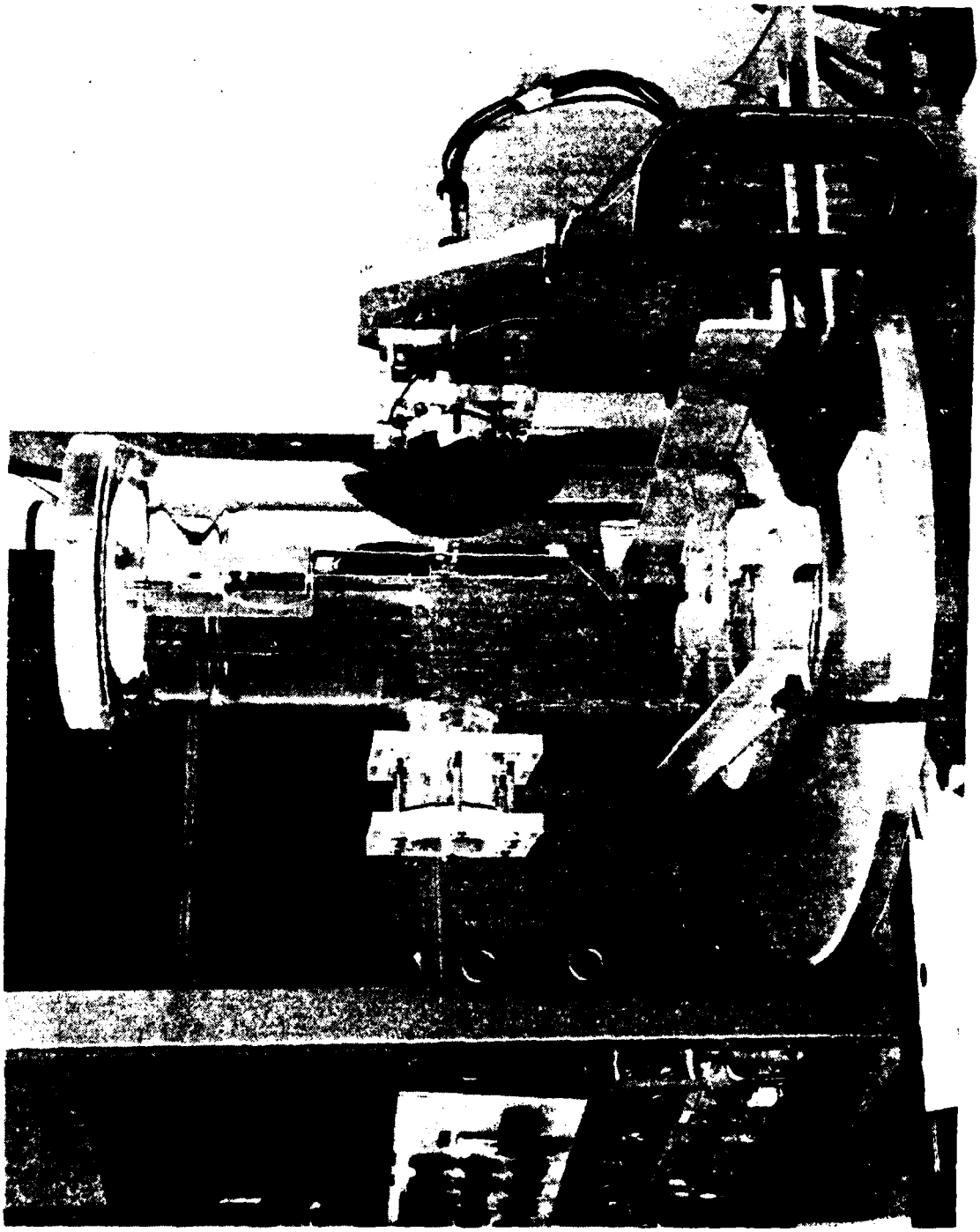

Figure 4 Demountable CL System with Glass Chamber

Table 6

Cathodoluminescent Brightness, Lot #2

Faceplate No/Kev.	52	53	56	55	56	58	59	60	62
8	10.6	16.0	13.2	9.6	8.0	12.0	13.7	88	8.4
9	34.4	38.4	60.0	36.0	27.2	42.0	46.2	32.9	38.0
10	112	87	120	94	77	95	133	91	102
11	178	164	208	163	152	176	198	160	176
12	292	296	336	304	272	290	363	312	304
13	451	482	525	440	401	444	462	424	468
14	640	640	723	652	600	609	688	676	744
15	806	840	836	800	704	752	814	760	848
16	964	1040	1012	1024	1000	948	1001	1028	1100
17	1080	1120	1160	1160	1040	1072	1100	1080	1200
18	1310	1360	1320	1320	1280	1240	1250	1300	1420

Raster Size: $0.1 \times 0.1\ cm^2$

Screen Current: $5.0\ \mu A$

Pressure: 2×10^{-7} Torr

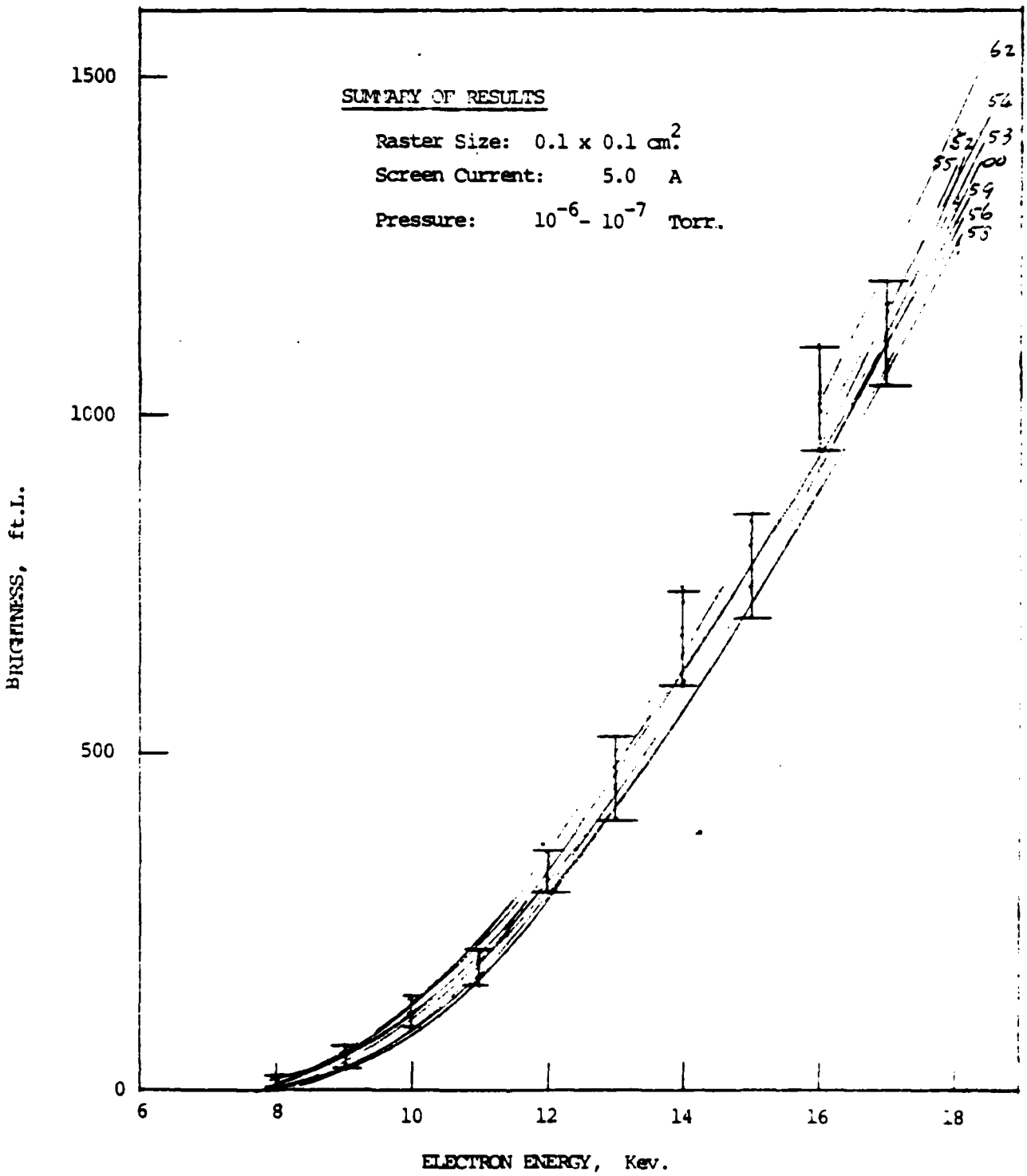

Fig. 5 Cathodoluminescence, Summary, Lot #2

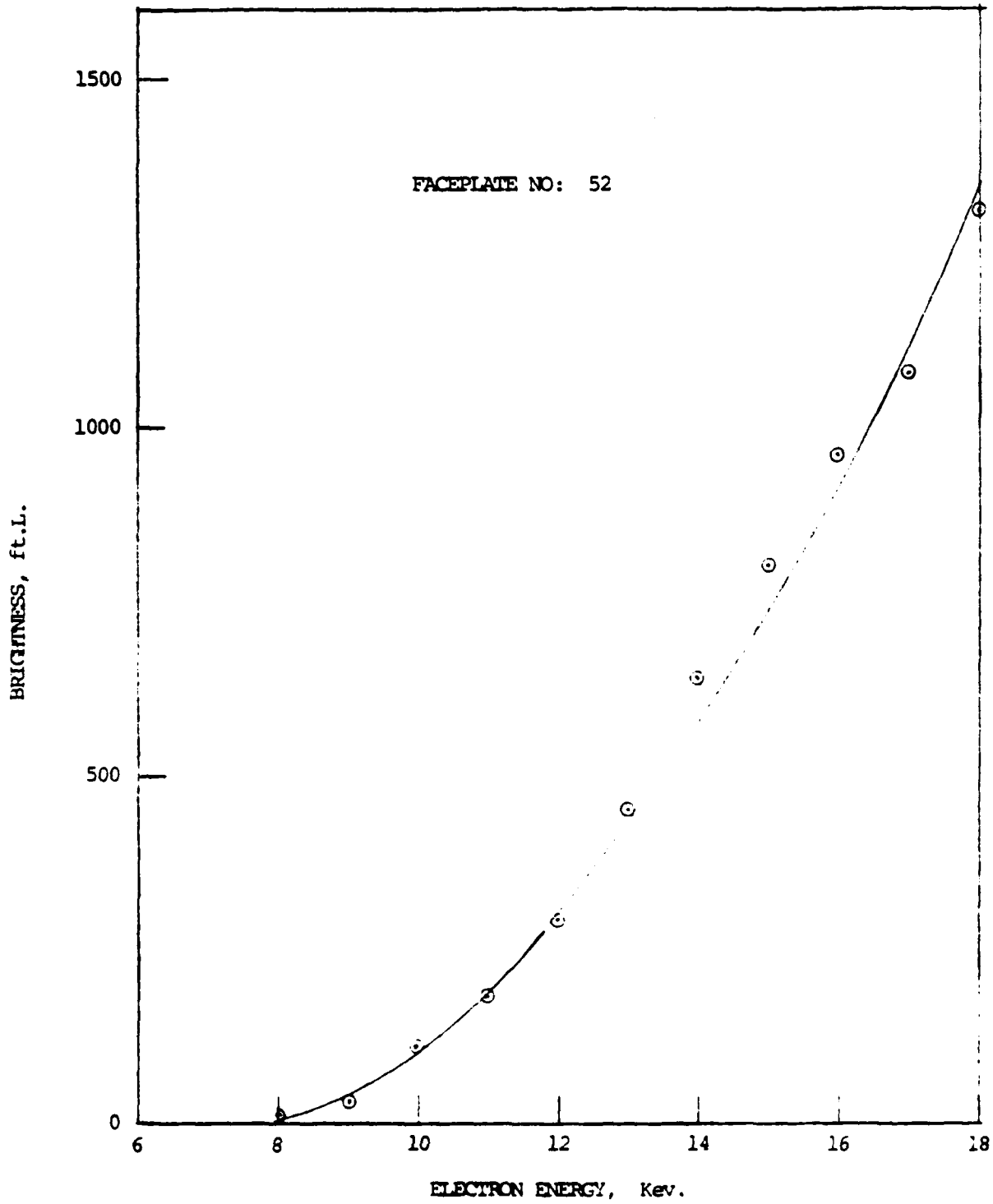

Fig. 6 Cathodoluminescence, Faceplate No. 52

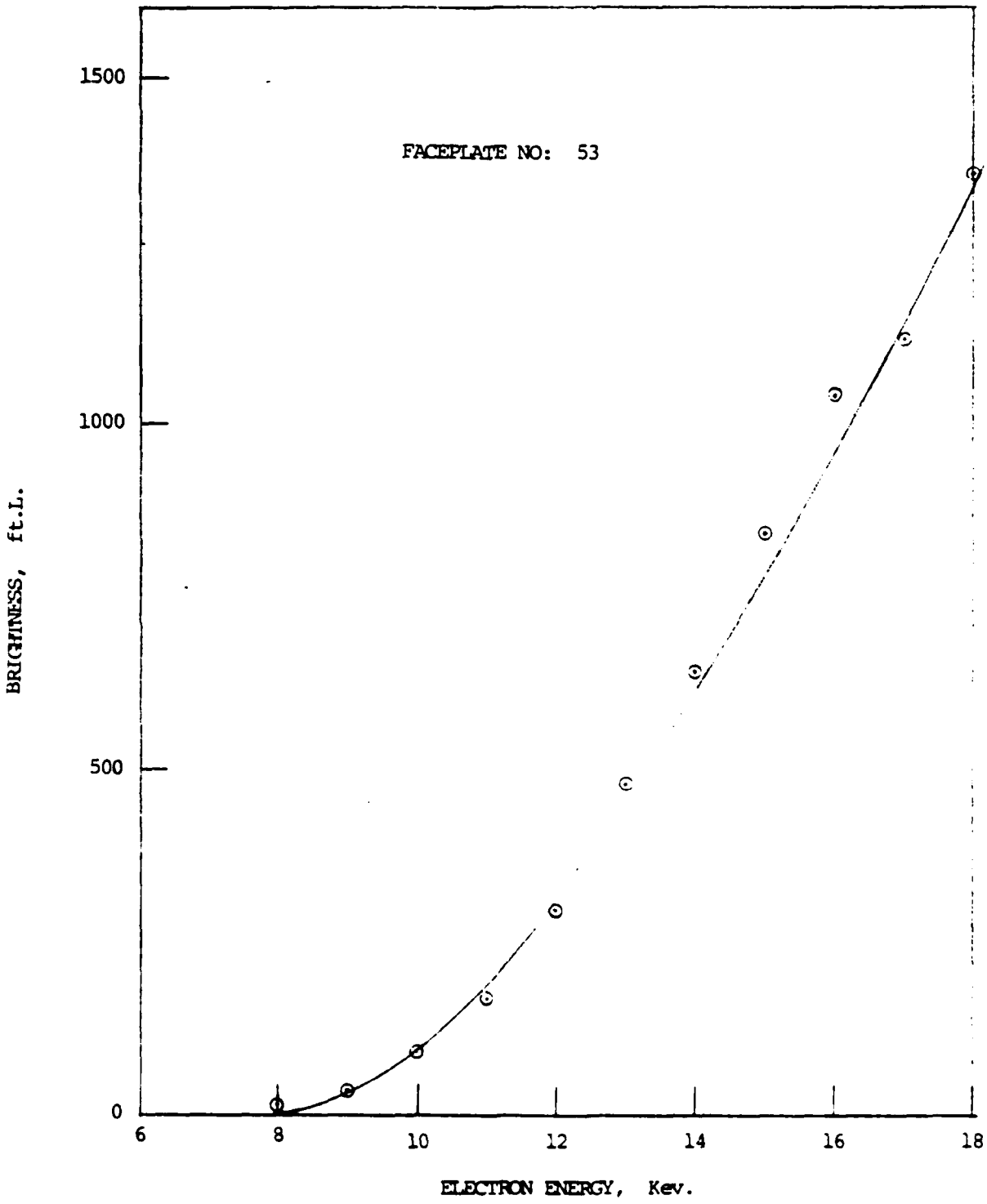

Fig. 7 Cathodoluminescence, Faceplate No. 53

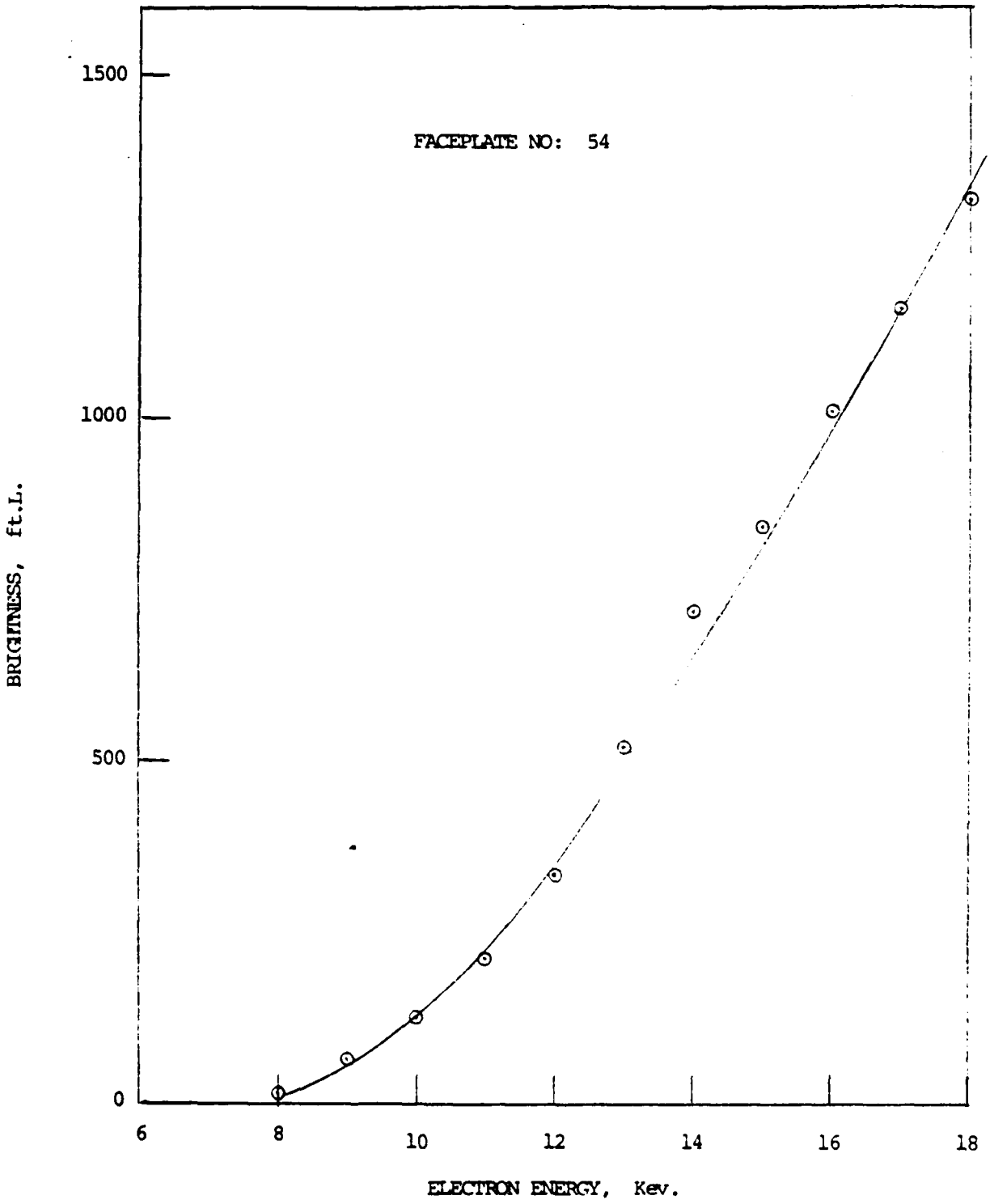

Fig. 8 Cathodoluminescence, Faceplate No. 54

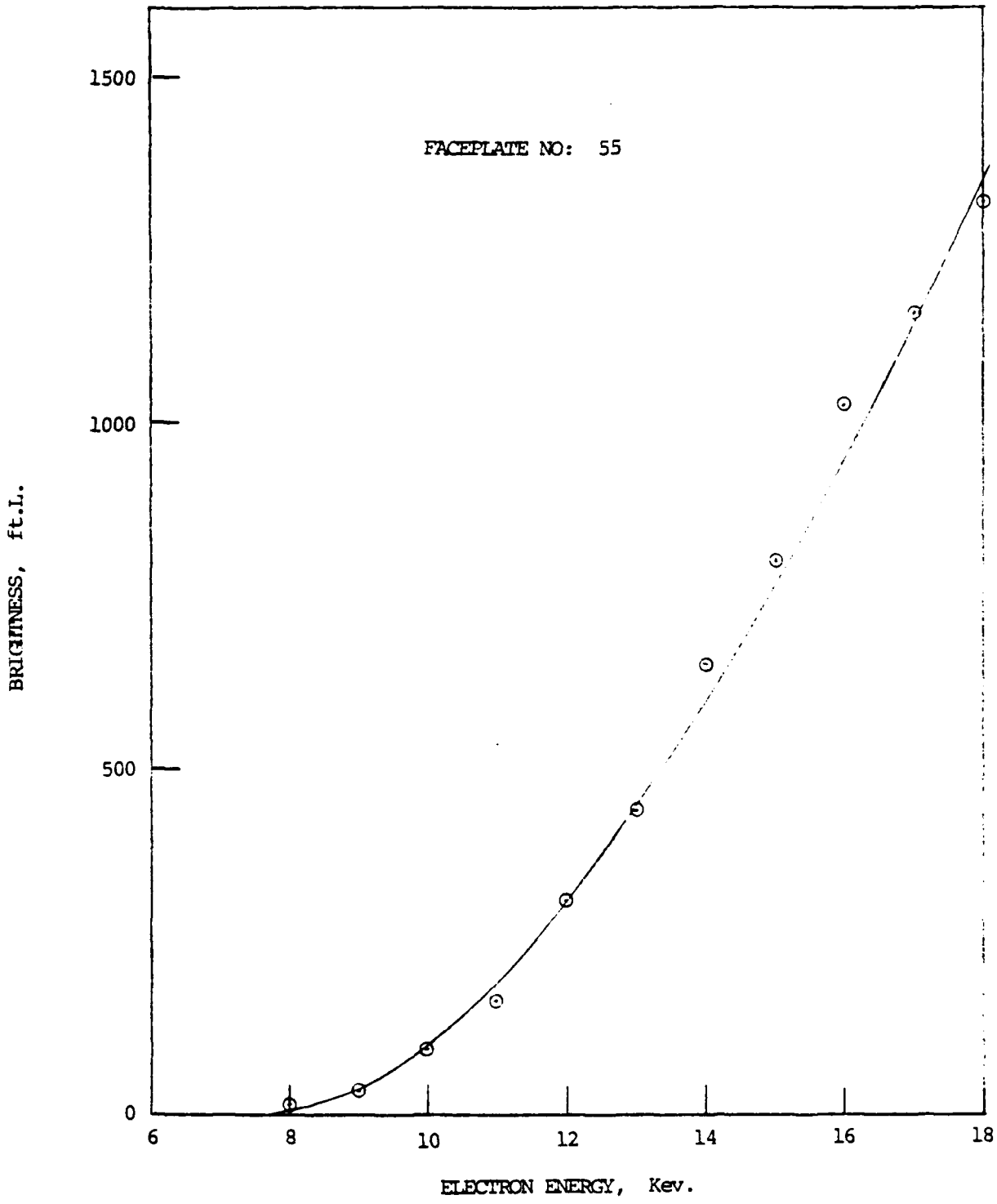

Fig. 9 Cathodoluminescence, Faceplate No. 55

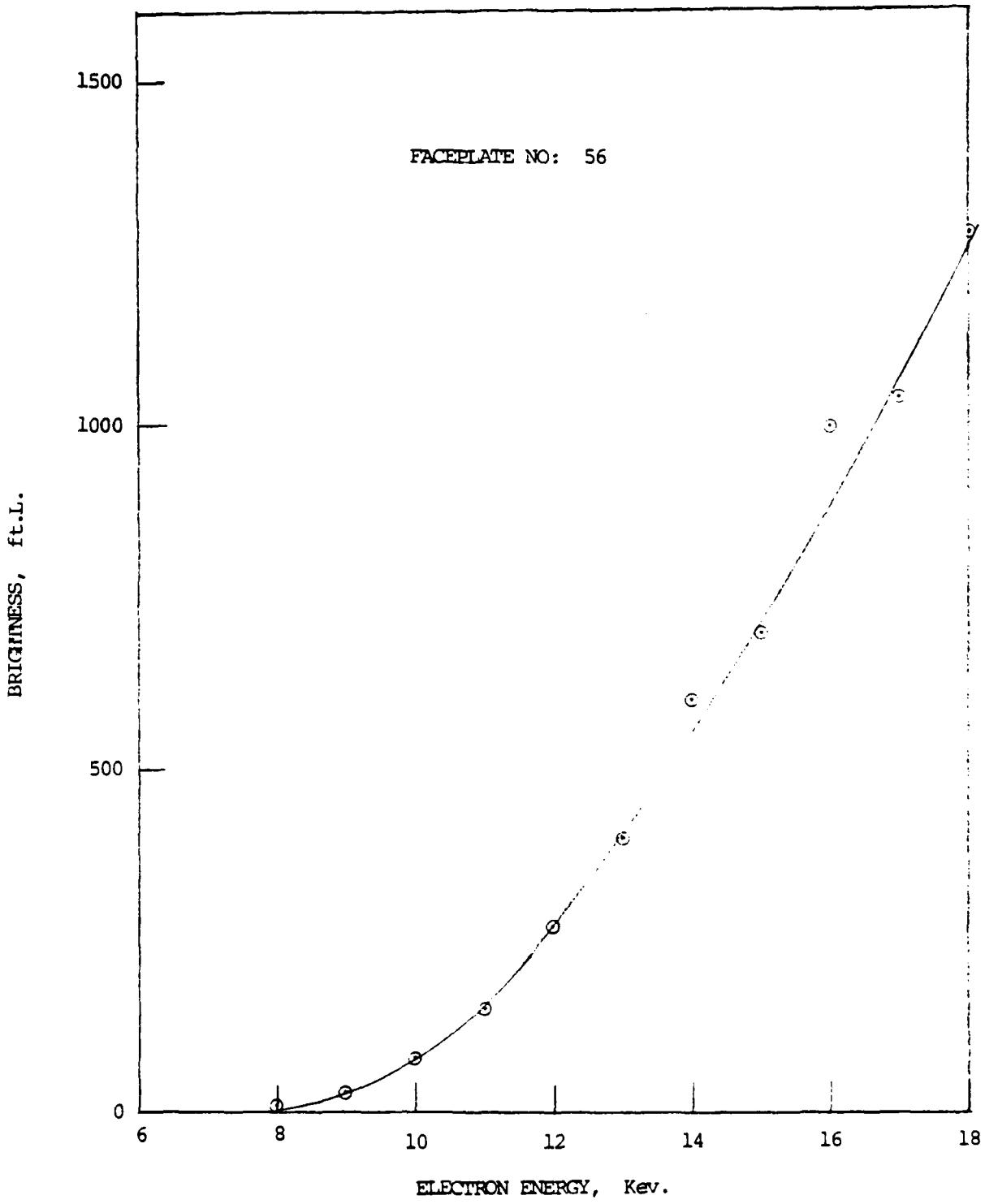

Fig. 10 Cathodoluminescence, Faceplate No. 56

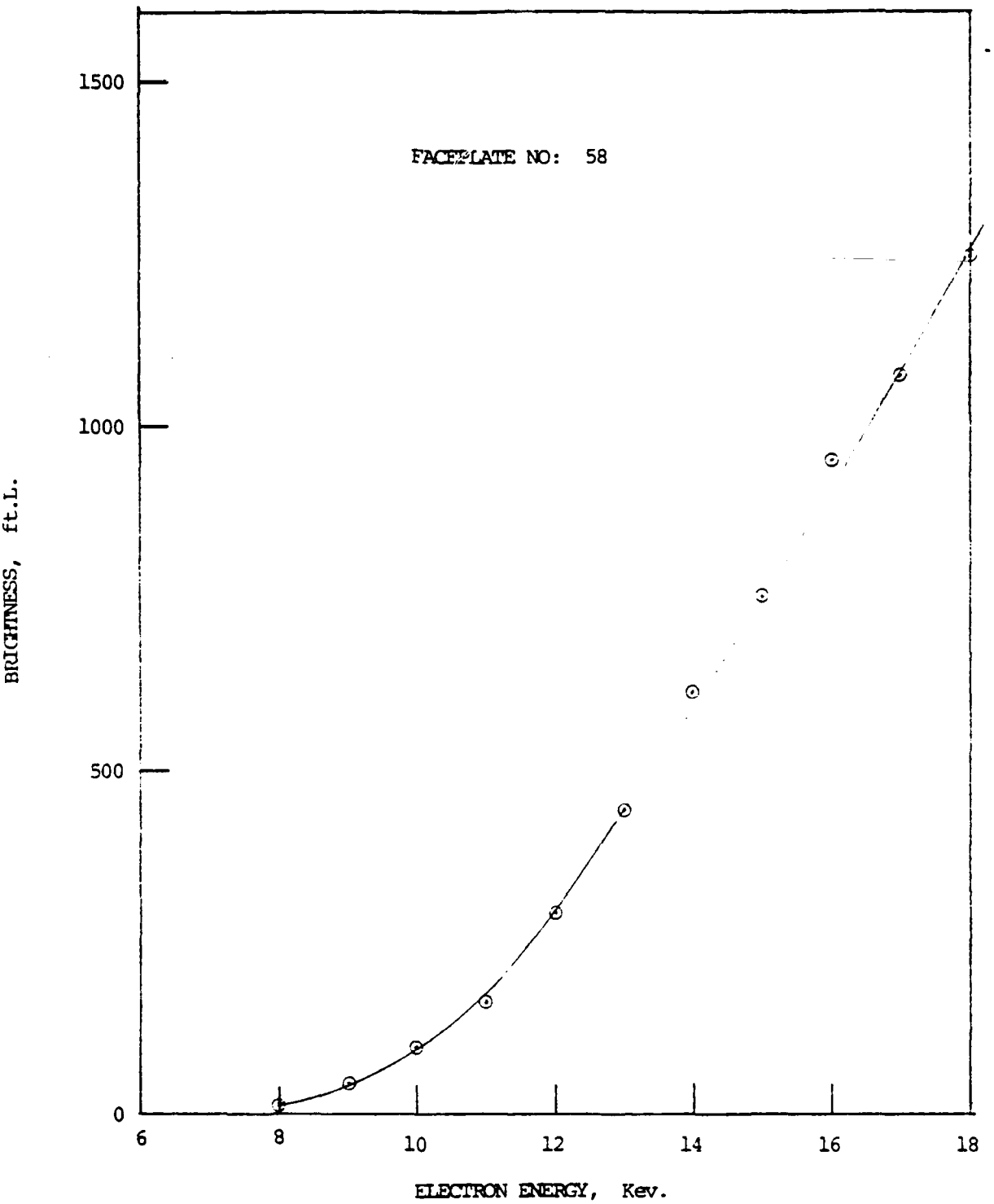

Fig. 11 Cathodoluminescence, Faceplate No. 58

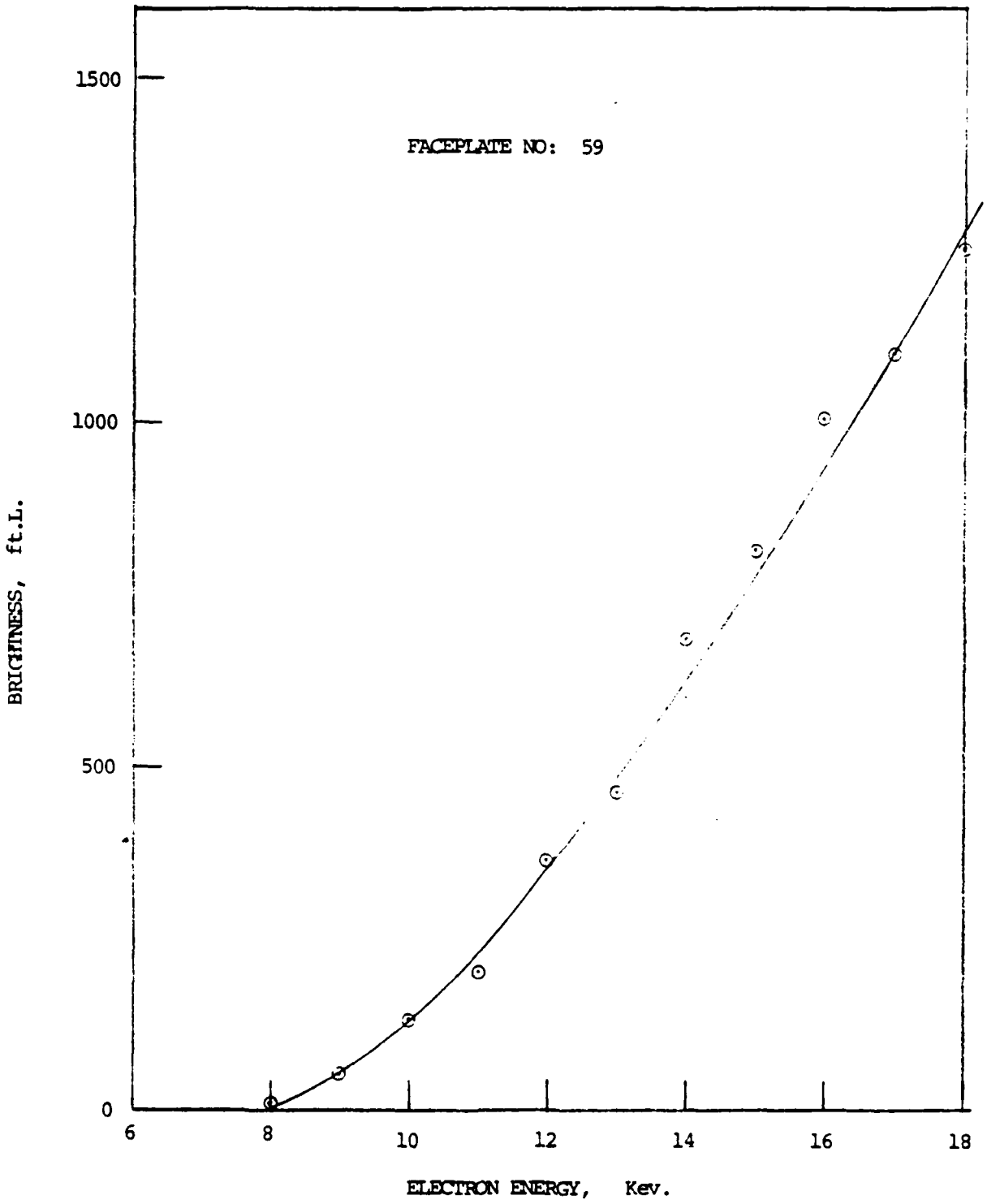

Fig. 12 Cathodoluminescence, Faceplate No. 59

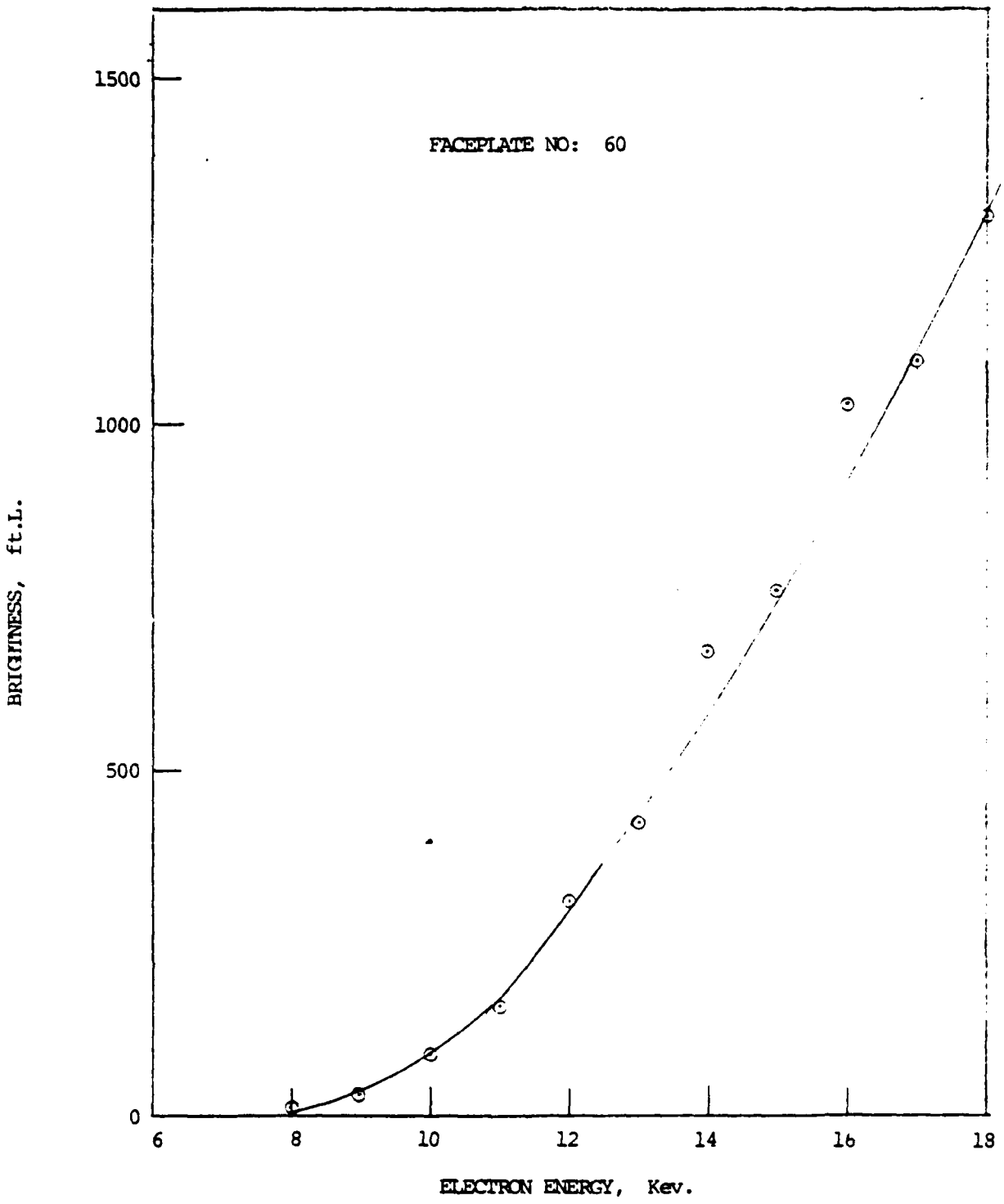

Fig. 13 Cathodoluminescence, Faceplate No. 60

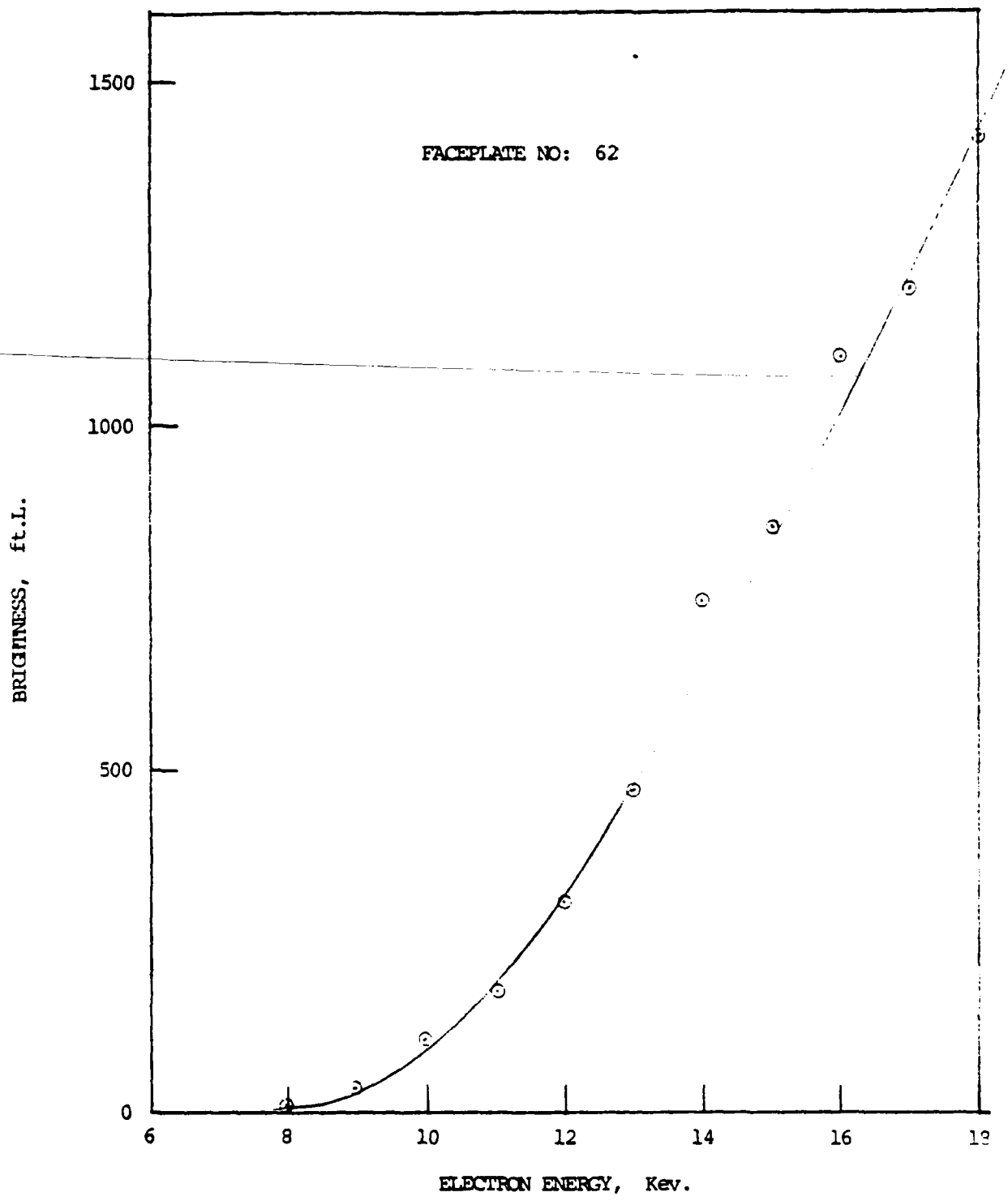

Fig. 14 Cathodoluminescence, Faceplate No. 62

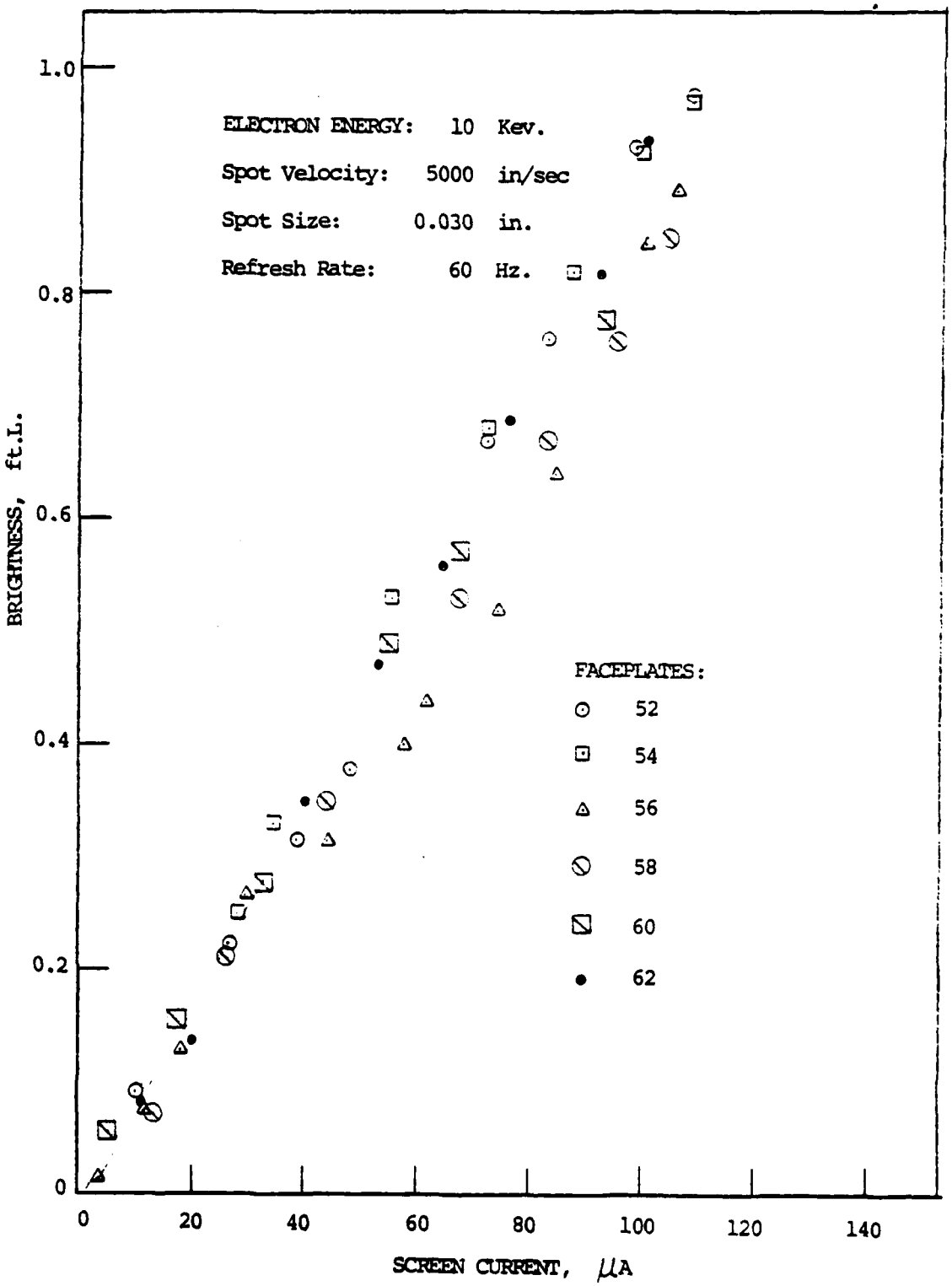

Fig. 15 Cathodoluminescence at 500 in./sec., Lot #2

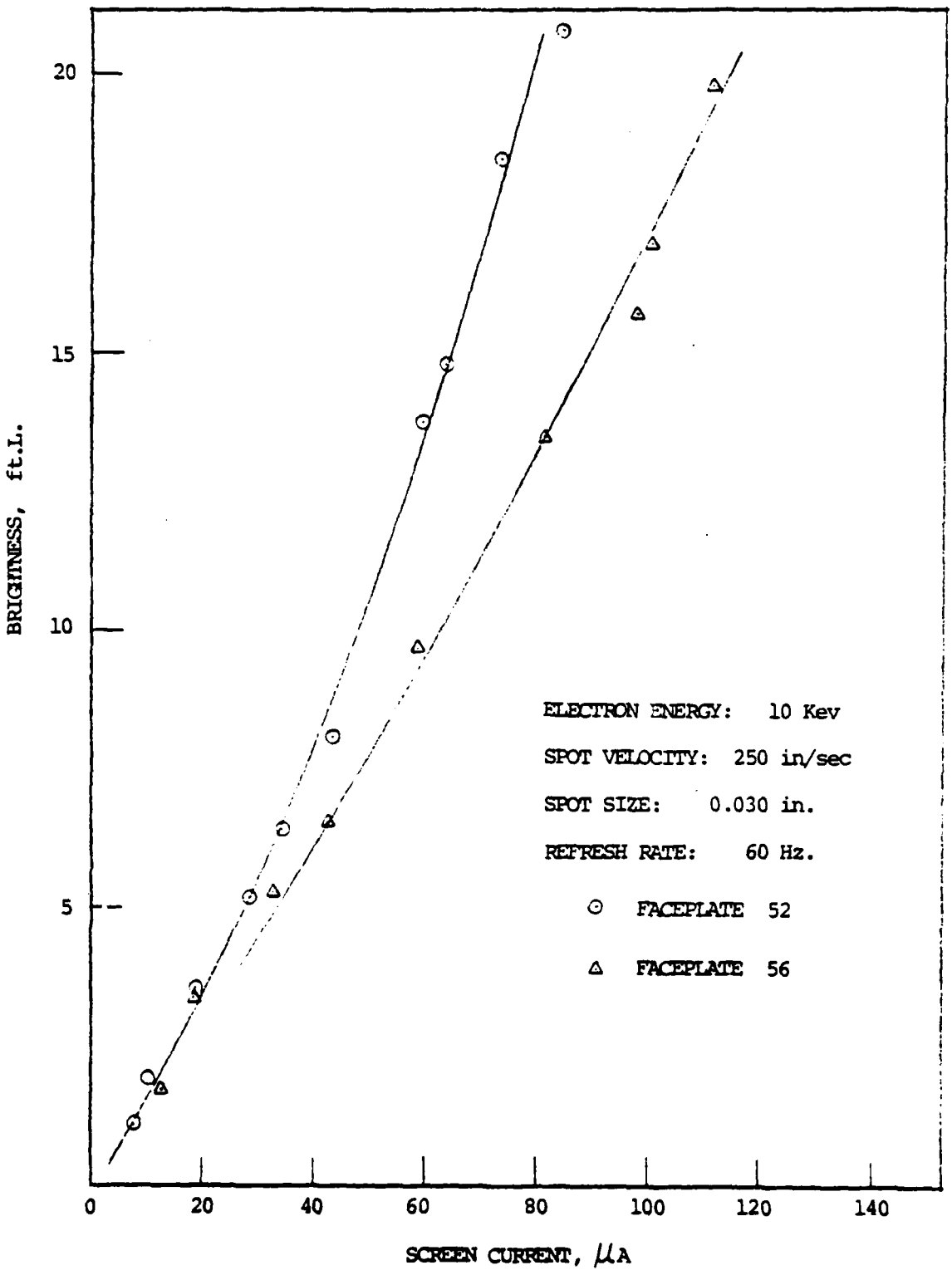

Fig. 16 Cathodoluminescence at 250 in./sec.

Table 7

Cathodoluminescent Brightness, Lot #3

(Foot - Lamberts)

Faceplate No./Kev	66	67	68	69	70	71	72	73	74	64
8	5.05	10.8	7.65	5.21	6.25	4.22	4.42	8.69	6.20	10.1
9	12.1	12.2	18.1	14.5	16.1	11.0	11.7	10.5	15.0	17.4
10	20.5	43.4	52.4	30.6	31.2	22.6	22.8	37.4	32.3	44.8
11	39.2	68.7	54.6	53.4	58.3	40.6	453	63.6	57.4	77.5
12	60.8	101	77.6	90.4	88.2	64.0	66.7	97.0	91.5	116
13	101	144	129	127	141	108	102	150	135	179
14	130	189	174	191	177	143	137	203	190	259
15	194	244	224	257	258	202	182	274	235	324
16	228	284	277	301	282	250	222	320	312	398
17	305	325	324	380	371	293	272	364	387	471
18	344	356	354	397	390	357	330	435	432	498
19	450	435	415	459	477	398	373	471	450	/

Raster Size: $0.5 \times 0.5\ cm^2$

Screen Current: $5.0\ \mu A$

Pressure: 2×10^{-7} Torr.

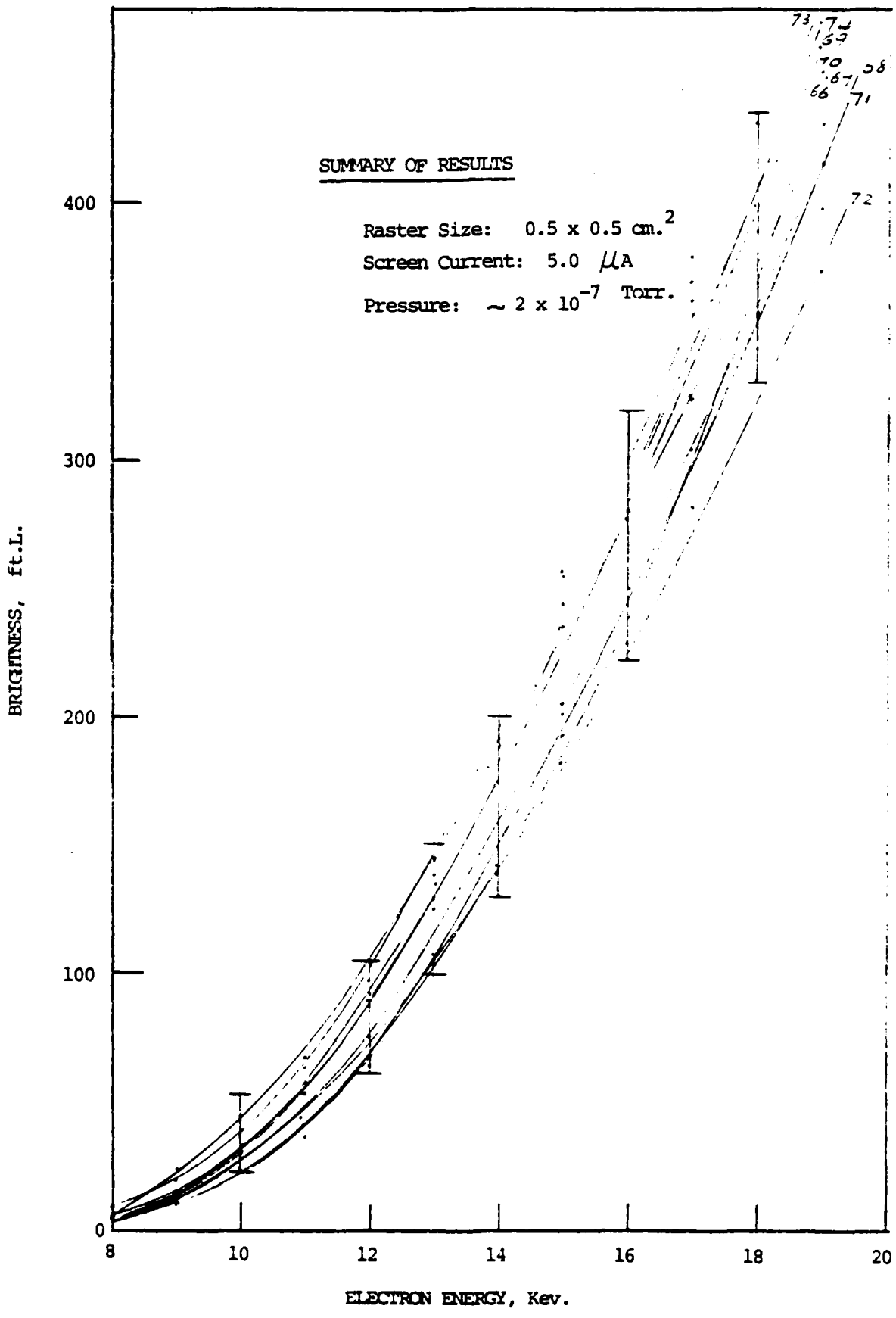

Fig. 17 Cathodoluminescence Summary, Lot #3

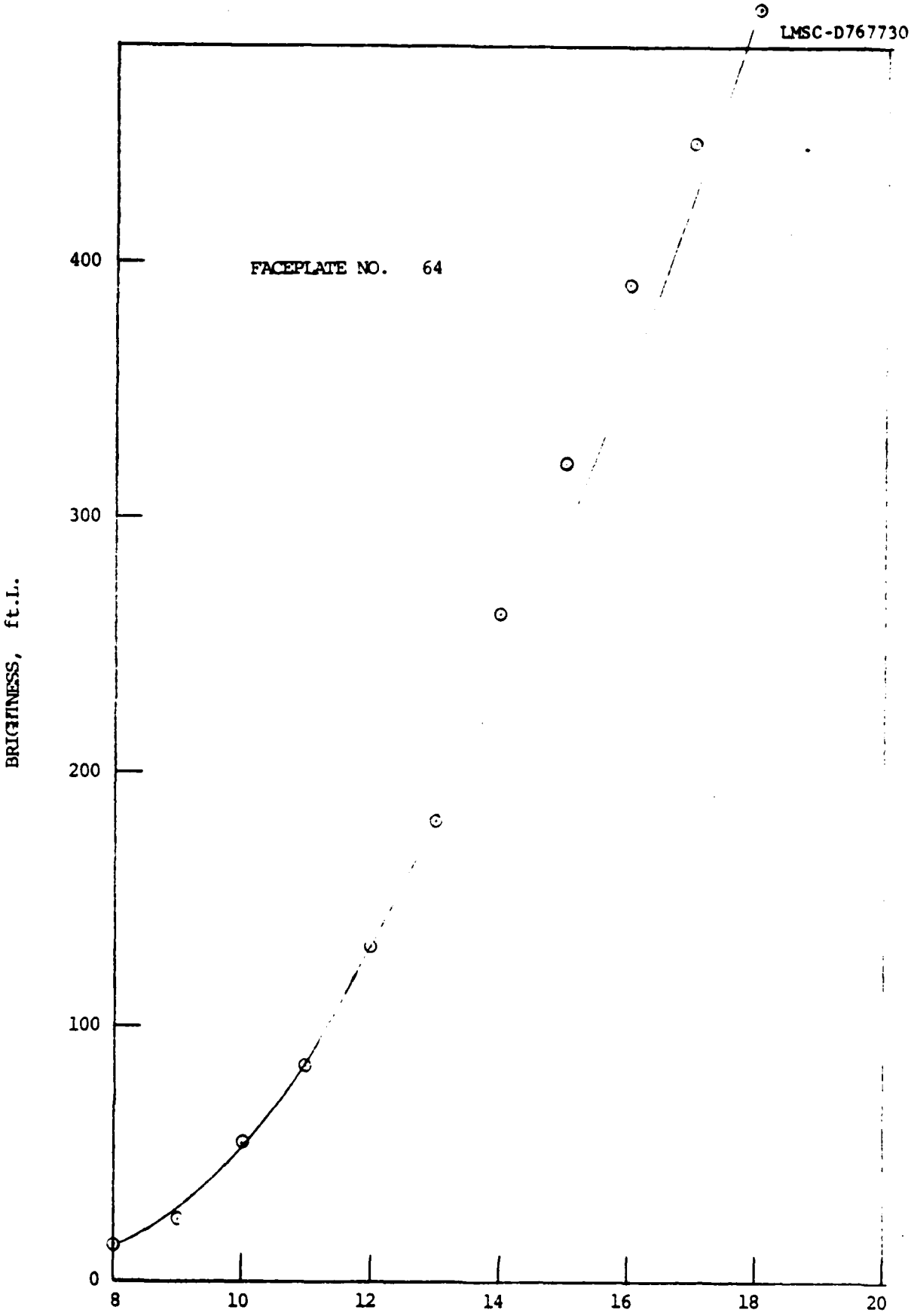

Fig. 18 Cathodoluminescence, Faceplate No. 64

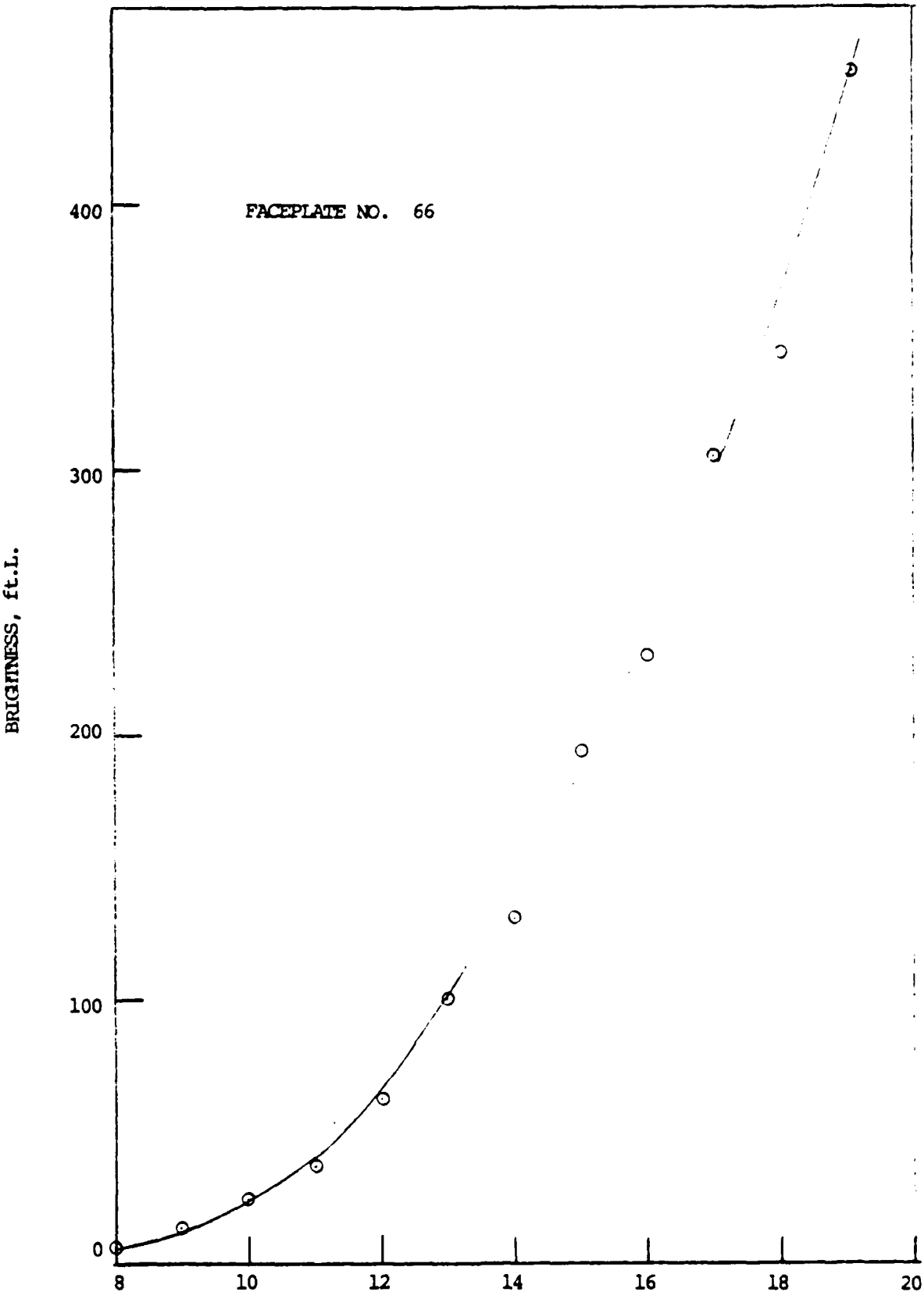

Fig. 19 Cathodoluminescence, Faceplate No. 66

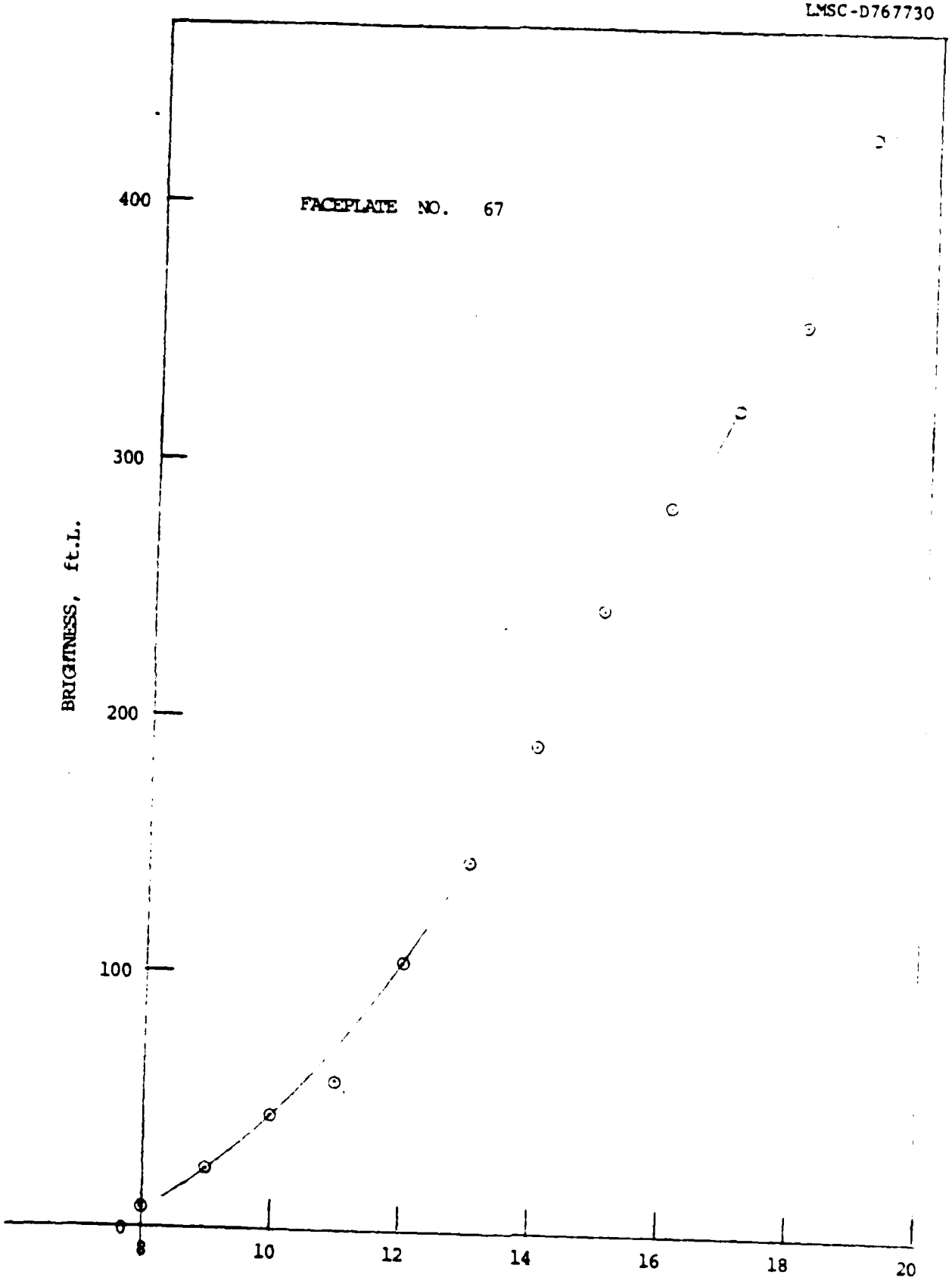

Fig. 20 Cathodoluminescence, Faceplate No. 67

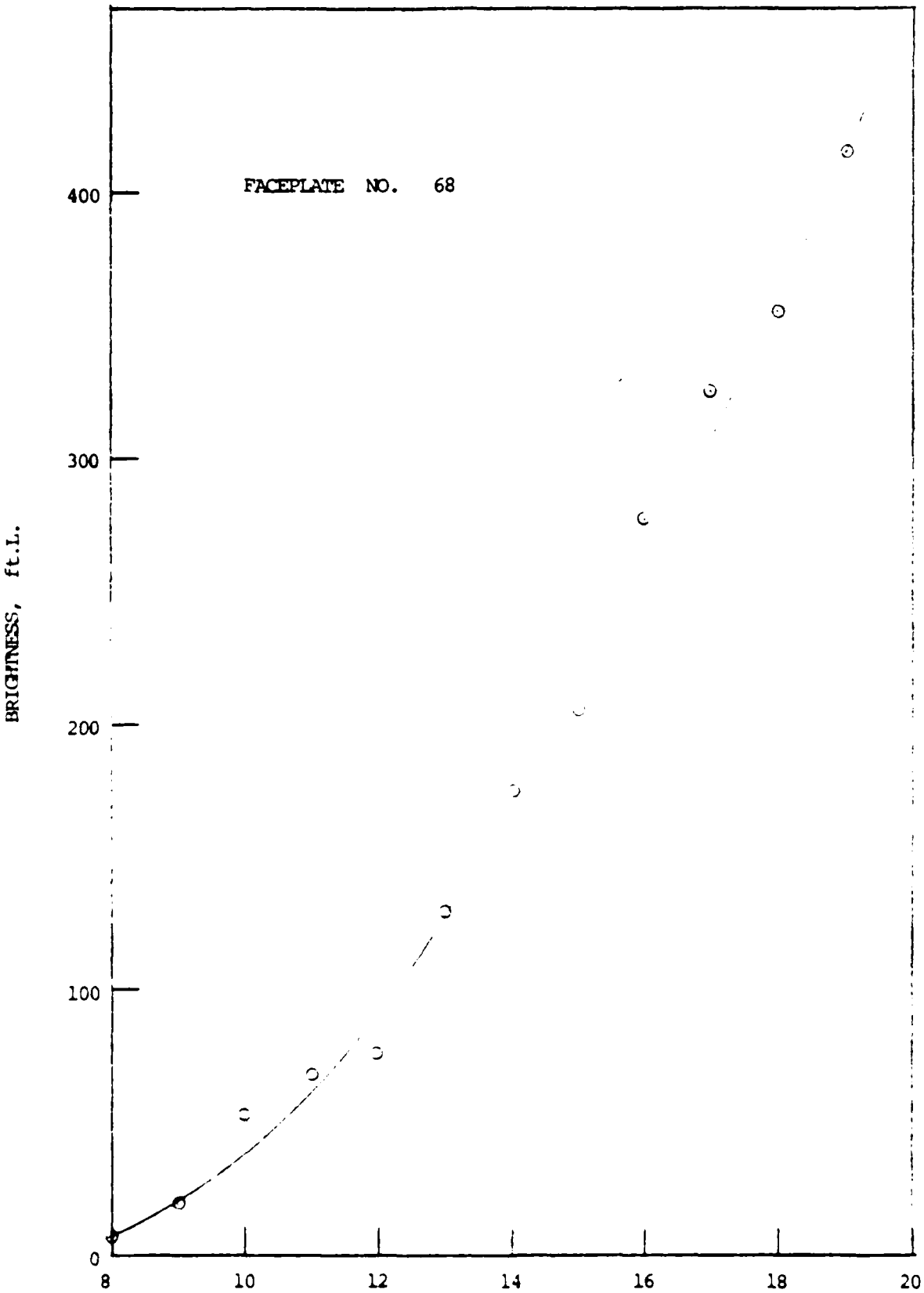

Fig. 21 Cathodoluminescence, Faceplate No. 68

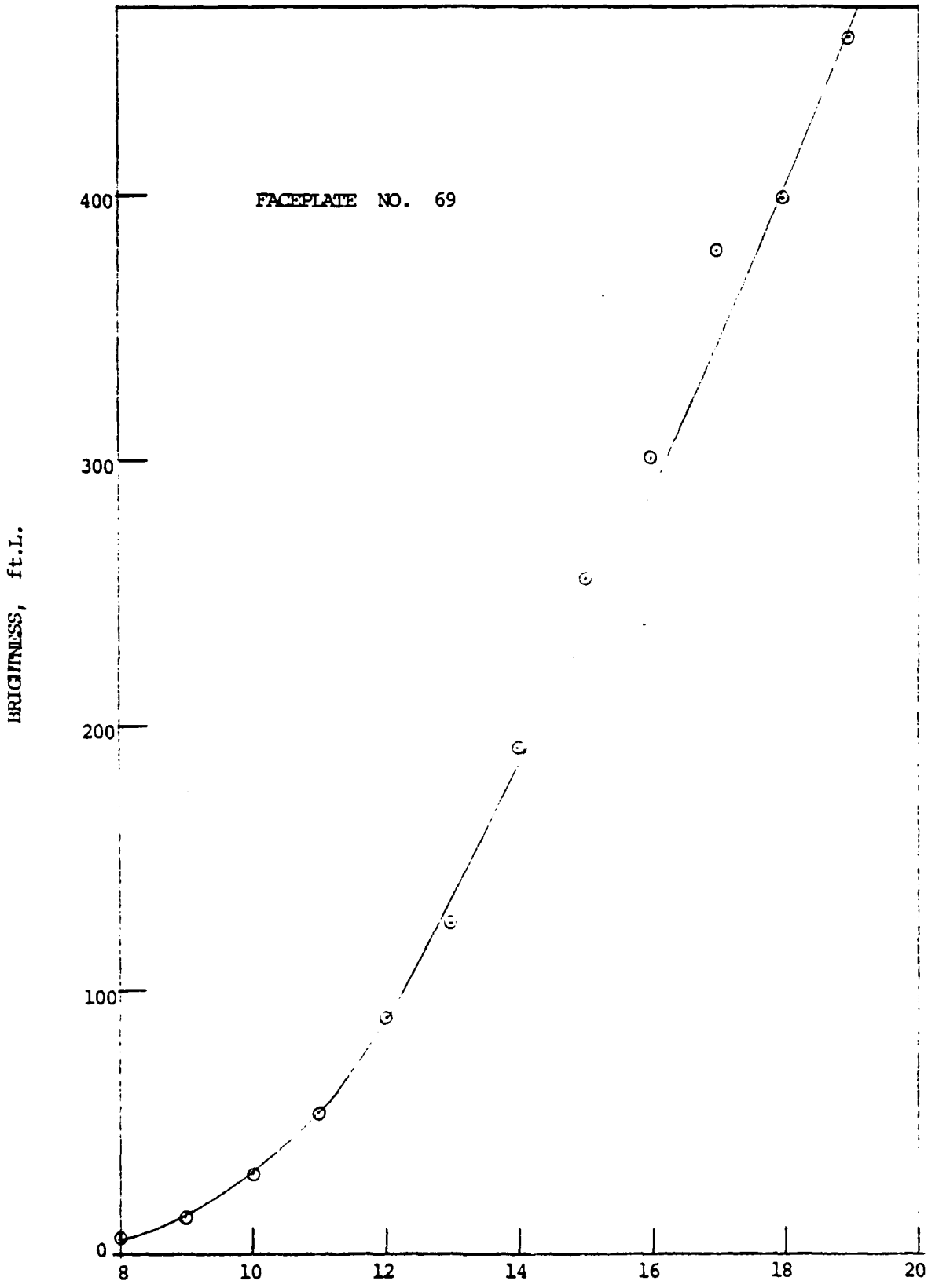

Fig. 22 Cathodoluminescence, Faceplate No. 69

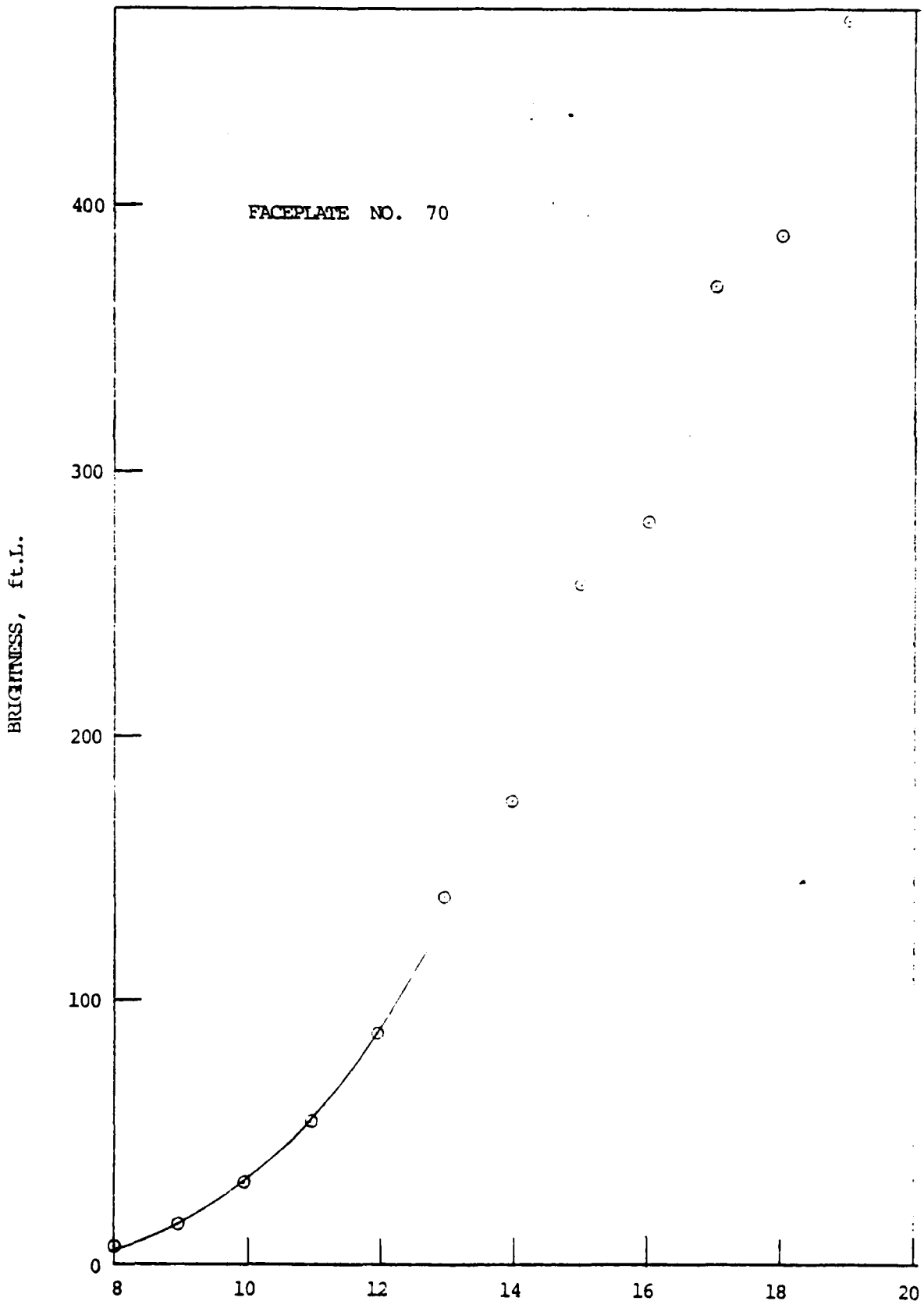

Fig. 23 Cathodoluminescence, Faceplate No. 70

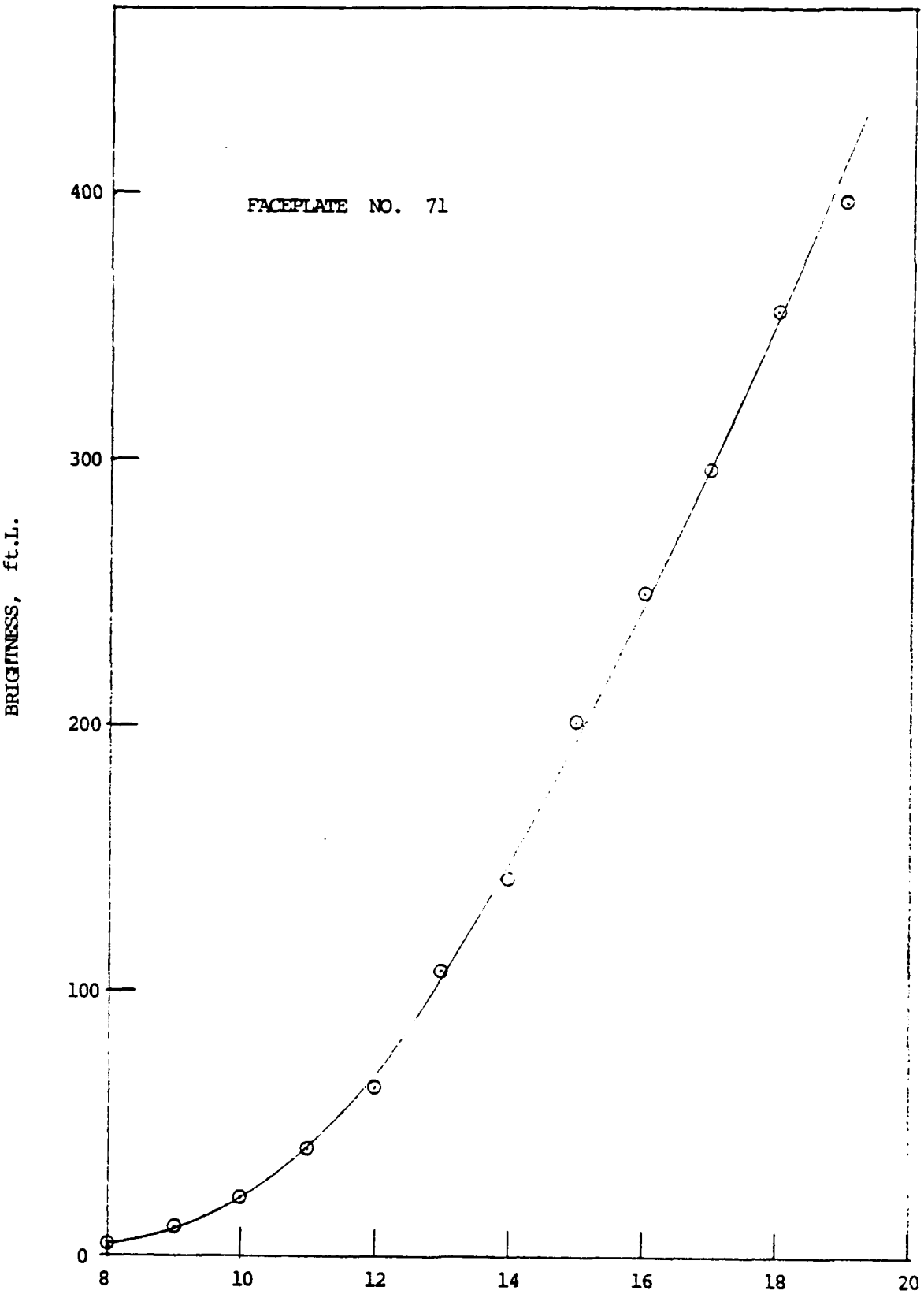

Fig. 24 Cathodoluminescence, Faceplate No. 71

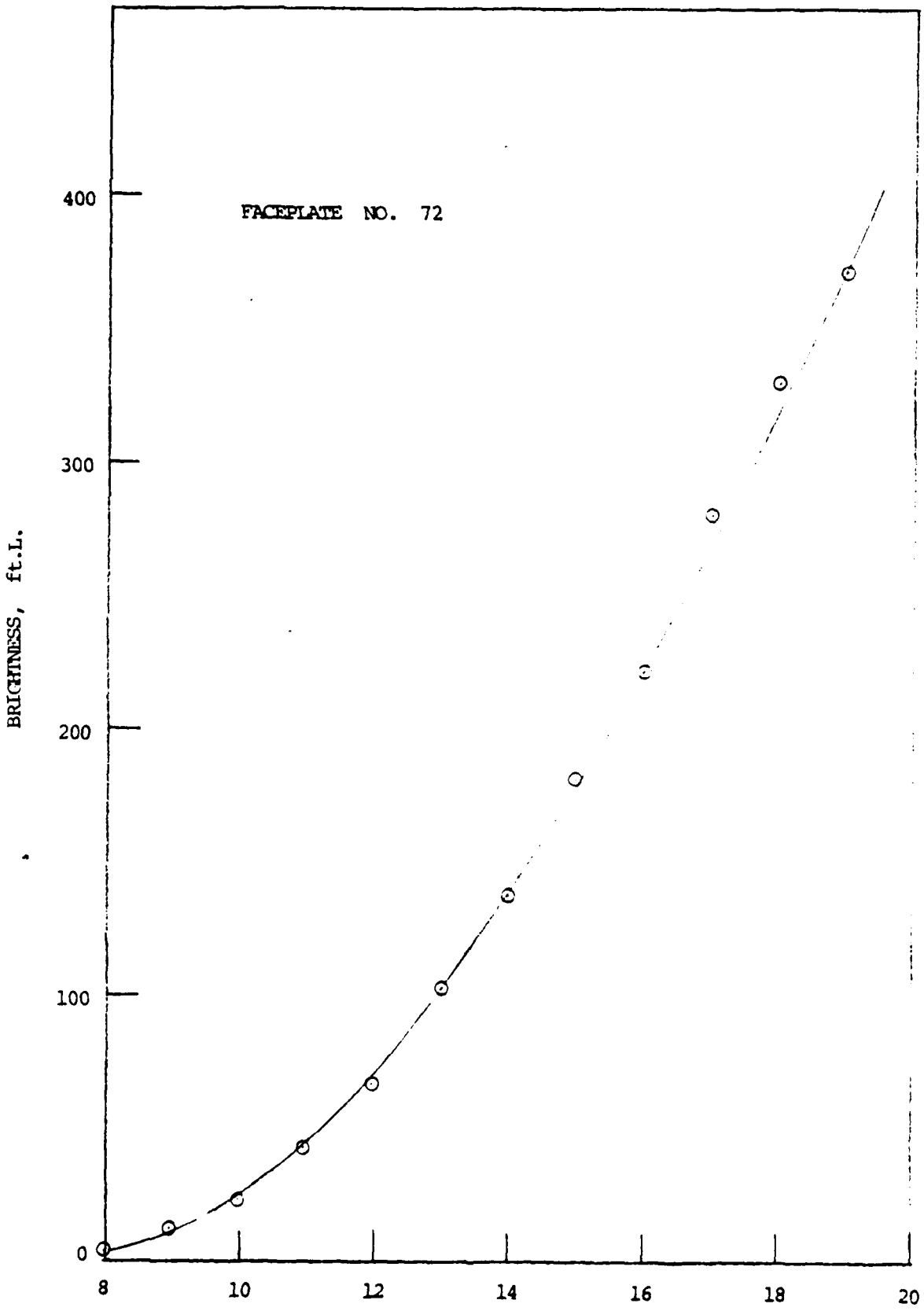

Fig. 25 Cathodoluminescence, Faceplate No. 72

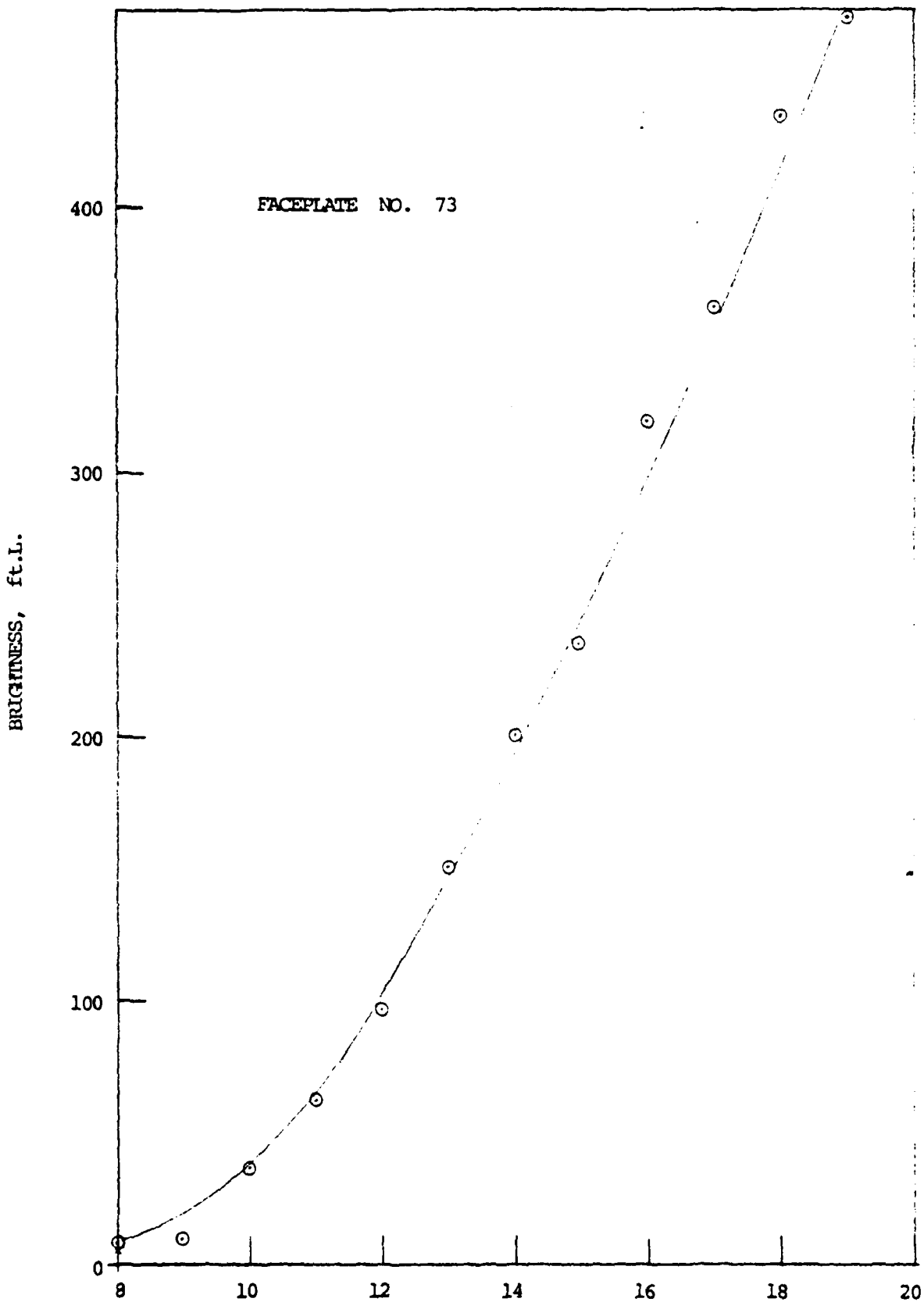

Fig. 26 Cathodoluminescence, Faceplate No. 73

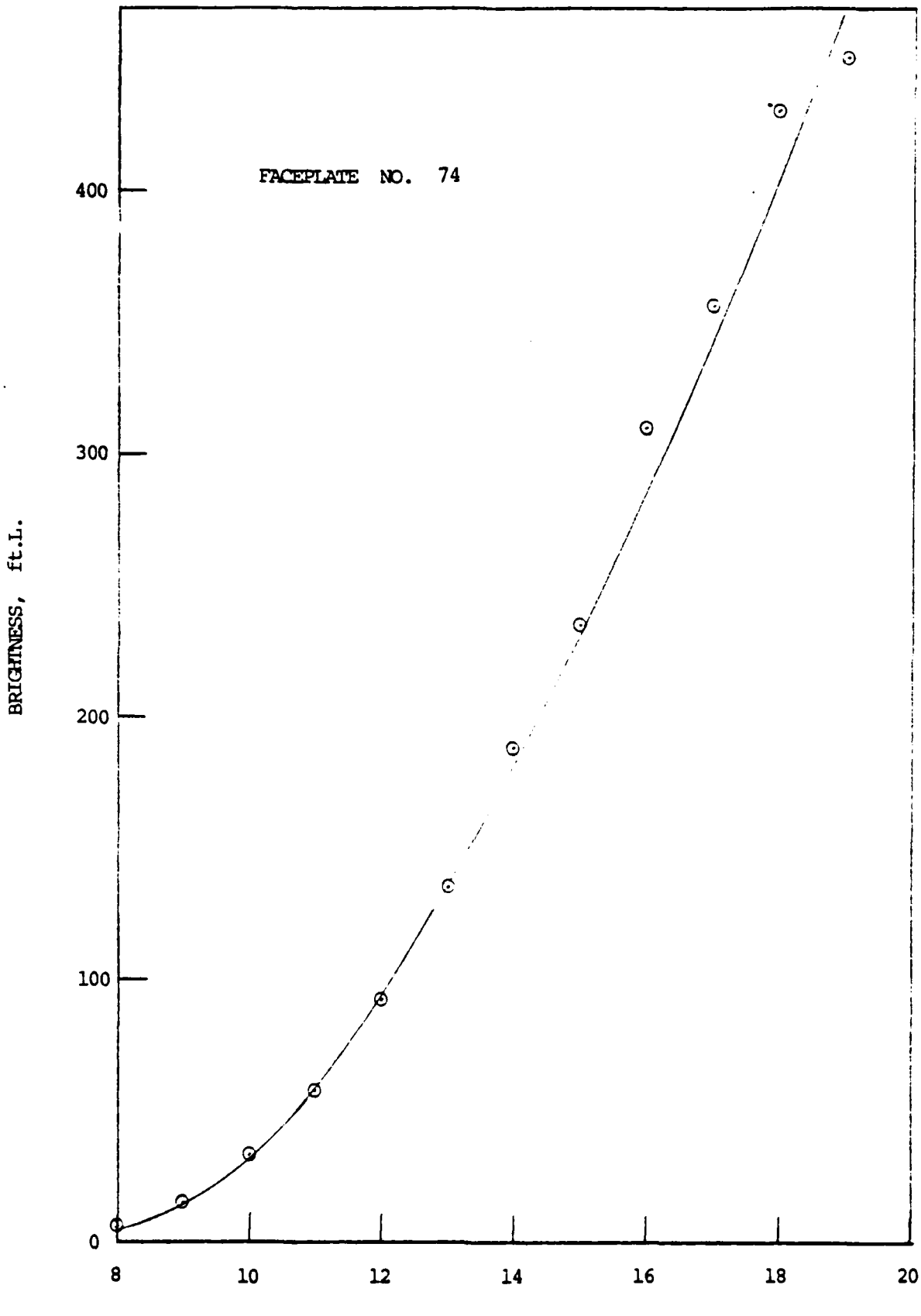

Fig. 27 Cathodoluminescence, Faceplate No. 74

4.5 Optical Reflectance Measurements

The purpose of the measurement was to determine the specular reflectance value and to evaluate the diffuse reflectance for each faceplate. The most accurate determination of diffuse reflectance requires the use of an integrating sphere. As such a sphere was not available, a bidirectional technique was used.

In a bidirectional measurement, a light beam is directed at the sample at a fixed angle of incidence as near to normal as practicable. The detector is then moved through several degrees about the specular reflection angle, with the light intensity recorded at each position of the detector. With a narrow beam of well-collimated light, a plot of intensity vs. detector angle should exhibit a narrow peak at the specular reflection angle. Any diffuse reflection would produce lateral tails symmetrically disposed about the peak.

The assembly shown in Figure 28 was for the bidirectional reflectance measurement of the Lot #1 faceplates. It was built around a Gaertner Model L103 spectrometer. The light source was a microscope illuminator operated via a Sola line voltage regulator. A 1/8 in. circular aperture was used in place of the slit. A Pritchard Model 1970 PR photometer with a fixed 4-in. Micro-Spectar Lens (1962-PD) was used as the light sensing instrument. The faceplate to be measured was placed on the prism platform and the collimation was accomplished using the existing optical system of the spectrometer. Since it was not convenient to move the rather bulky photometer around, the traditional technique of using a stationary light source in bidirectional reflectance measurement was modified. In the present measurement, the photometer was fixed in position, but the light source together with the faceplate was rotated through an angle α about the pivot point of the platform.

The optical axes of the light source and the photometer were initially separated by about 25°. A front surface mirror with known reflectance was first placed on the platform and so rotated as to produce a maximum reflectance in order to establish the angle of specular reflection. (See Figure 29). The mirror was then replaced with the sample faceplate and a maximum reflectance again

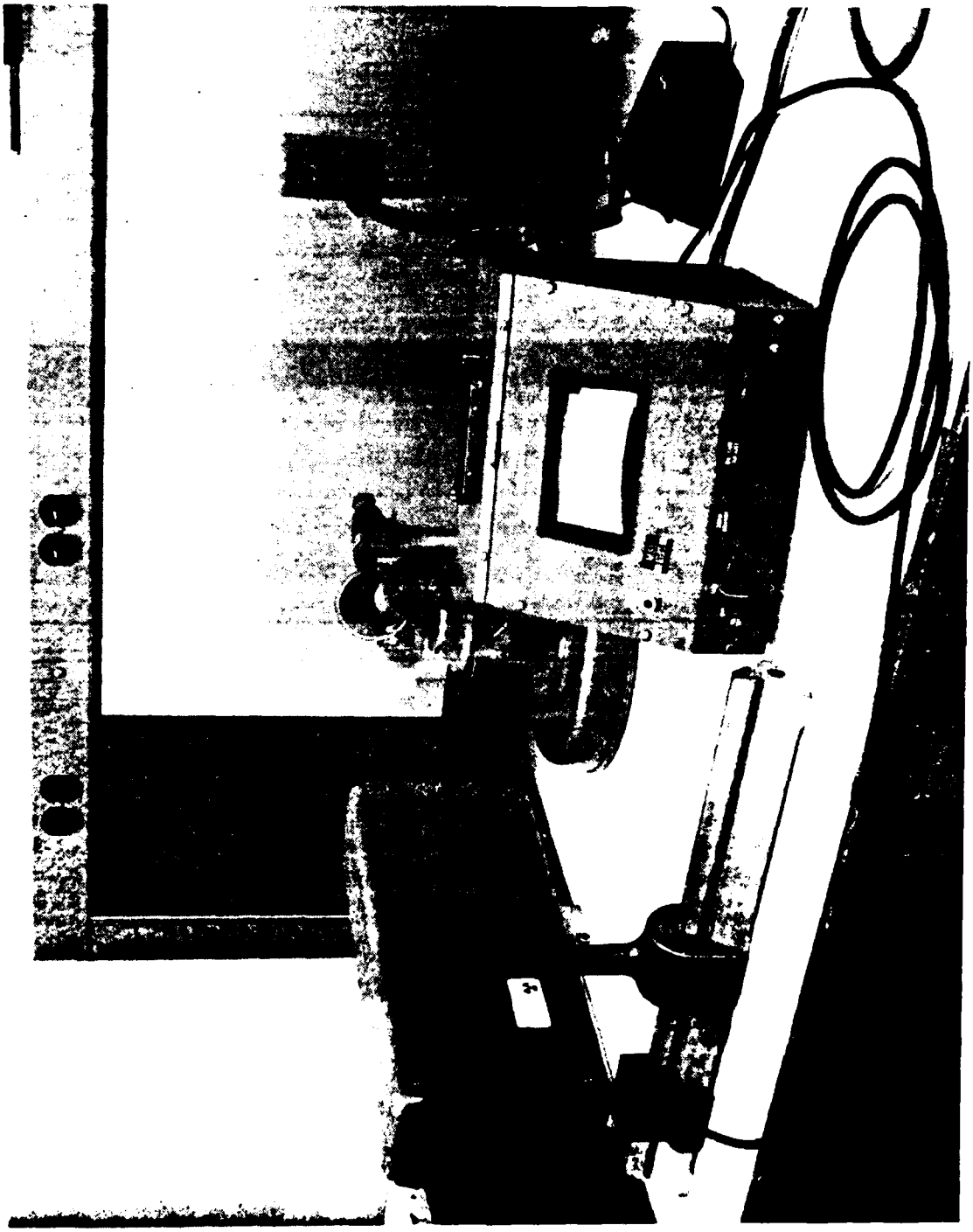

Fig. 28 Original Assembly for Optical Reflectance Measurement

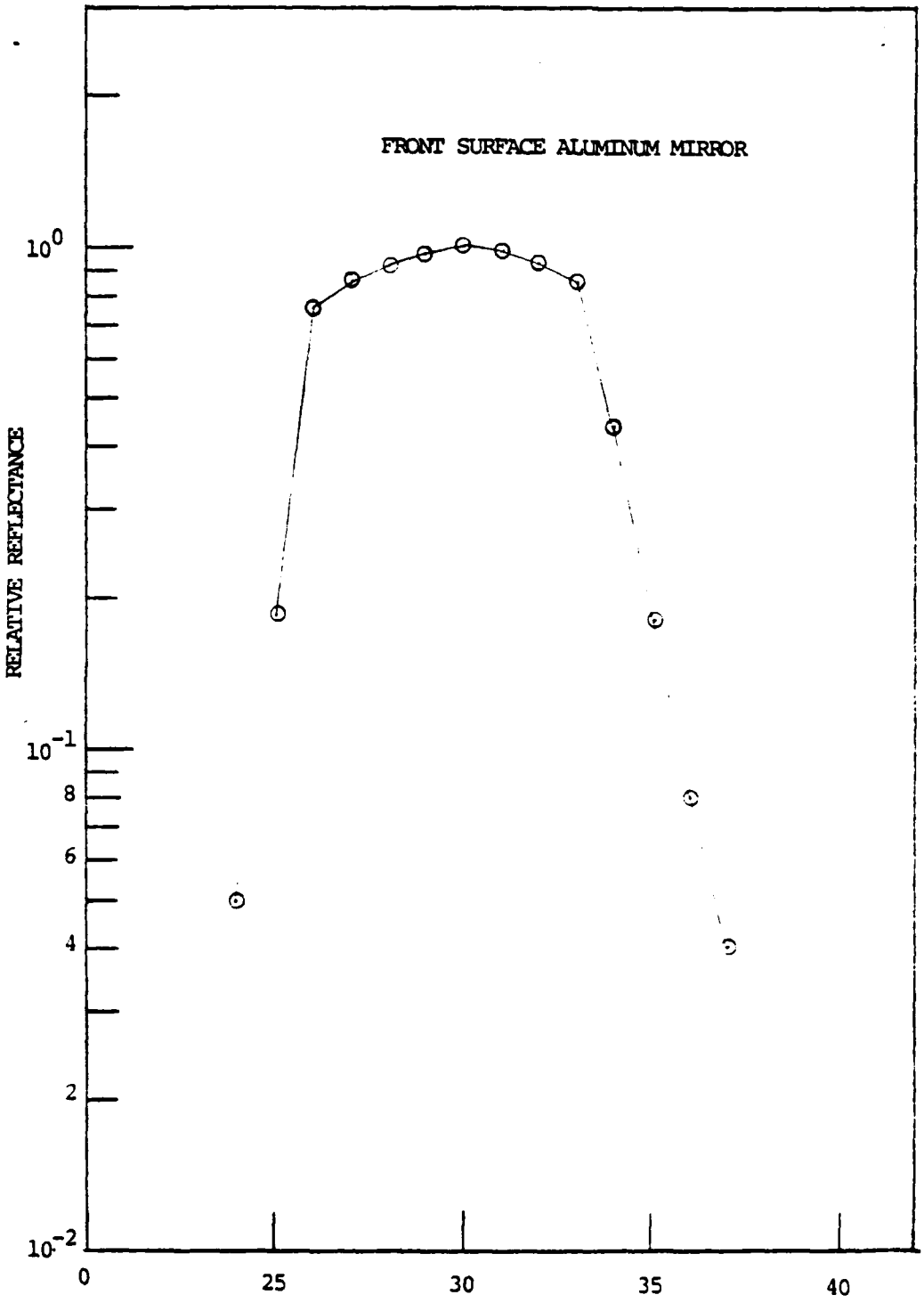

Fig. 29 Optical Reflectance, Mirror

established. The light source together with the faceplate was then rotated about the pivot at successive angular displacements of 1° apart over a range of $\pm 10^{\circ}$ from the specular reflectance angle and the reflected luminance at each angular displacement was recorded.

4.5.1 Lot #1

Bidirectional reflectance of the Lot #1 faceplates is presented in Figures 30 through 39. The measured specular reflectance values are summarized in Table 8. The plots of measurements on Lot #1 show a broad maximum at the specular reflection angle, contrary to an expected sharp peak. No tails characteristic of diffuse reflectance appear.

A discussion of these results with P. F. Krzyzkowski led to the conclusion that the broad peak was due to insufficient collimation of the incident light beam. It was suggested that increasing the source to sample and sample to detector distances should improve the collimation. A new setup for the measurements was then assembled, comparable to that employed at ERADCOM. In the meantime, Lot #1 was shipped to ERADCOM to meet scheduled delivery. ERADCOM has indicated that Lot #1 will be returned to permit remeasurement with the new assembly.

4.5.2 Lot #2

The optical assembly that eventually evolved for the measurement is depicted in Figure 40 and the placement of components is schematically represented in Figure 41. It was noted initially that the specular reflectance angle, as anticipated, was small, so that the light source was placed quite far (~ 75 in.) from the sample surface in order to give more accurate angular displacement as well as ease of light beam collimation. In addition, since the photometer used as a light sensing instrument is rather bulky in comparison to the light source, the usual bidirectional reflectance measurement technique of using a fixed light source but rotating sensor has been reversed. In the present experiment, the photometer is fixed in position, but the light source is rotated through an end of α about the pivot point onto which the sample rests. All components were carefully aligned and leveled to ensure that the surface of the faceplate sample was at right angles to the light beam at all times.

Table 8

Specular Reflectance, Lot #1

Faceplate	Specular Reflectance, %
38	6.0
39	7.7
40	6.8
41	8.7
42	6.5
43	6.3
44	6.4
45	6.9
46	7.2
48	7.9

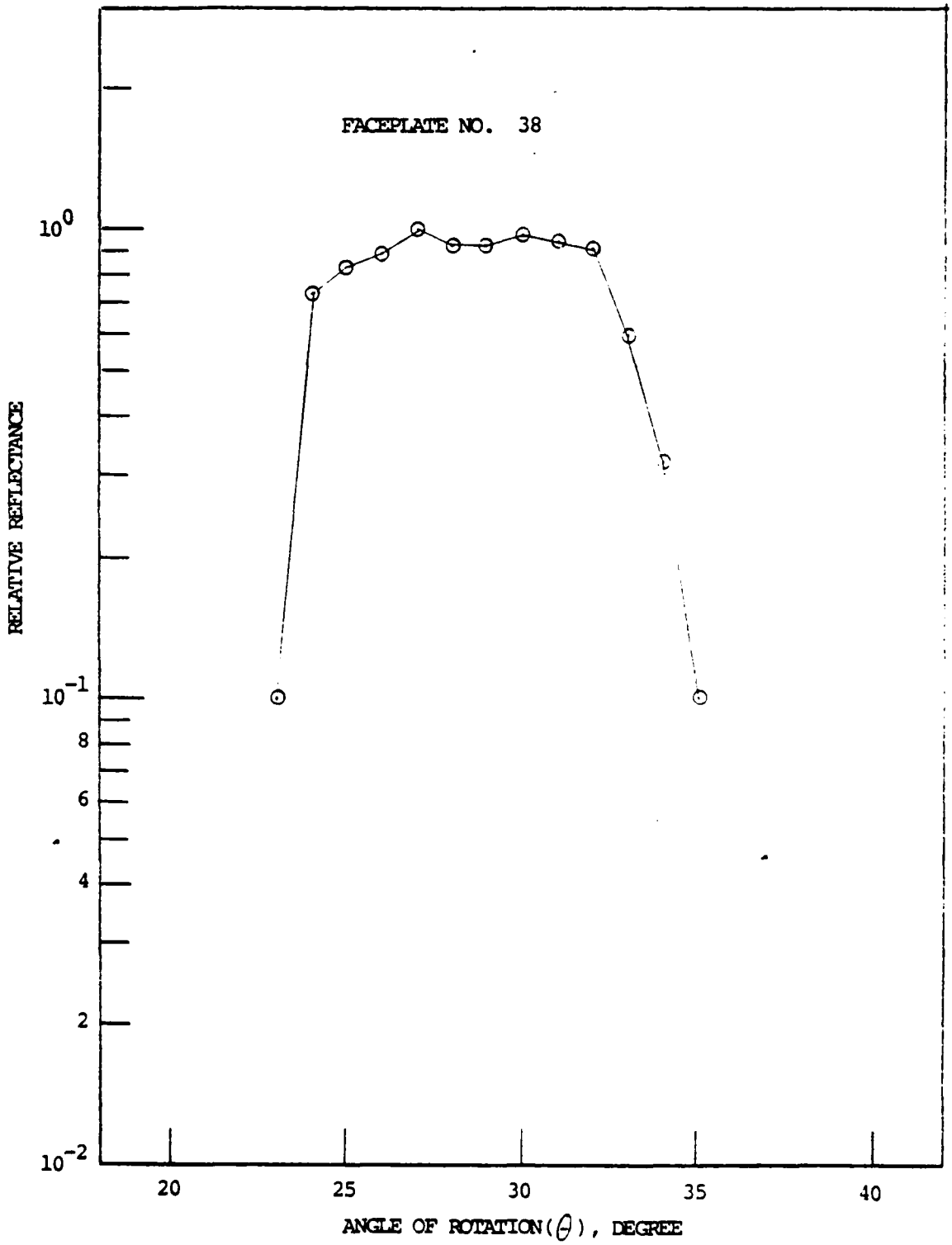

Fig. 30 Optical Reflectance, Faceplate No. 38

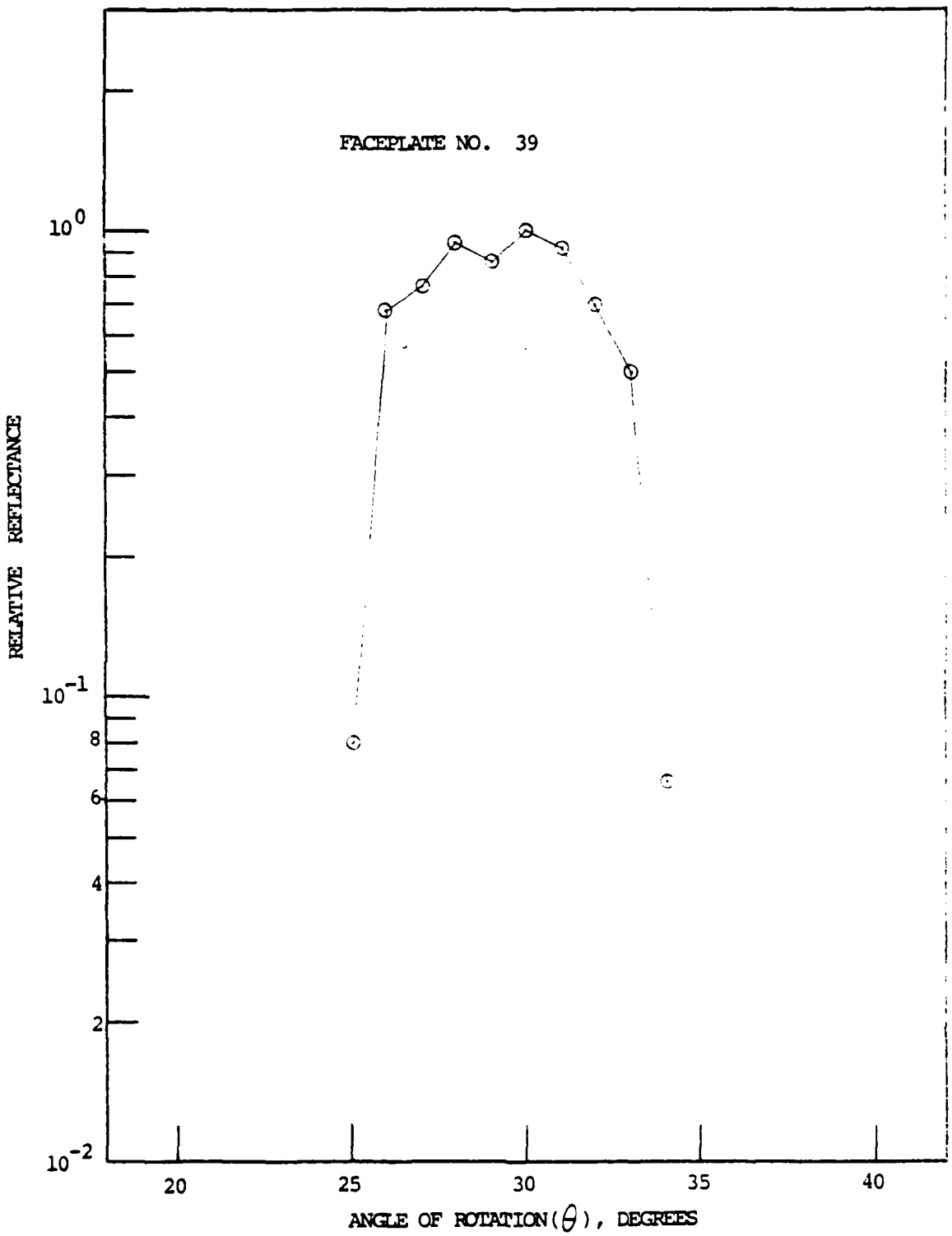

Fig. 31 Optical Reflectance, Faceplate No. 39

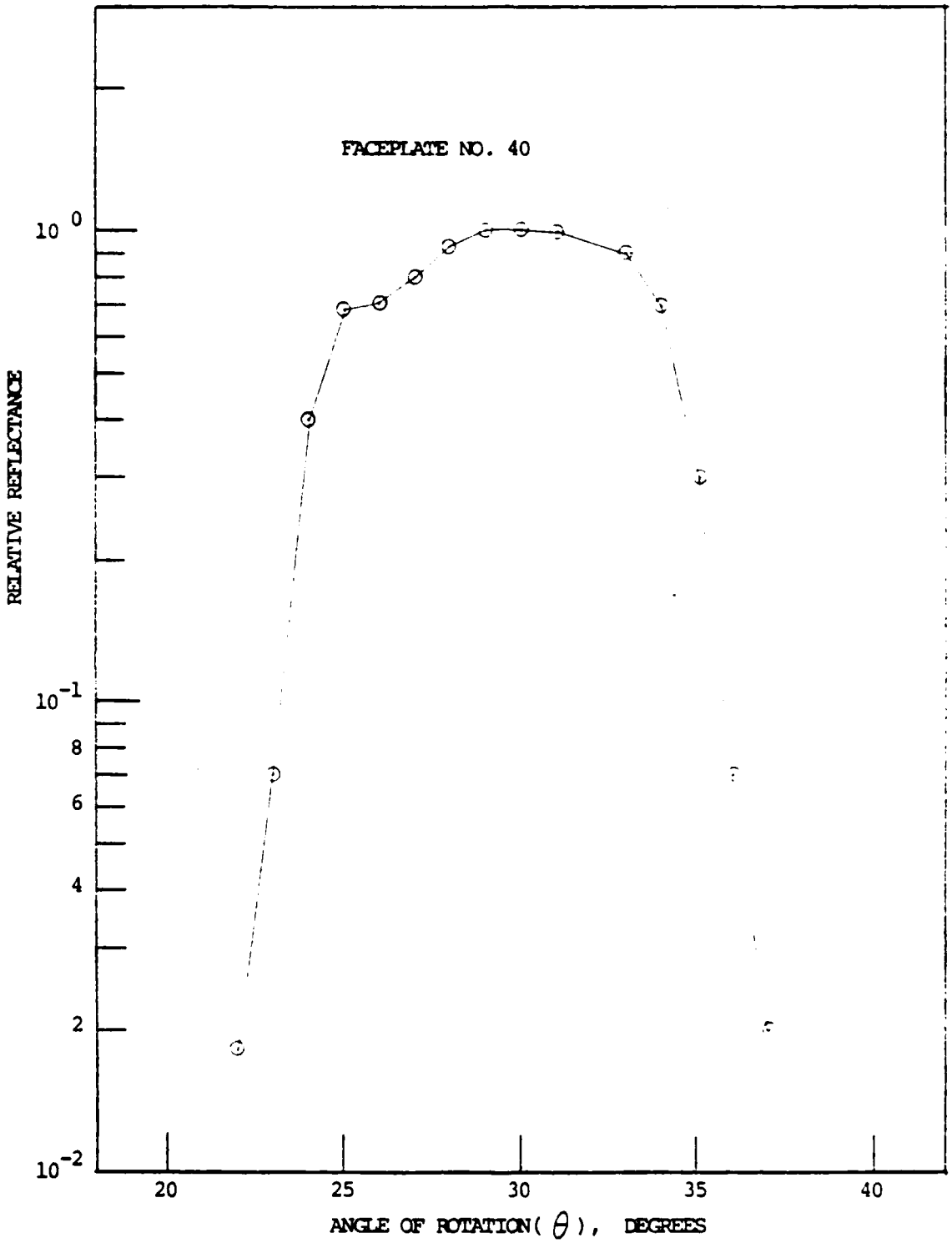

Fig. 32 Optical Reflectance, Faceplate No. 40

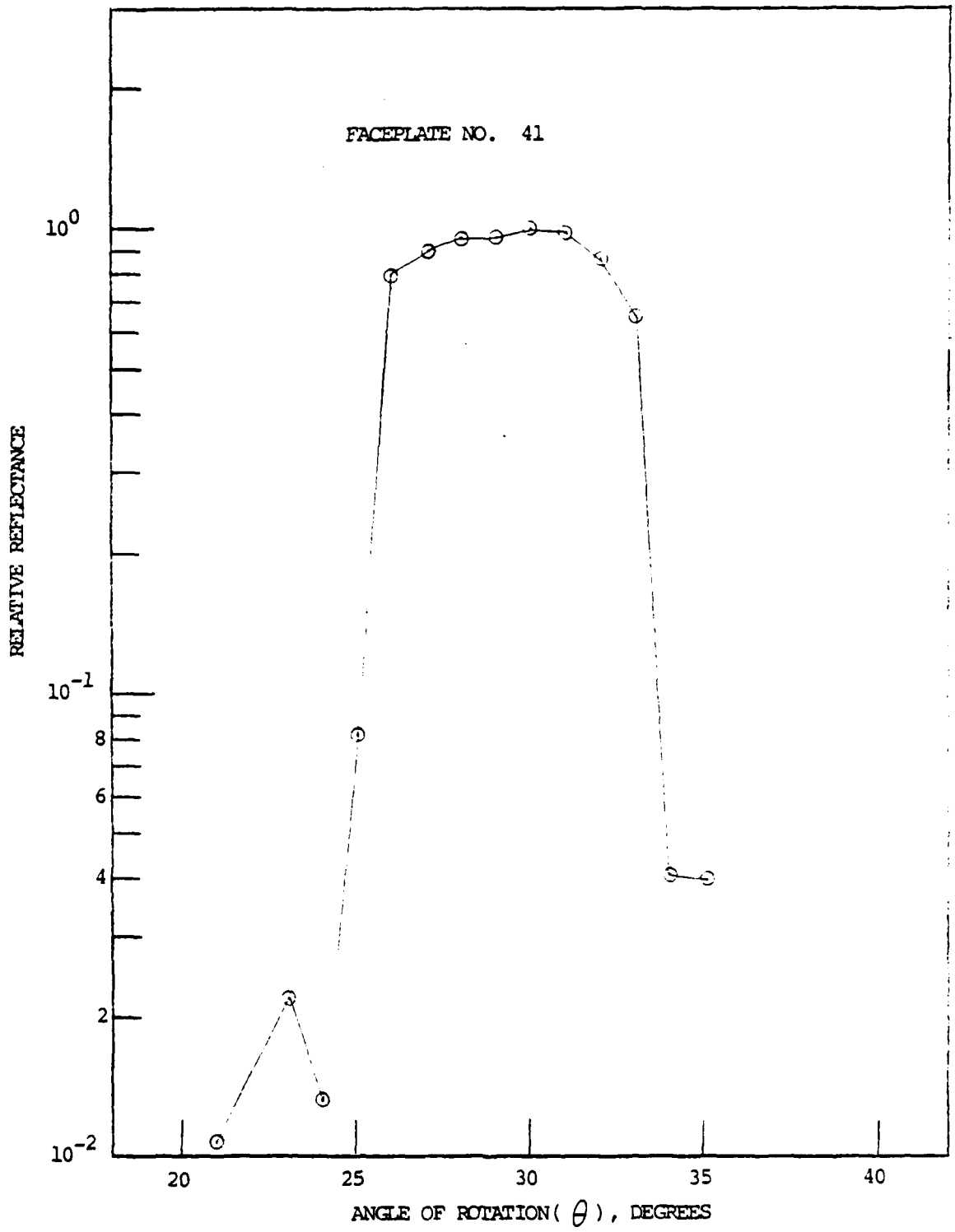

Fig. 33 Optical Reflectance, Faceplate No. 41

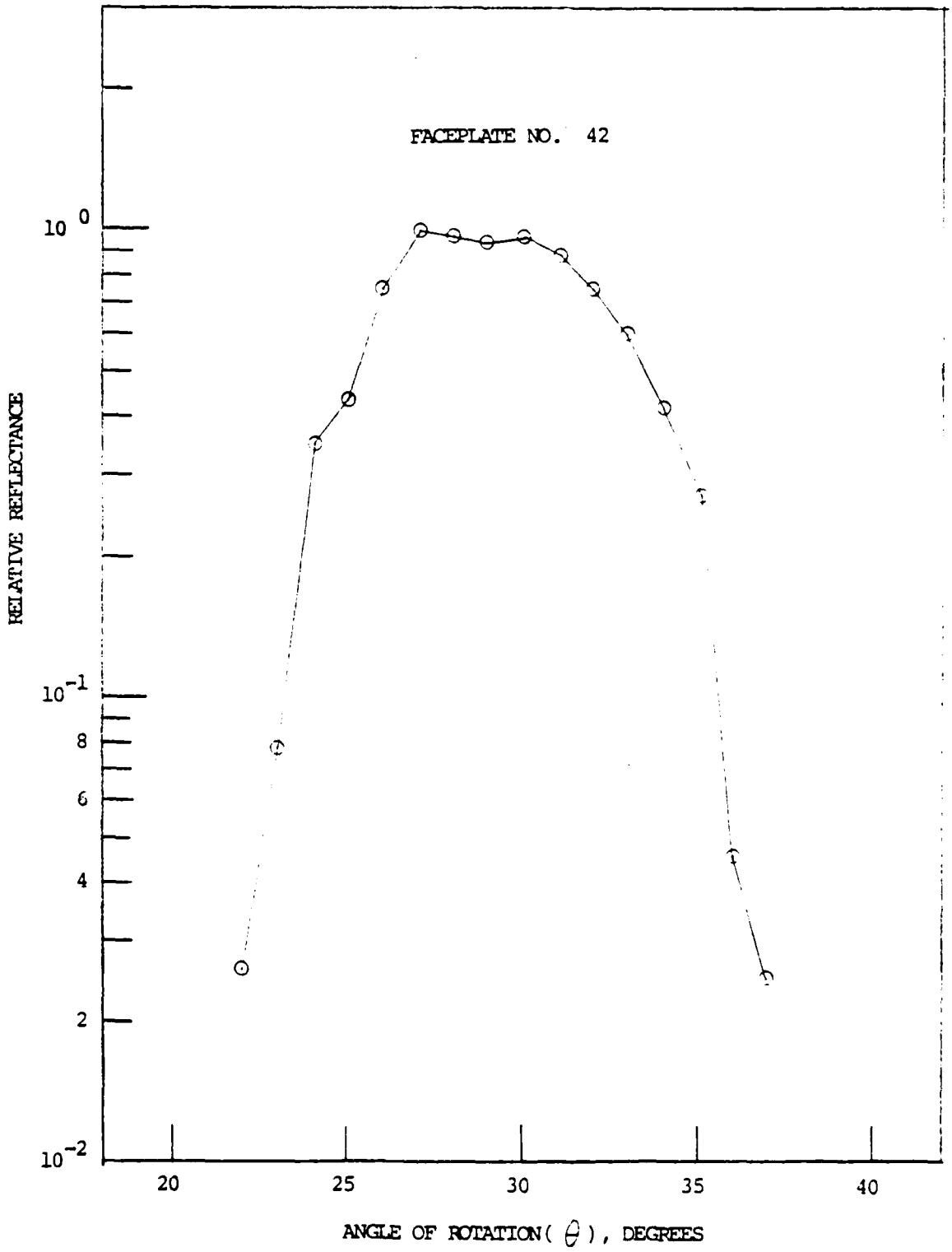

Fig. 34 Optical Reflectance, Faceplate No. 42

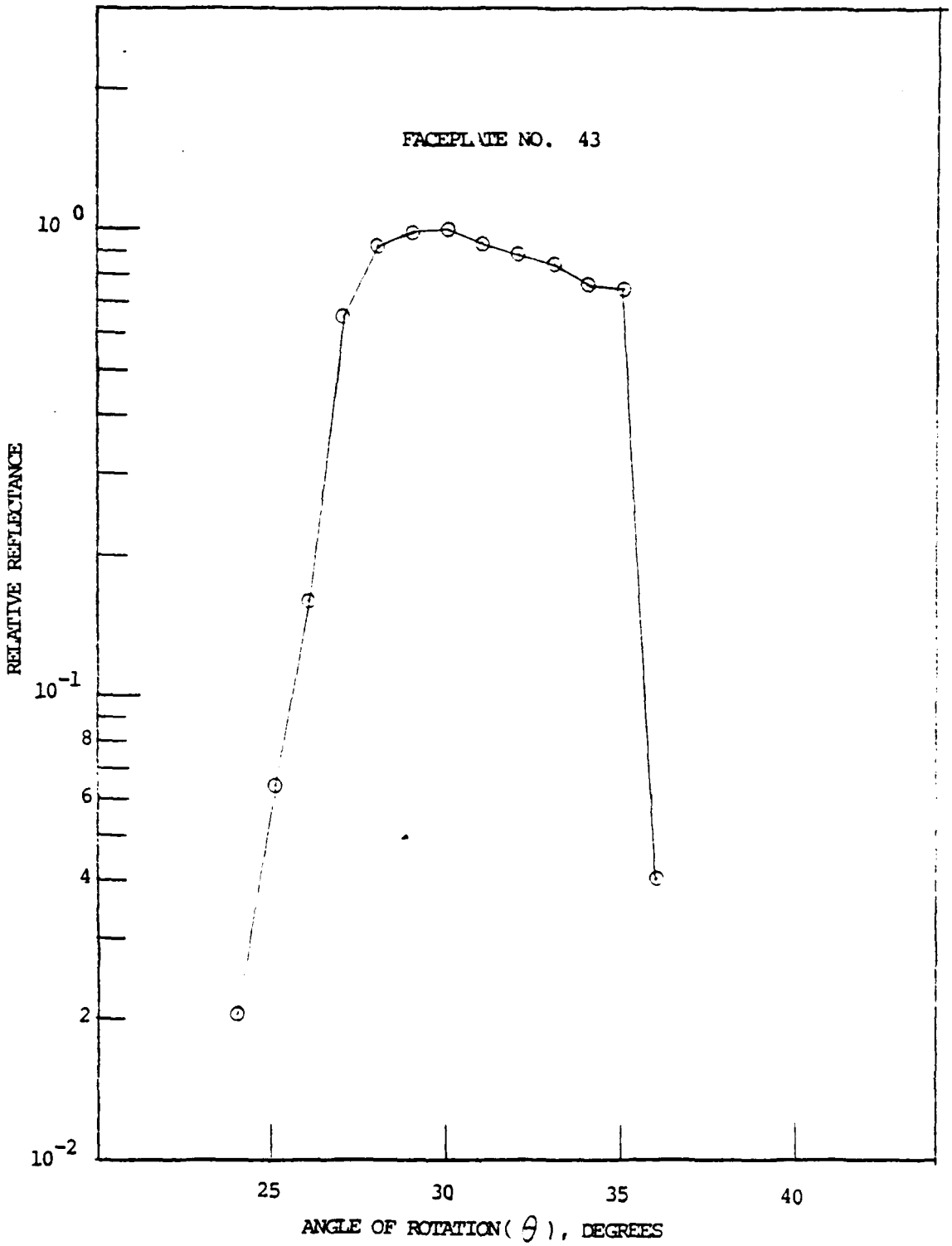

Fig. 35 Optical Reflectance, Faceplate No. 43

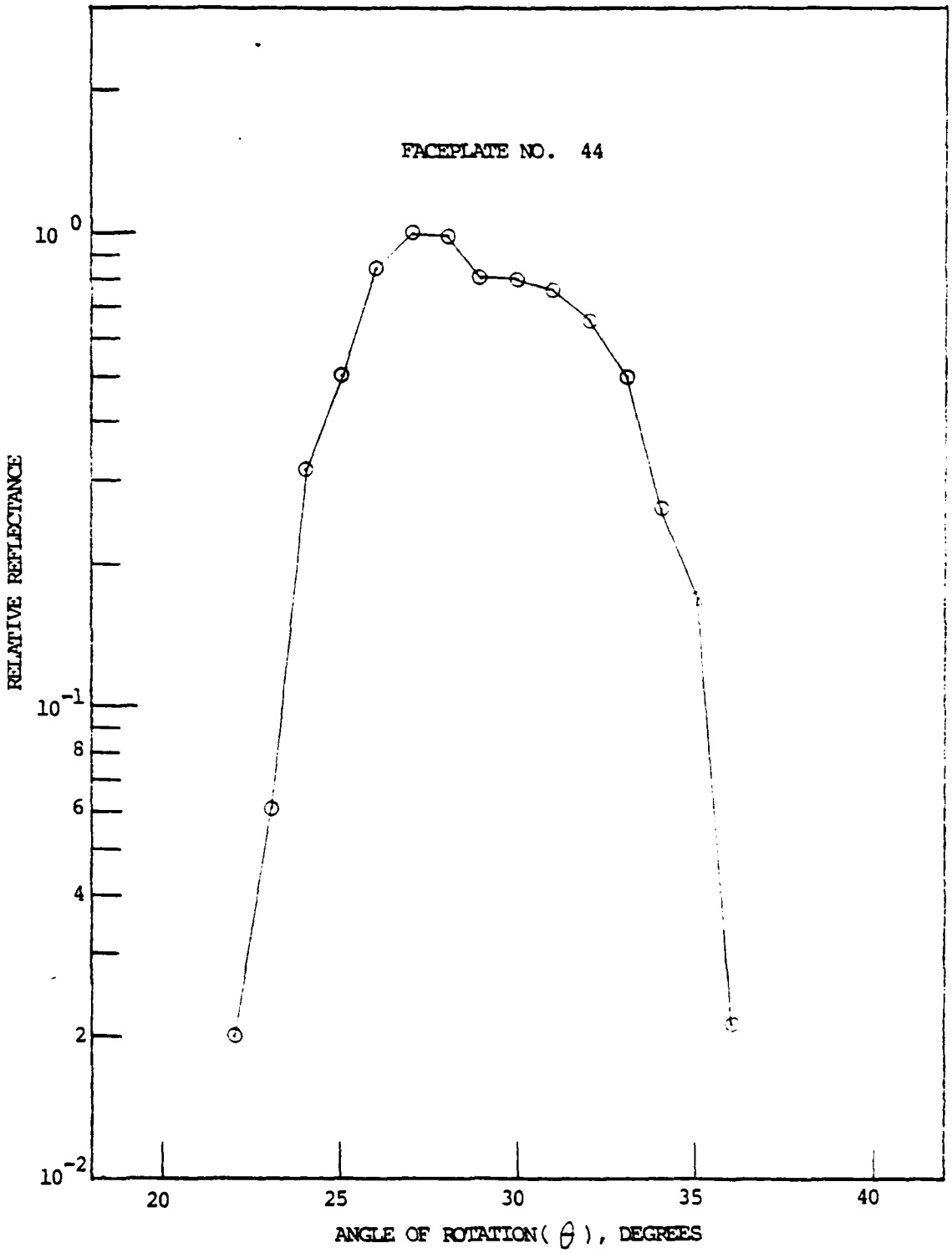

Fig. 36 Optical Reflectance, Faceplate No. 44

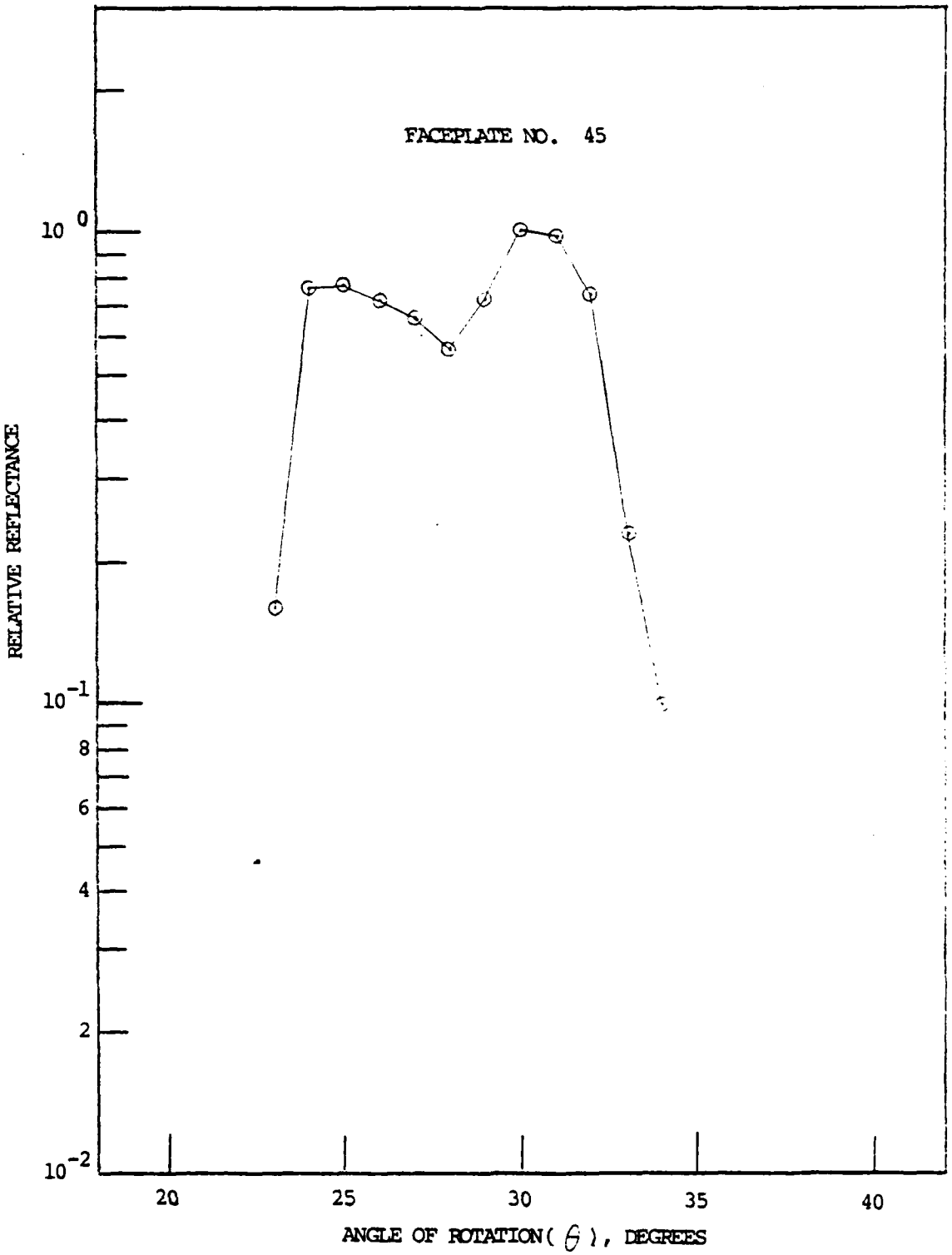

Fig. 37 Optical Reflectance, Faceplate No. 45

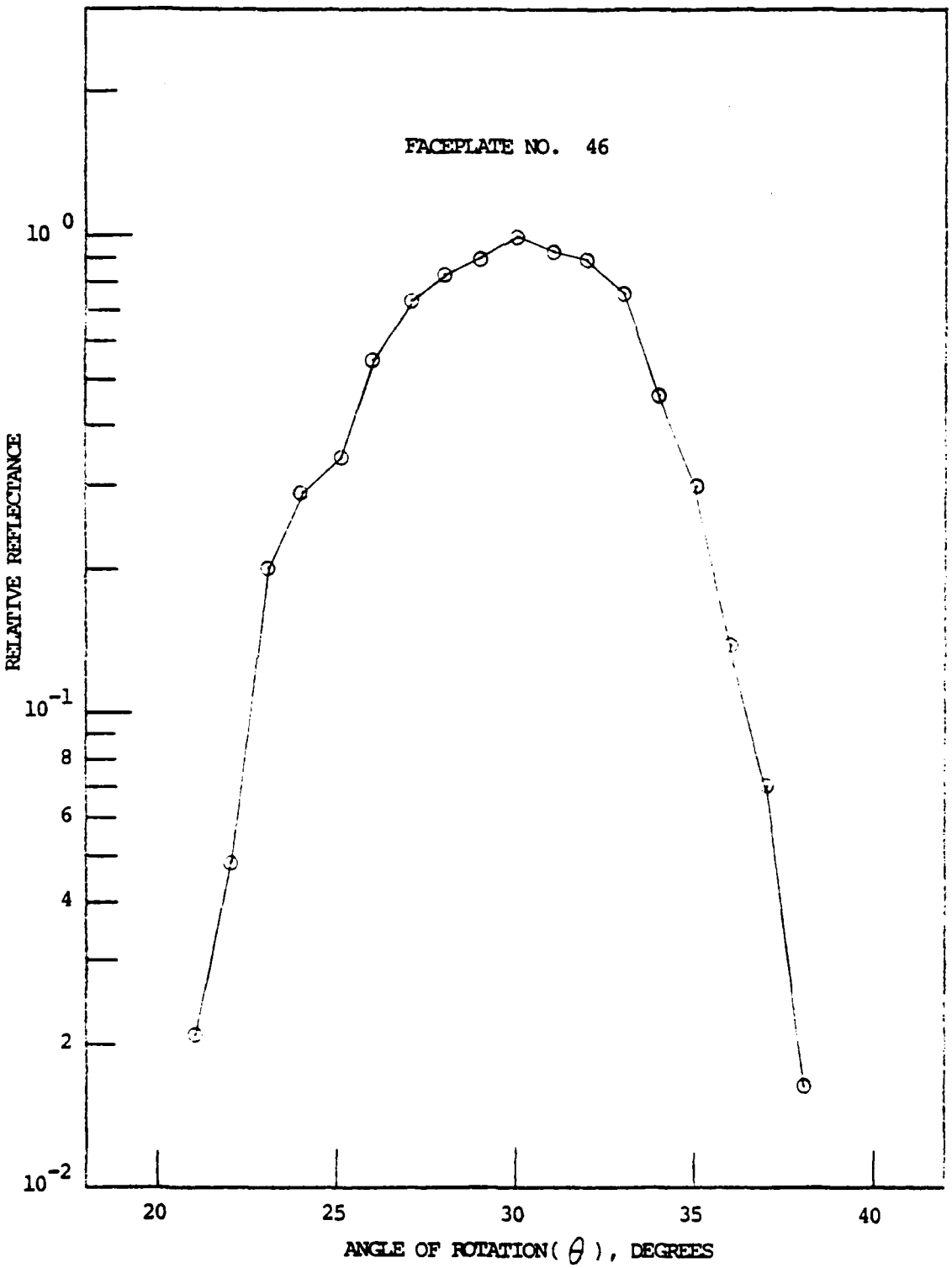

Fig. 38 Optical Reflectance, Faceplate No. 46

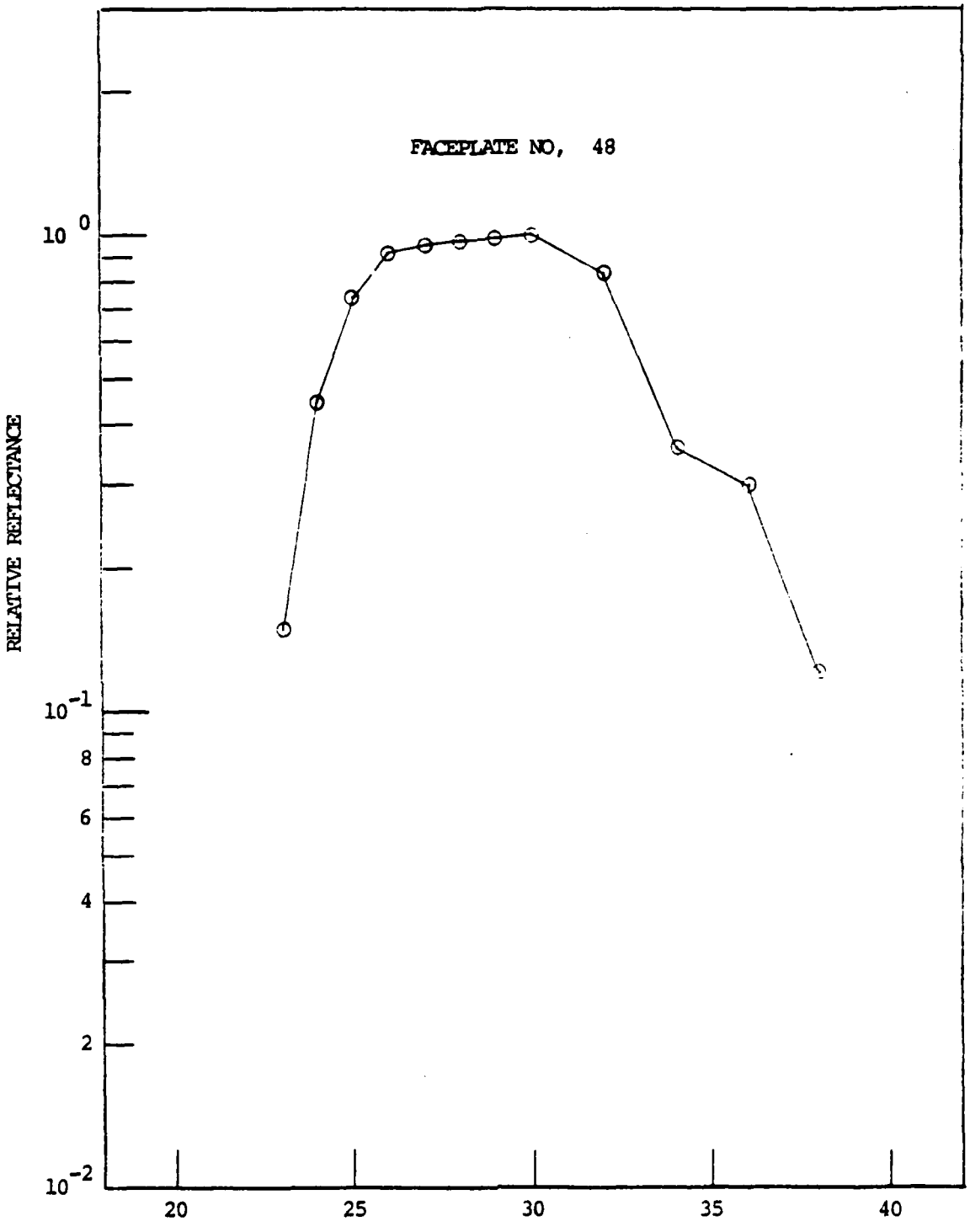

Fig. 39 Optical Reflectance, Faceplate No. 48

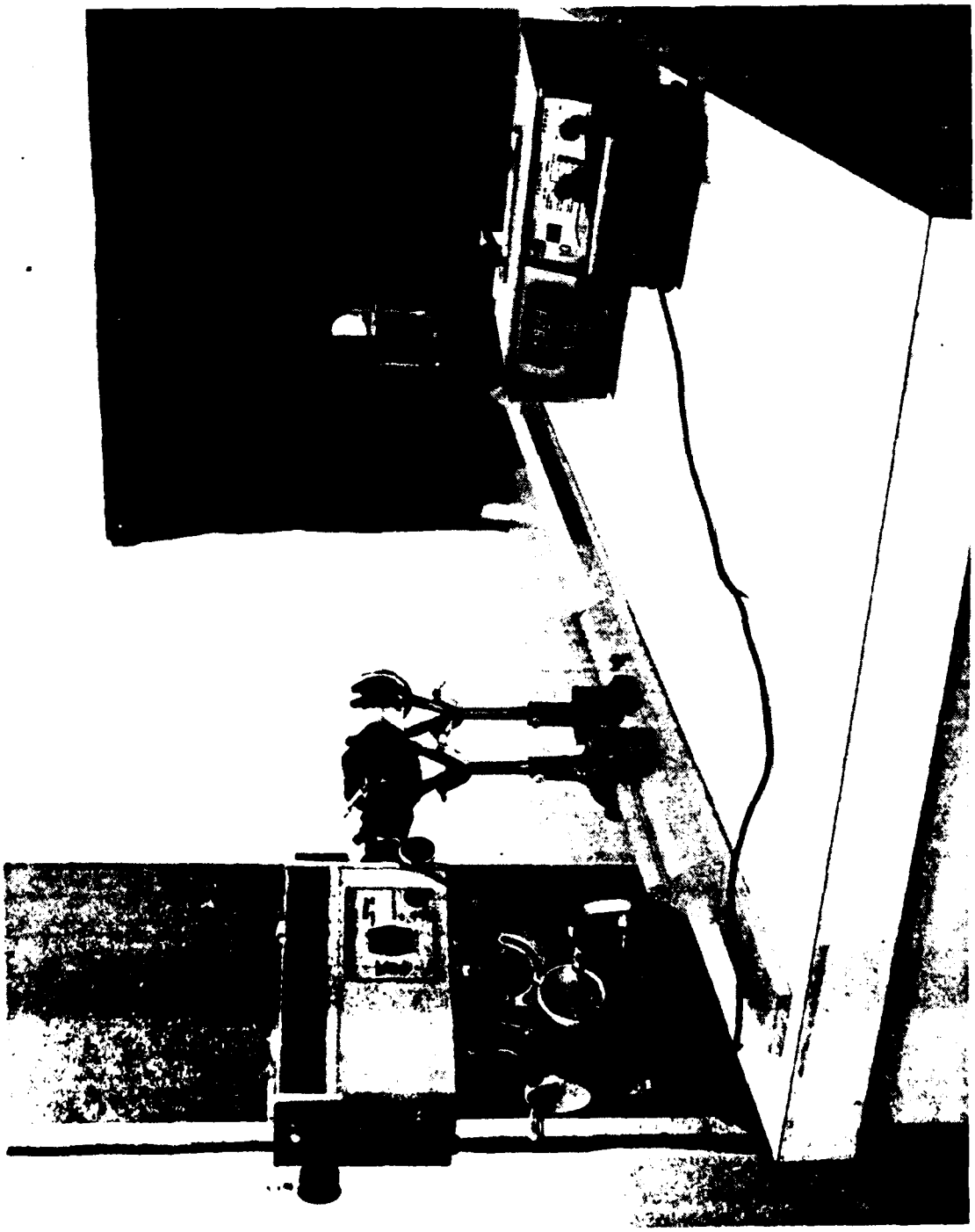

Fig. 40 Assembly for Optical Reflectance Measurement

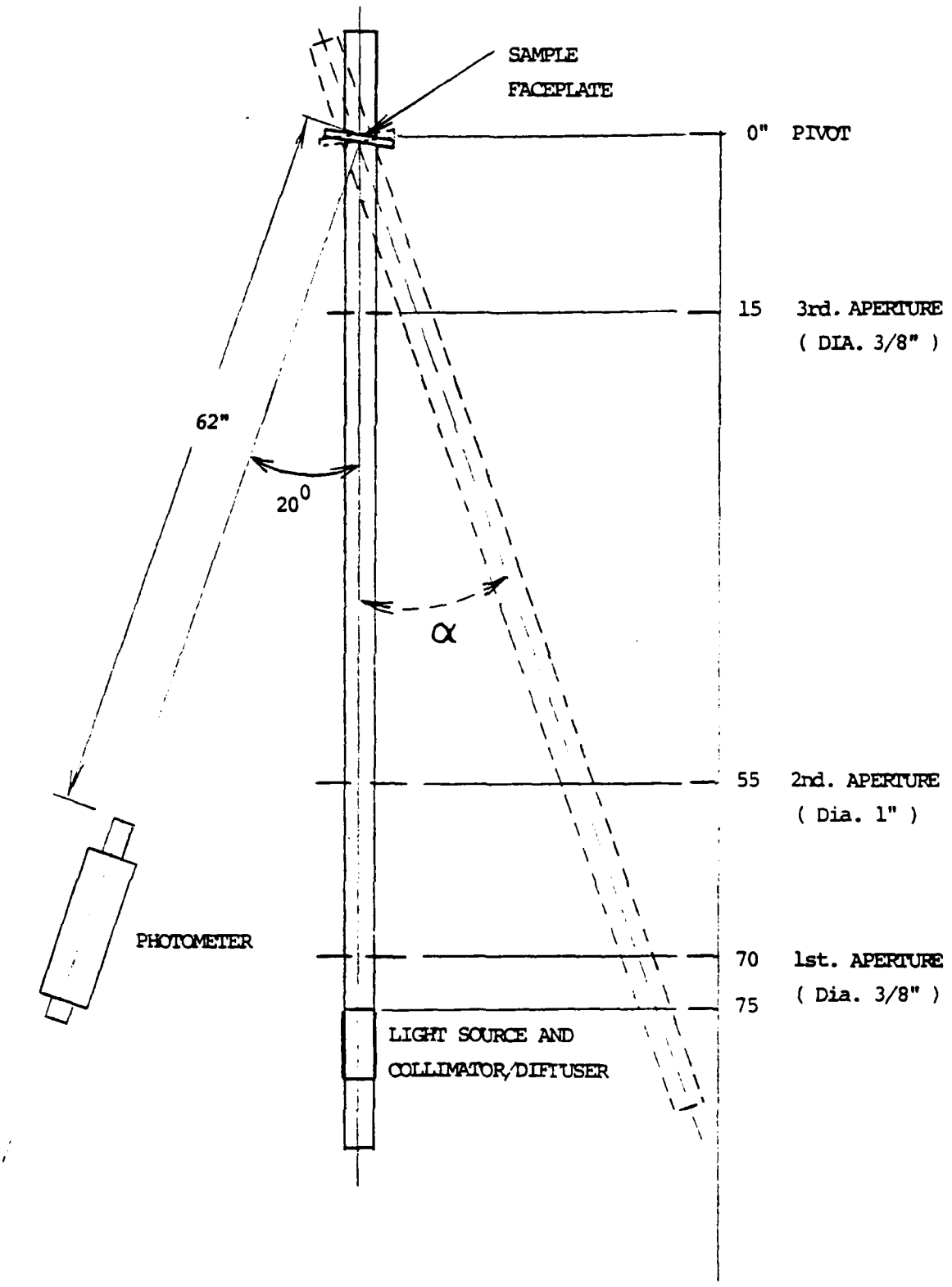

Fig. 41 Schematic of Reflectance Measurement

The light source is an Osram 8110 tungsten filament bulb operated with a voltage regulated variable transformer. The bulb is contained in a metal enclosure and convection-air cooled together with a lens made of frosted glass as the collimator. It was found necessary to use another Sola line voltage regulator in conjunction with the transformer to obtain long term ability of the light output. The light source was operated at about 6V and 4.2A and gave a luminance of 12,685 ft. L. at a distance of 132 inches. The light beam was restricted through a series of apertures to a 1/2 in. dia. circle near the center of the sample surface.

A Pritchard Model 1980A-PL photometer with the standard 7" objective lens was used to measure the brightness of the reflected light. The distance between the lens and the sample surface is 62 in., so with a 20-minute aperture, the field coverage is about 0.36 in., well within the 0.5 in. light beam on the sample surface.

The optical axes of the light source and photometer are initially separated by 20°. At the pivot point, a front surface mirror is first placed on the sample platform and so rotated as to give a maximum light brightness reading on the photometer monitor, indicating a specular reflection. The mirror is then replaced with the sample whose bidirectional reflectance is to be measured. This is carried out by rotating the source about the pivot through angle α equal to -2, -1, 0, 1, 2, 3, 4, 5, 10, 15, 20 and 30°. After this, the mirror is again put in place to check if there has been any significant change in the incident light intensity. When the change is within 1%, the experiment is continued for the next sample without further adjustment.

The results for faceplate Lot #2 are presented in Figures 44-52, and also summarized in Table 9. For comparison, measurements also made on an aluminum front surface mirror (92% reflectance at normal incidence) and on a magnesium carbonate block, an almost perfect diffuse reflector. Results for these are shown in Figures 42 and 43. Reflection from a planar diffuse reflecting surface follows Lambert's cosine law $I = I_o \cos \theta$ where θ is the angle between the direction of measurement and the normal to the surface, I_o is the incident intensity and I is the reflected intensity (Ref. 17).

Table 9

Reflectance of Faceplates, Lot #2

In Percentage

Faceplate No.	Angular Displacement from Specular Angle						
	0	1	3	5	10	15	30
Mirror	9.20×10^{1}	2.23×10^{0}	4.28×10^{-3}	2.17×10^{-3}	8.12×10^{-4}	4.16×10^{-4}	4.71×10^{-5}
52	6.07×10^{0}	1.50×10^{-1}	2.48×10^{-3}	3.05×10^{-4}	1.84×10^{-4}	1.51×10^{-4}	4.02×10^{-5}
53	6.40×10^{0}	5.78×10^{-1}	2.03×10^{-3}	1.93×10^{-3}	1.70×10^{-3}	1.37×10^{-3}	2.80×10^{-4}
54	5.36×10^{0}	1.15×10^{-1}	2.29×10^{-3}	9.22×10^{-4}	7.00×10^{-4}	5.23×10^{-4}	9.85×10^{-5}
55	4.87×10^{0}	3.94×10^{-1}	7.39×10^{-4}	6.03×10^{-4}	5.33×10^{-4}	4.51×10^{-4}	8.67×10^{-5}
56	6.74×10^{0}	2.48×10^{-1}	1.01×10^{-3}	8.20×10^{-4}	7.02×10^{-4}	5.94×10^{-4}	1.15×10^{-4}
58	5.10×10^{0}	1.73×10^{-1}	7.96×10^{-4}	7.57×10^{-4}	6.35×10^{-4}	4.94×10^{-4}	1.20×10^{-4}
59	5.45×10^{0}	7.89×10^{-1}	2.90×10^{-3}	2.22×10^{-3}	1.75×10^{-3}	1.31×10^{-3}	1.82×10^{-4}
60	6.86×10^{0}	4.83×10^{-1}	5.68×10^{-4}	4.89×10^{-4}	4.21×10^{-4}	2.66×10^{-4}	5.80×10^{-5}
62	5.75×10^{0}	1.47×10^{-1}	6.40×10^{-4}	5.63×10^{-4}	4.60×10^{-4}	3.86×10^{-4}	1.13×10^{-4}
$MgCO_3$ Block	1.68×10^{-4}	-	-	1.63×10^{-4}	1.58×10^{-4}	1.53×10^{-4}	1.29×10^{-4}

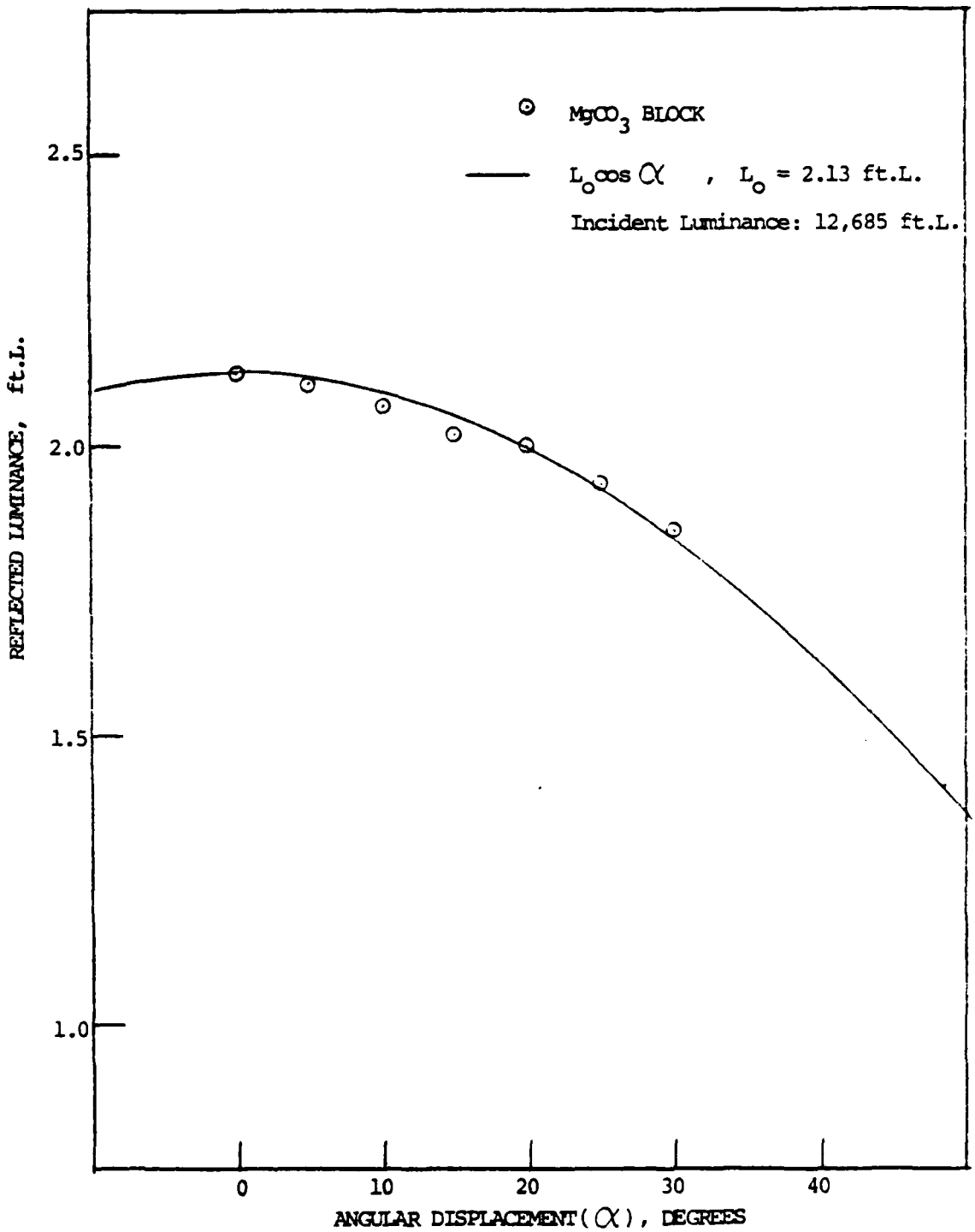

Fig. 42 Reflectance of $MgCO_3$

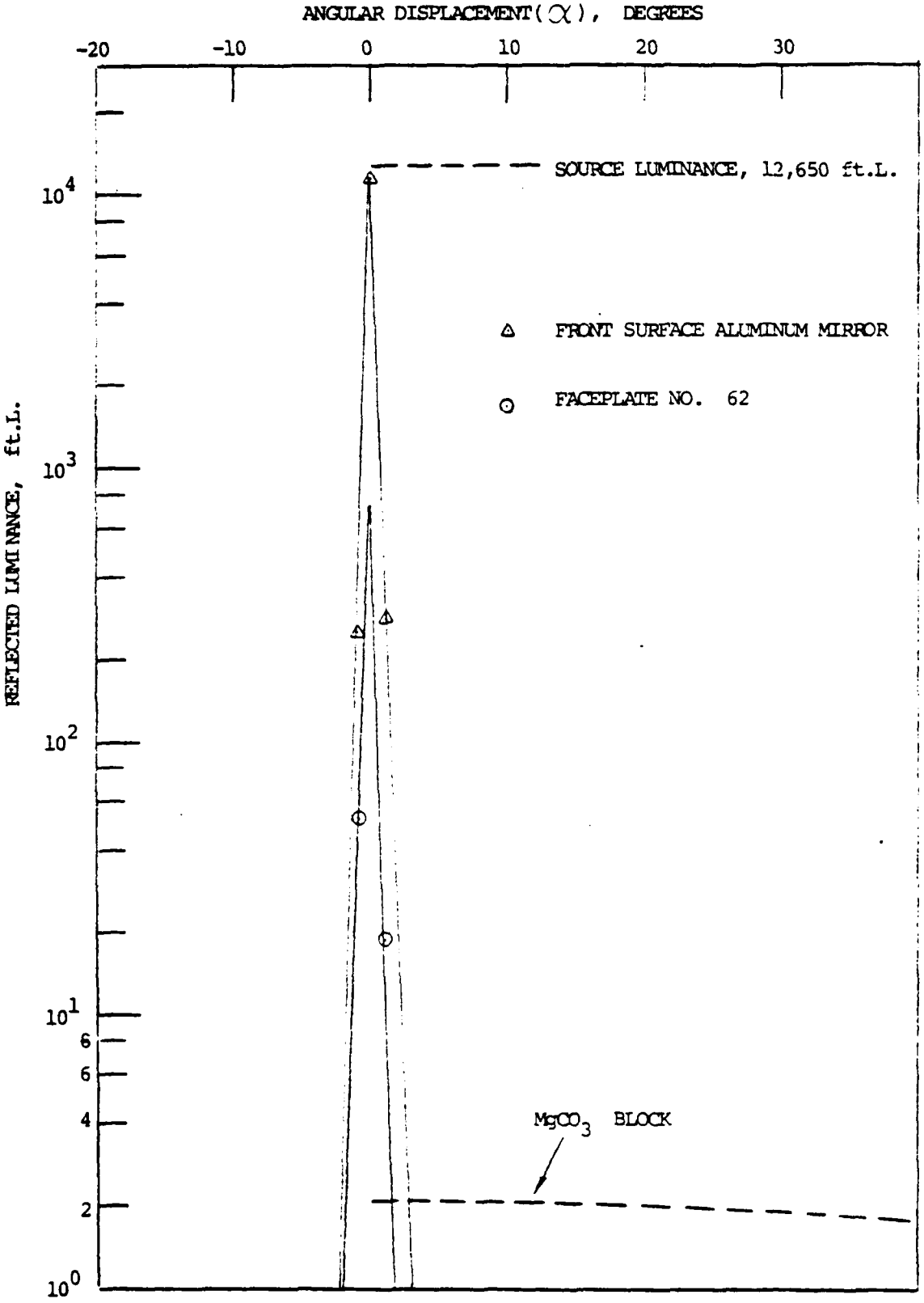

Fig. 43 (Upper) Reflected Luminance - $MgCO_3$, Mirror and Faceplate No. 62

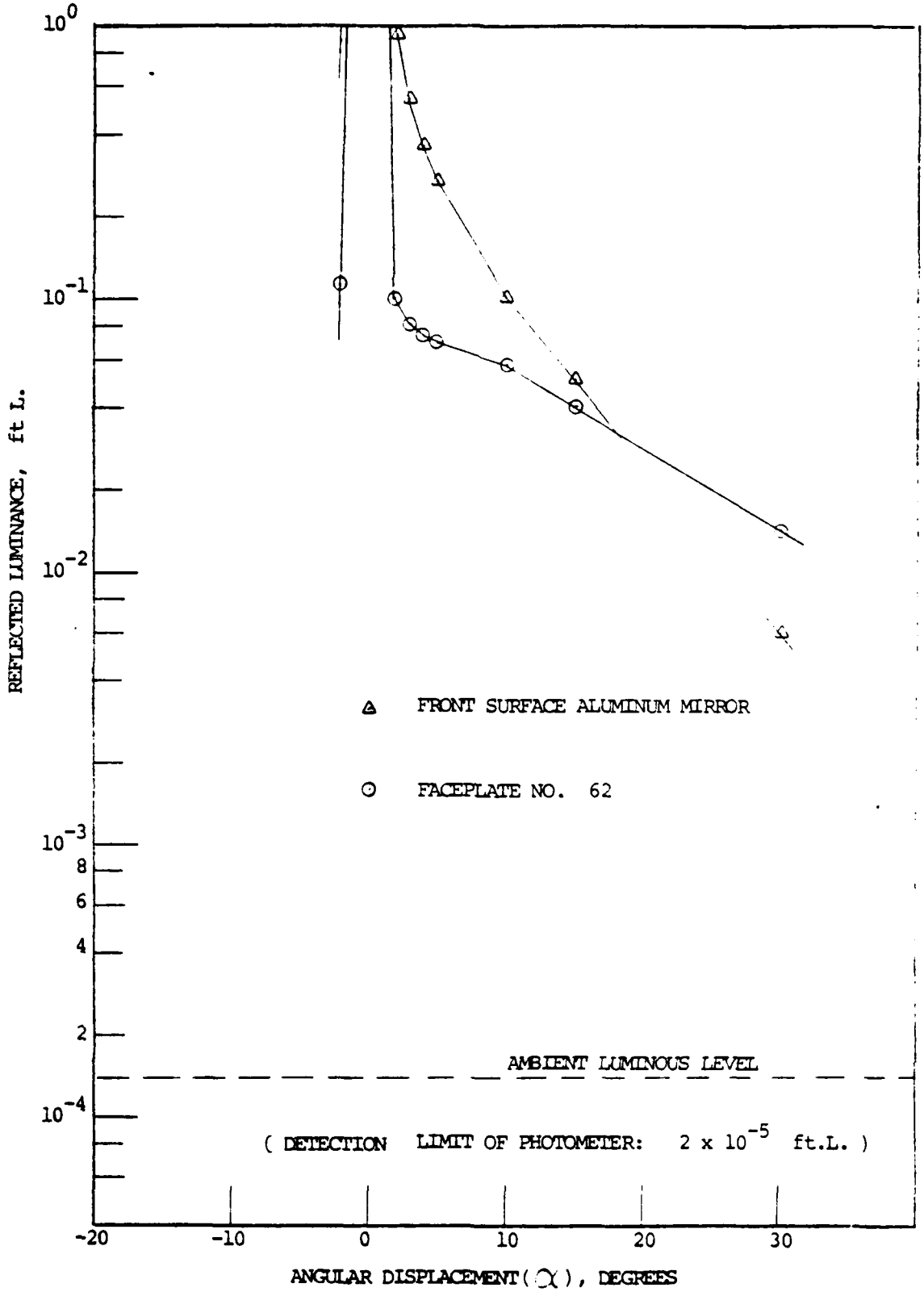
REFLECTED LUMINANCE, ft L.
10^0
10^{-1}
10^{-2}
10^{-3}
8
6
4
2
10^{-4}
FRONT SURFACE ALUMINUM MIRROR
FACEPLATE NO. 62
AMBIENT LUMINOUS LEVEL
(DETECTION LIMIT OF PHOTOMETER: 2×10^{-5} ft.L.)
-20
-10
0
10
20
30
ANGULAR DISPLACEMENT(α), DEGREES

Fig. 43 (Lower)

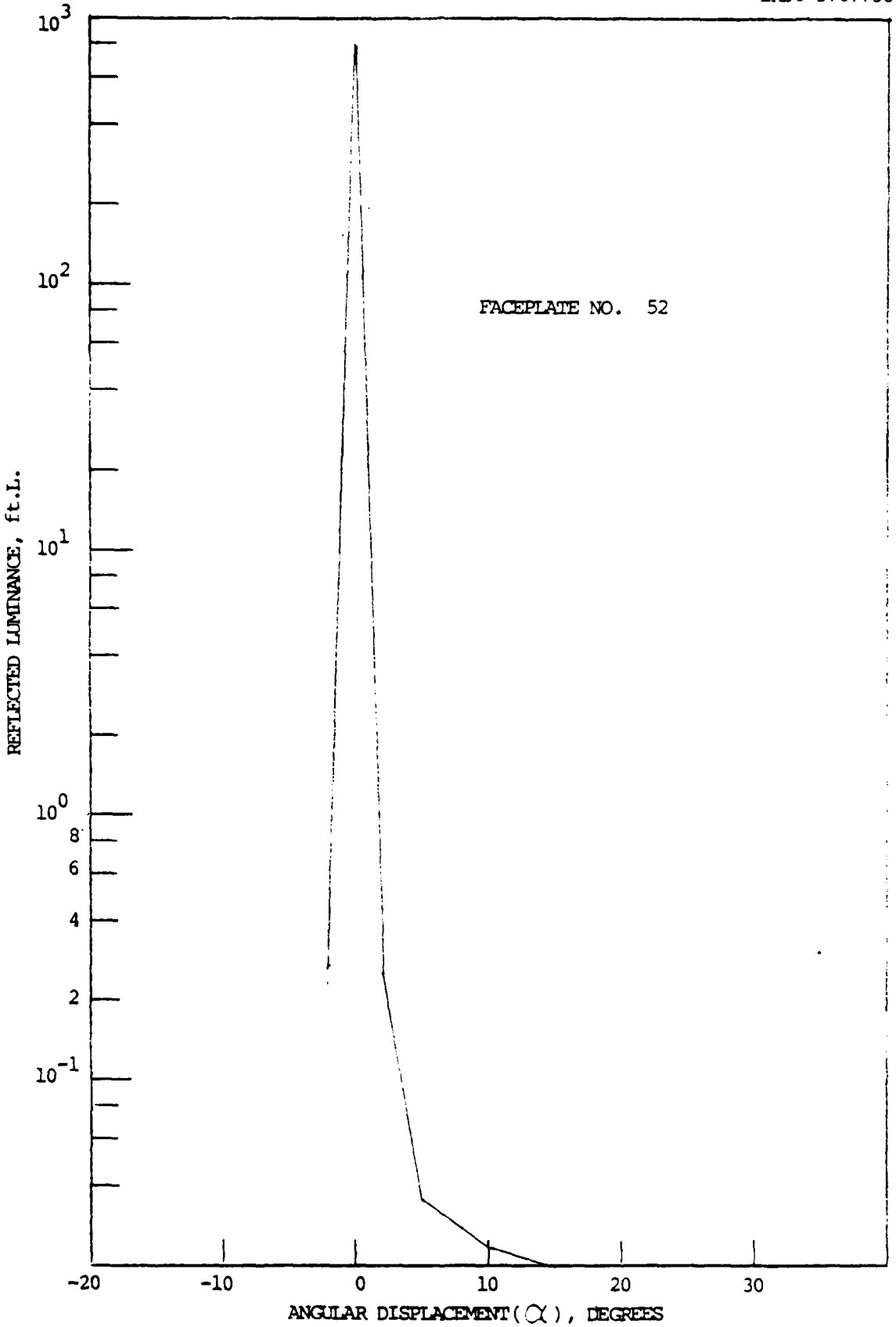

Fig. 45 Reflected Luminance, Faceplate No. 52

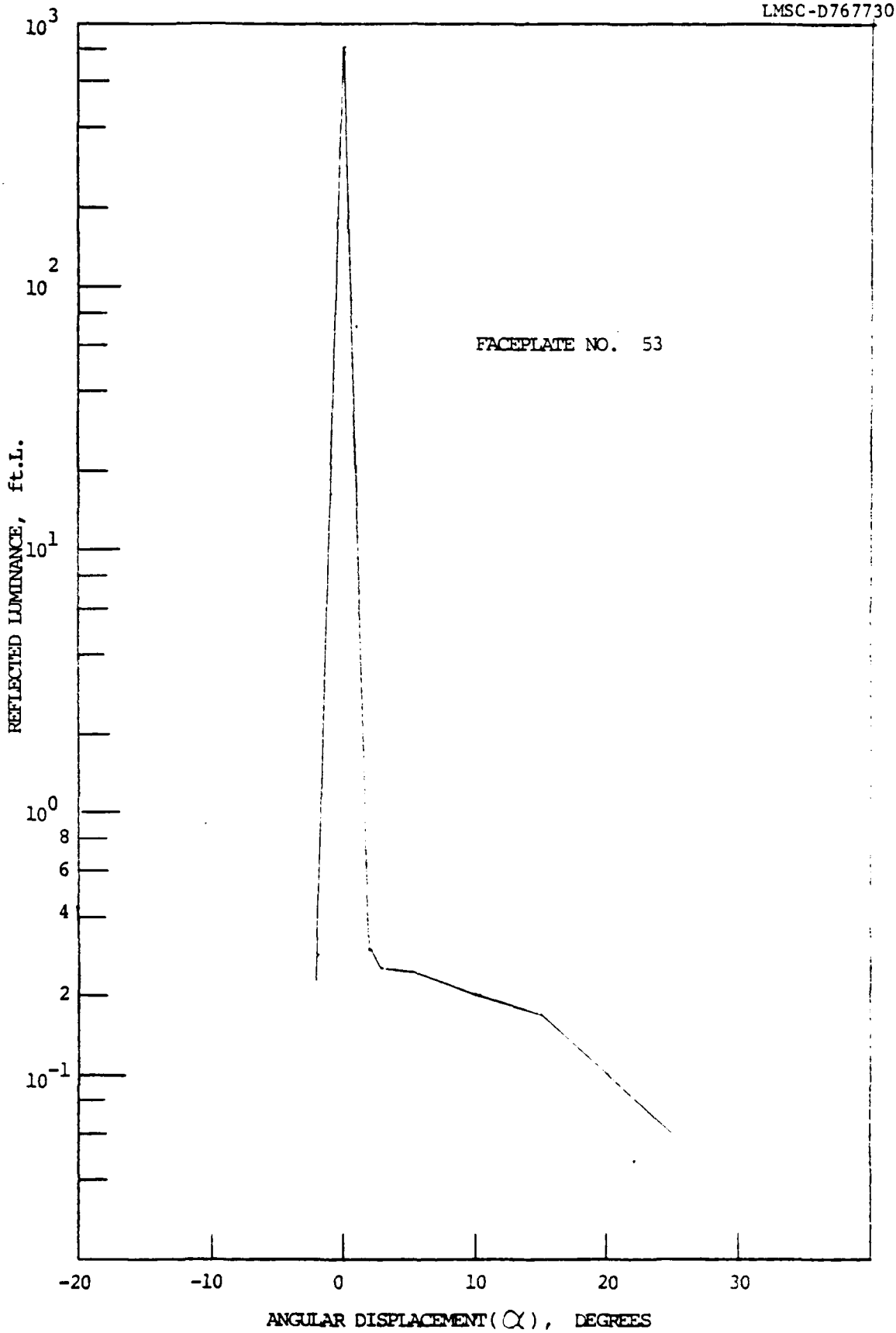

Fig. 46 Reflected Luminance, Faceplate No. 53

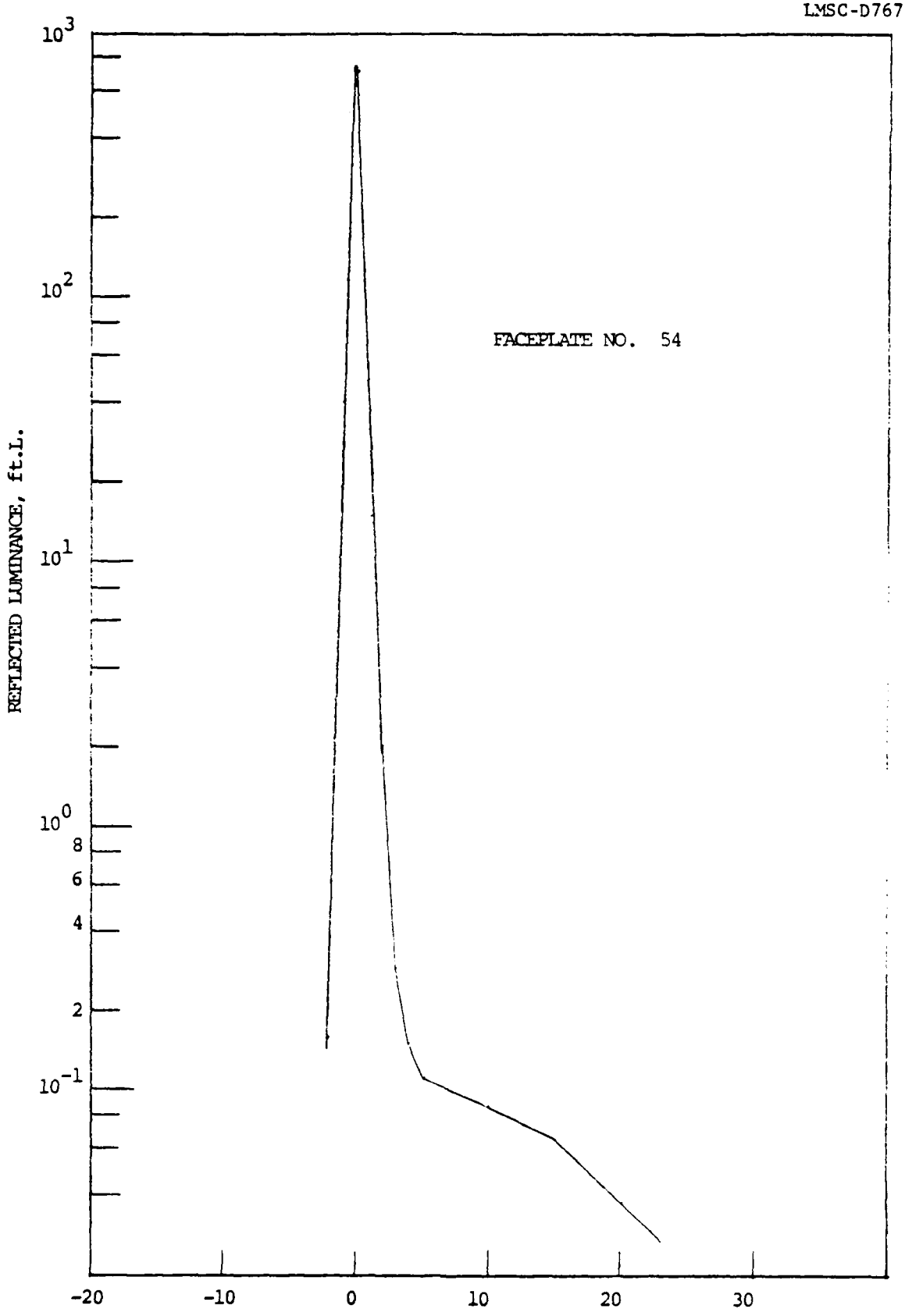

Fig. 47 Reflected Luminance, Faceplate No. 54

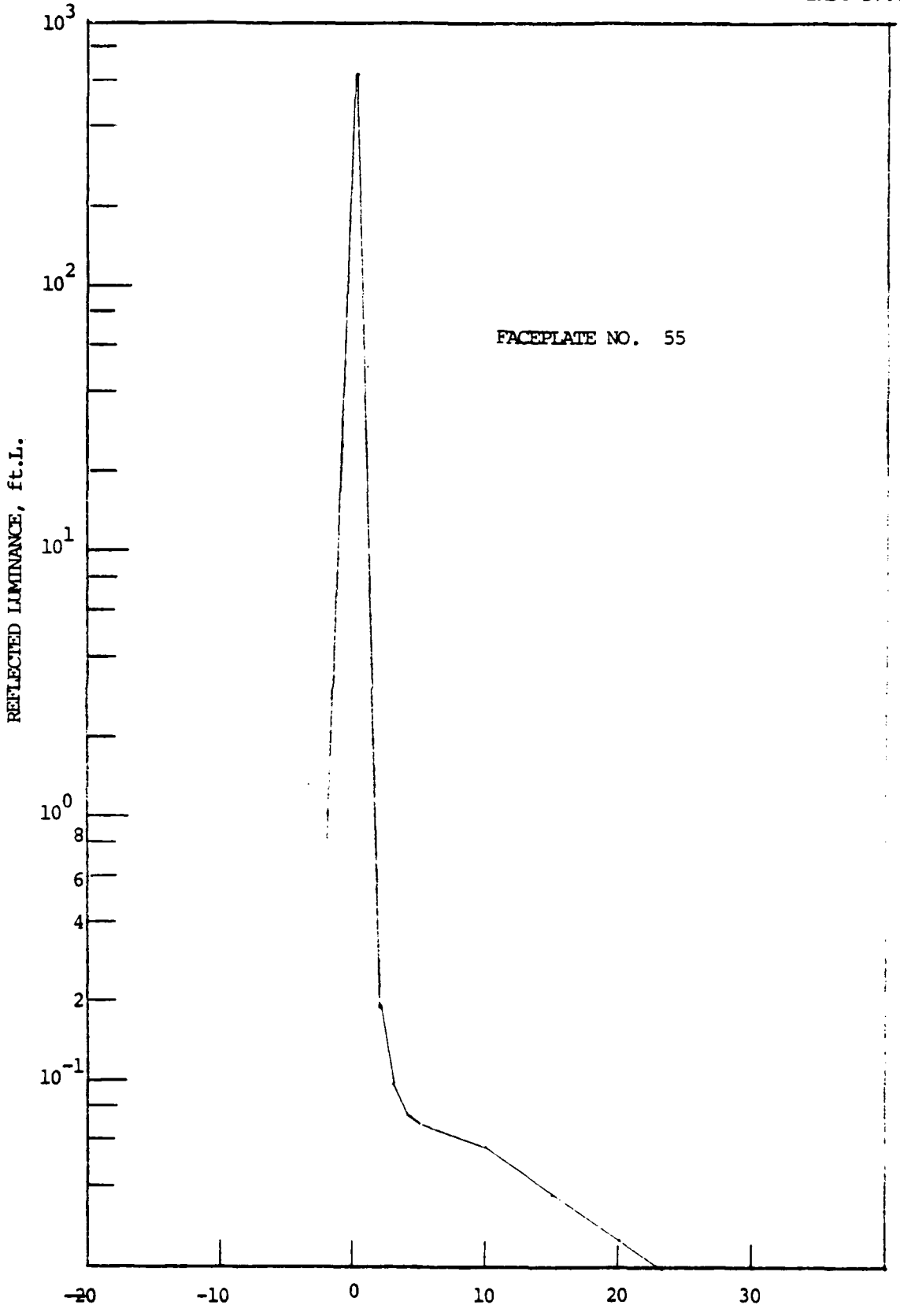

Fig. 48 Reflected Luminance, Faceplate No. 55

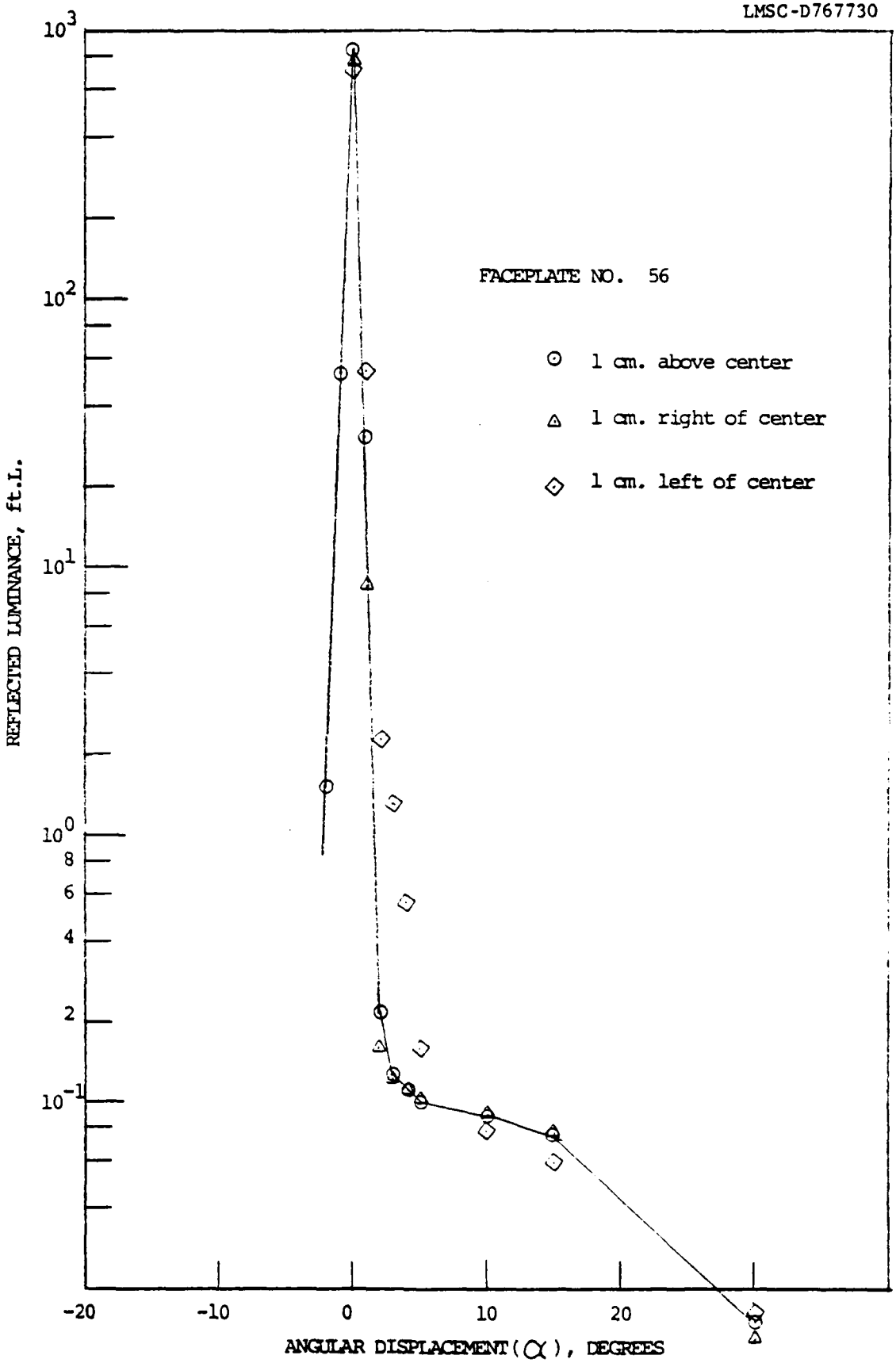

Fig. 49 Reflected Luminance, Faceplate No. 56

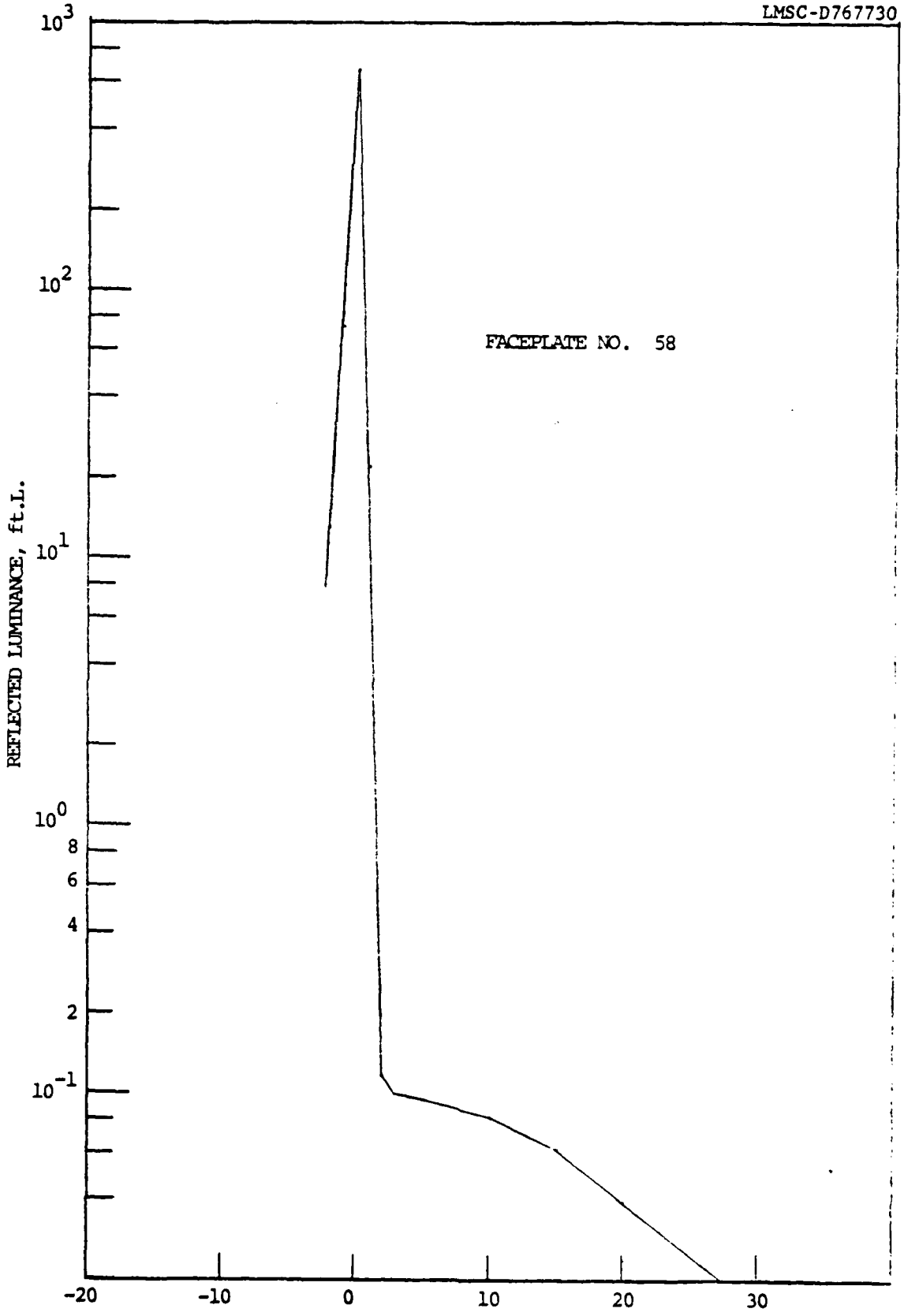

Fig. 50 Reflected Luminance, Faceplate No. 58

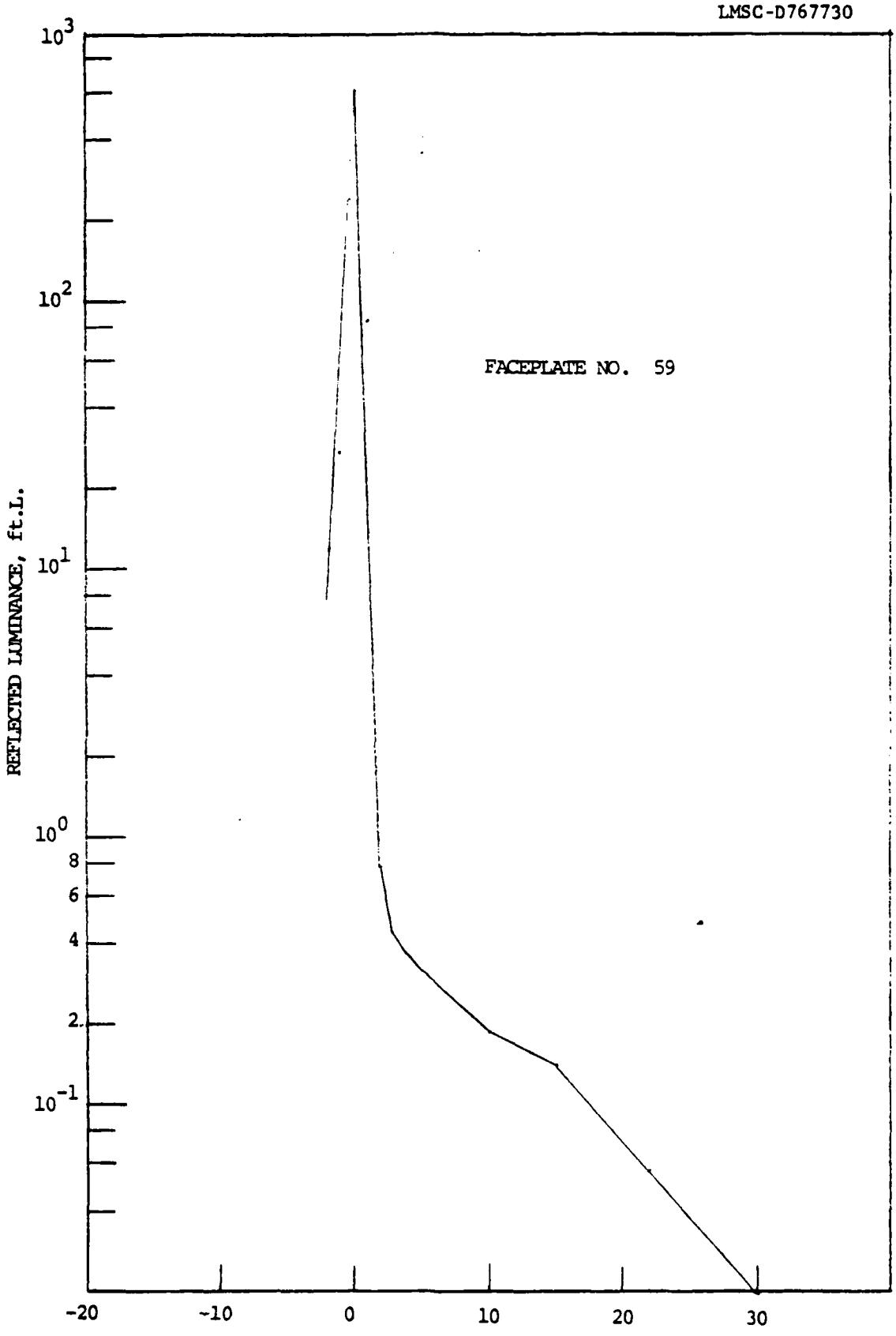

Fig. 51 Reflected Luminance, Faceplate No. 59

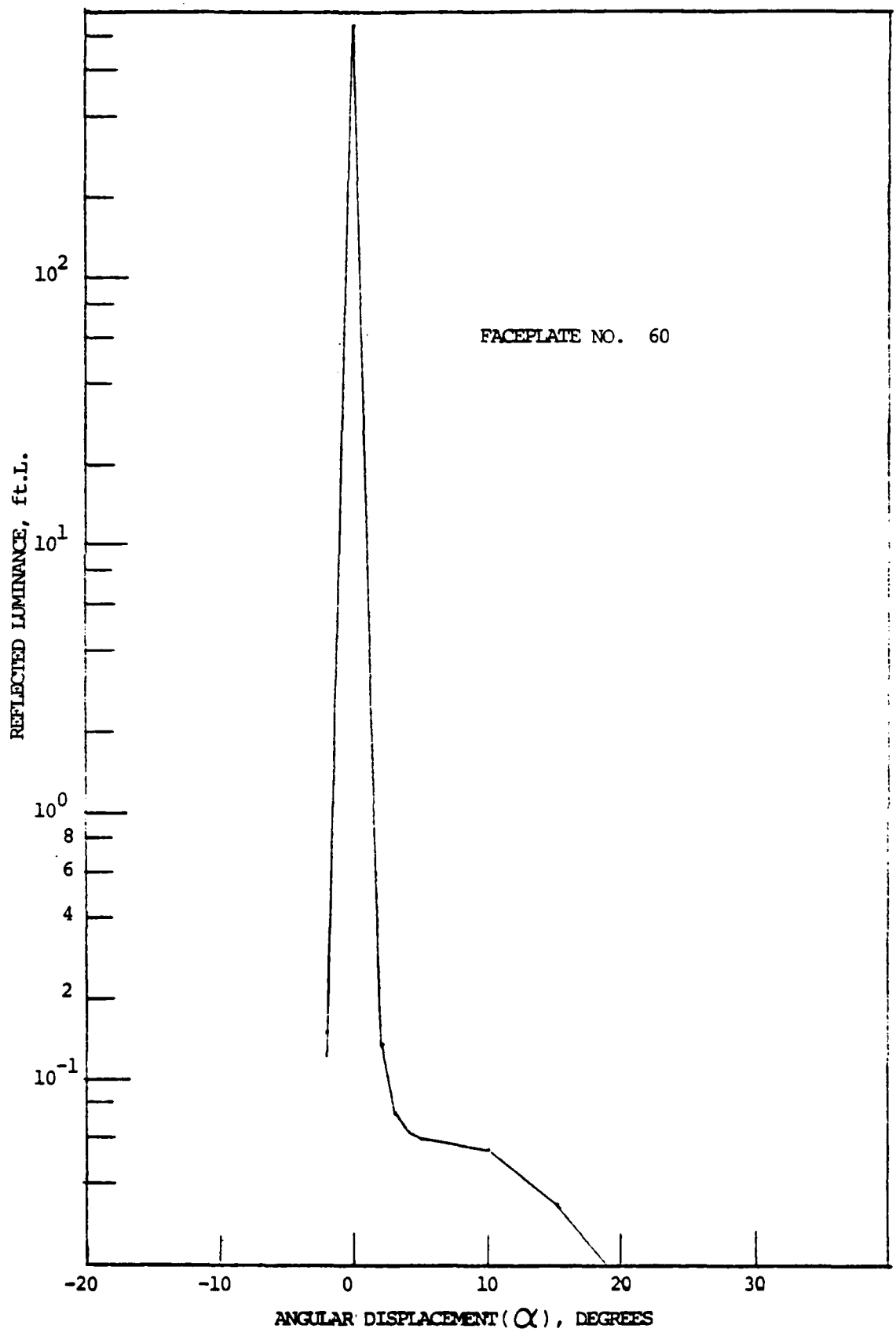

Fig. 52 Reflected Luminance, Faceplate No. 60

The figure for the faceplates are characterized by a sharp specular peak at the normal incidence angle (0 deg) and a tail evident at angles of 5 degrees and lower which is about four orders below the specular peak. Comparison with the figure for the $MgCO_3$ black indicates the tails on the faceplate plots are due to diffuse reflection.

4.5.3 Lot #3

The optical reflectances of the faceplates of Lot #3 were measured with the test assembly previously described for Lot #2. The results are shown in Figures 55 through 62. The plots are similar to those previously obtained for Lot #2. The measurements are summarized in Table 10.

4.6 Black Back Film Thickness

The black back film used in this program is a vanadium-based absorbing inhomogeneous film fabricated as described in U.S. Pat. No. 4,132,919. The method is based on RF sputtering, using a vanadium metal target and an argon atmosphere initially containing sufficient oxygen to produce an initial deposit of vanadium pentoxide. After deposition is started, the oxygen pressure is gradually reduced to zero. The result is a film which varies in composition from V_2O_5 at the phosphor surface to vanadium metal in the final stage of deposition. The oxygen pressure is controlled by the setting of a micrometer valve.

The schedule which was originally used to produce the film is shown in Table 11(a). It was found that films made according to the original schedule had thicknesses of about 2600 to 2900Å, and frequently exhibited a slight transmission, rather than being completely opaque. It appeared desirable to increase the thickness of the metal portion of the film; this would insure complete opacity and might also eliminate or at least minimize any change in optical properties of the film that might occur during exposure to the elevated temperatures of the glass sealing step in assembling the CRT.

The modified schedule shown in Table 11(b) was therefore adopted. The oxide portion of the schedule was reduced and the metal portion increased. Samples of films produced according to each schedule were submitted to ERADCOM for Auger analysis as part of the study to determine factors responsible for

Table 10

Reflectance of Faceplates, Lot #3

In Percentage

Faceplate No.	Angular Displacement from Specular Angle						
	0	1	3	5	10	15	30
66	6.26	1.43×10^{-1}	4.93×10^{-3}	4.05×10^{-3}	2.78×10^{-3}	2.26×10^{-3}	6.36×10^{-4}
67	6.20	1.10	7.48×10^{-4}	3.54×10^{-4}	2.48×10^{-4}	2.12×10^{-4}	6.29×10^{-5}
68	6.36	3.09	1.08×10^{-3}	7.72×10^{-6}	5.90×10^{-4}	4.45×10^{-4}	7.08×10^{-5}
69	7.03	3.43	1.43×10^{-3}	9.76×10^{-4}	7.09×10^{-4}	4.92×10^{-4}	6.20×10^{-5}
70	6.76	3.04	1.56×10^{-3}	9.61×10^{-4}	6.82×10^{-4}	4.10×10^{-4}	4.65×10^{-5}
71	7.58	1.78	1.55×10^{-3}	5.97×10^{-4}	2.83×10^{-4}	2.13×10^{-4}	5.04×10^{-5}
72	8.68	3.15	1.74×10^{-3}	9.73×10^{-4}	6.24×10^{-4}	4.18×10^{-4}	4.67×10^{-5}
73	8.91	3.46	4.53×10^{-3}	6.70×10^{-4}	3.89×10^{-4}	2.47×10^{-4}	3.88×10^{-5}
74	6.88	1.55	8.13×10^{-4}	4.22×10^{-4}	2.40×10^{-4}	1.82×10^{-4}	8.14×10^{-5}
64	5.38	1.10	1.12×10^{-3}	8.82×10^{-4}	7.61×10^{-4}	6.51×10^{-4}	1.25×10^{-4}

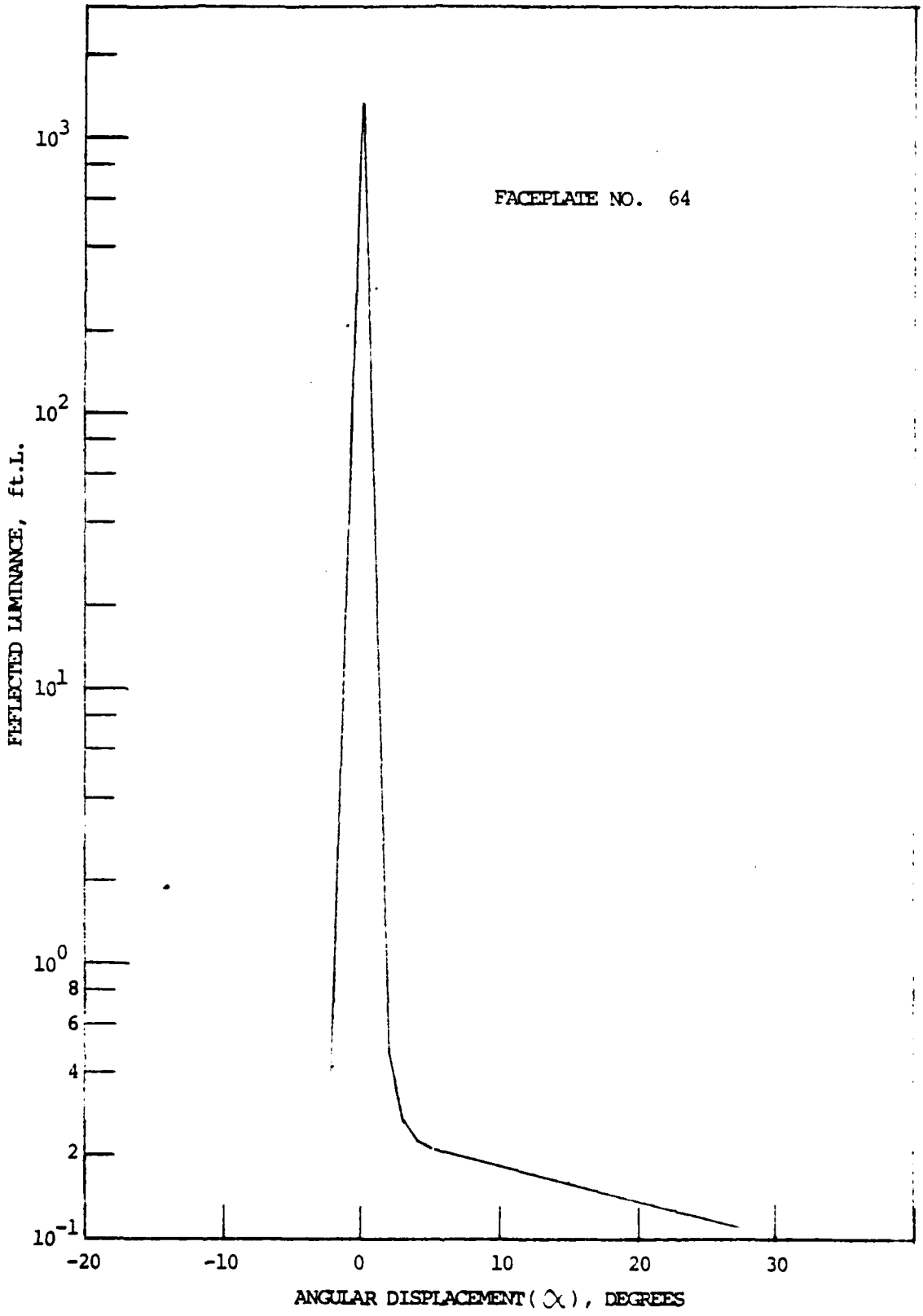

Fig. 53 Reflected Luminance, Faceplate No. 64

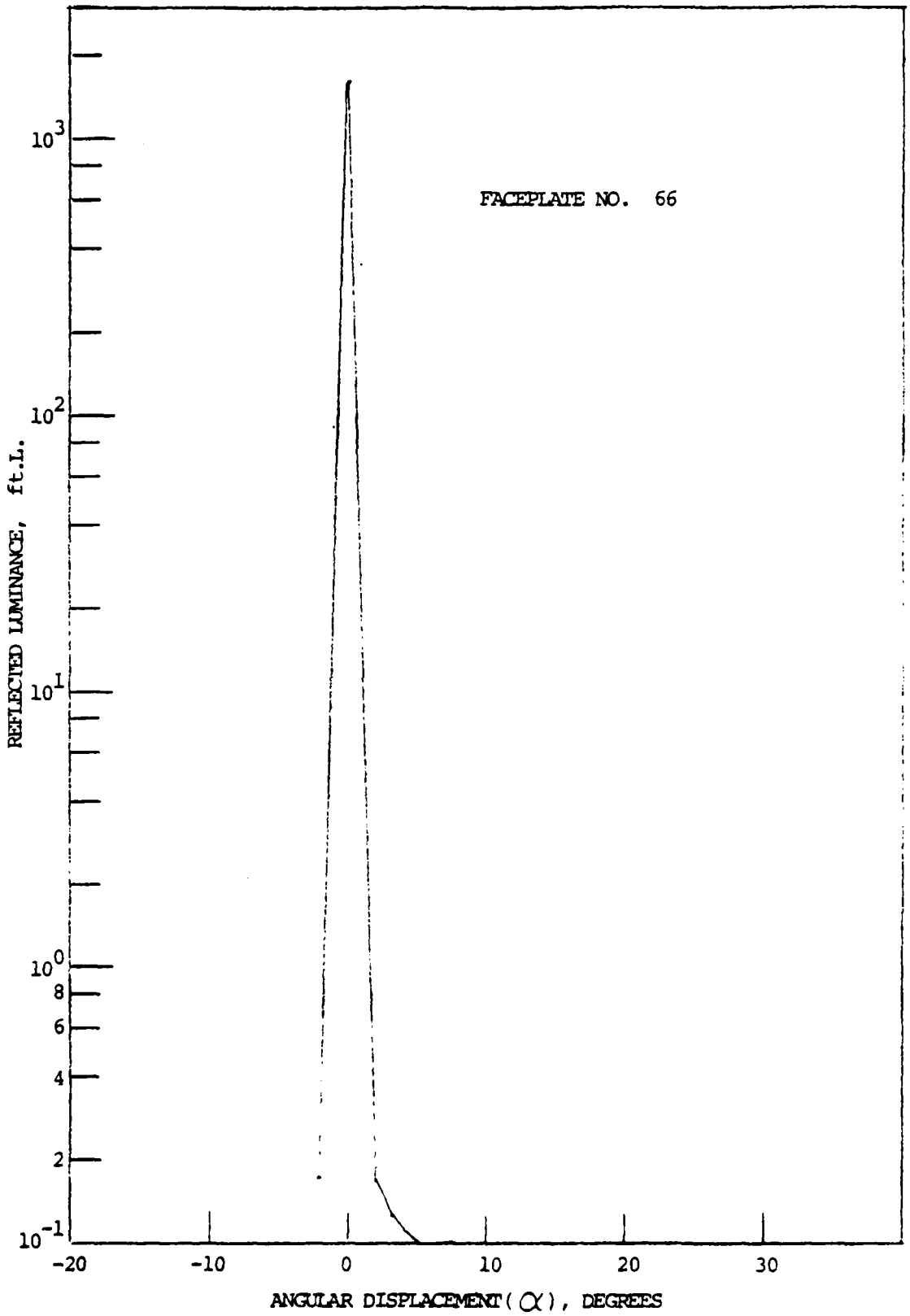

Fig. 54 Reflected Luminance, Faceplate No. 66

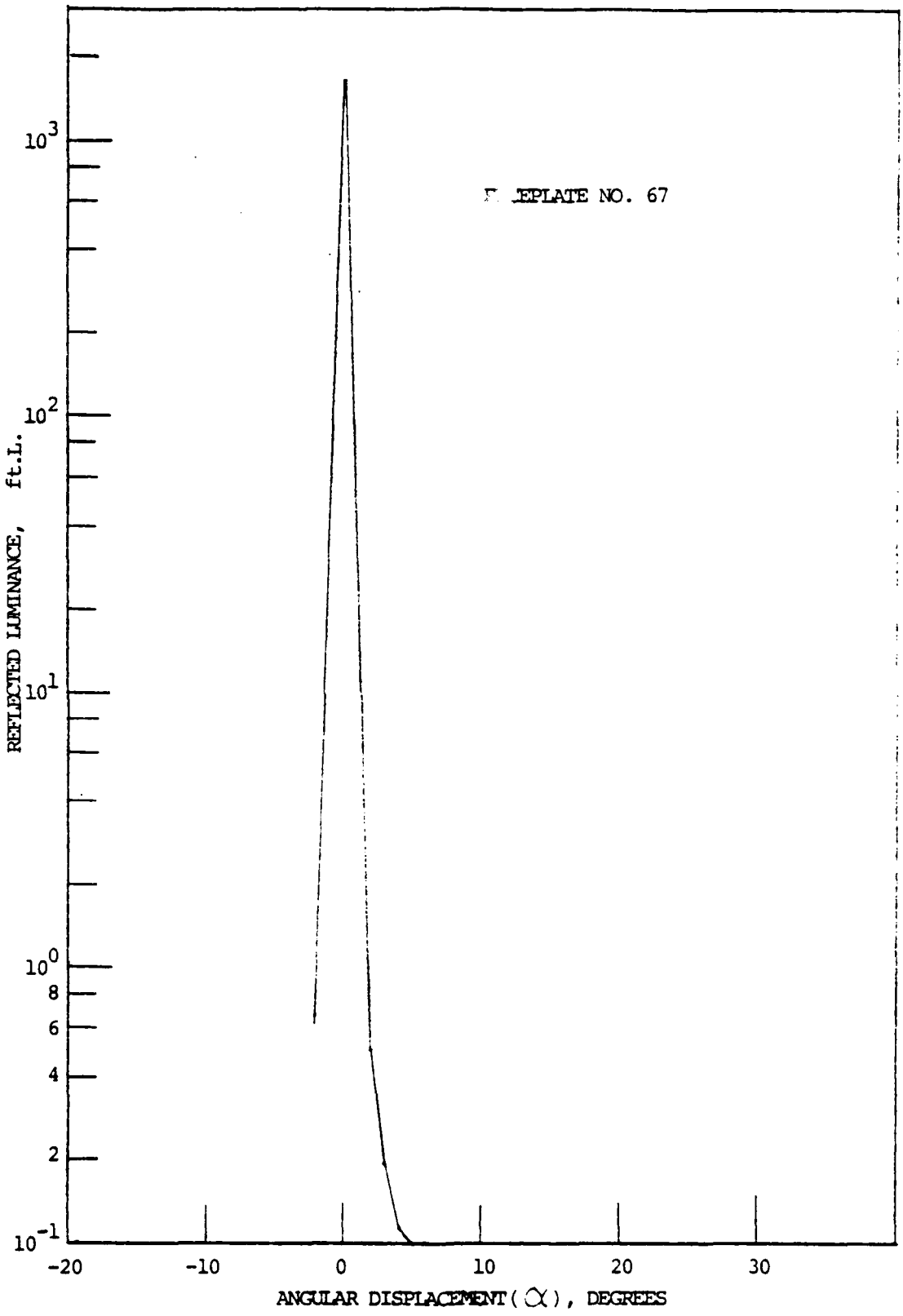

Fig. 55 Reflected Luminance, Faceplate No. 67

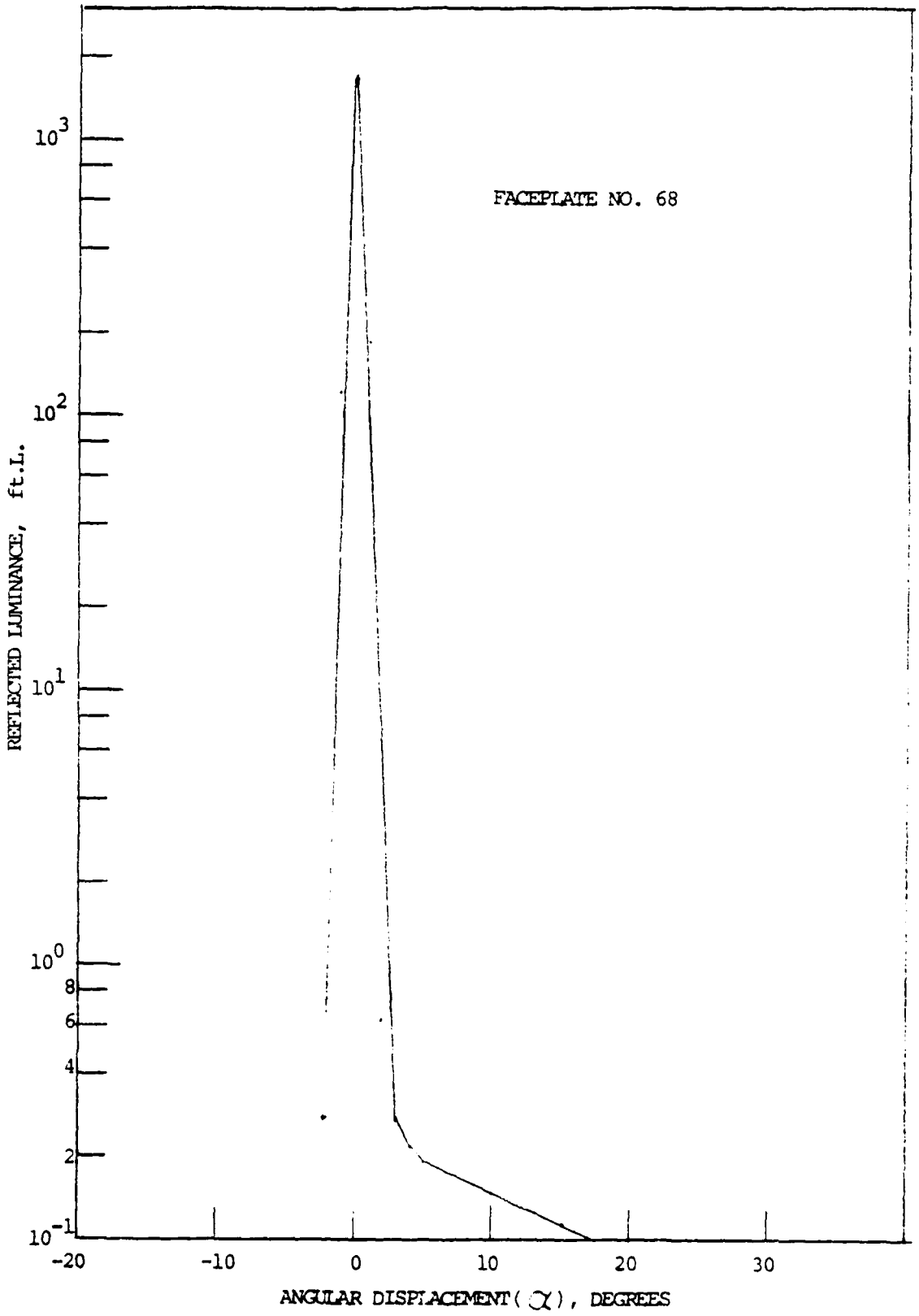

Fig. 56 Reflected Luminance, Faceplate No. 68

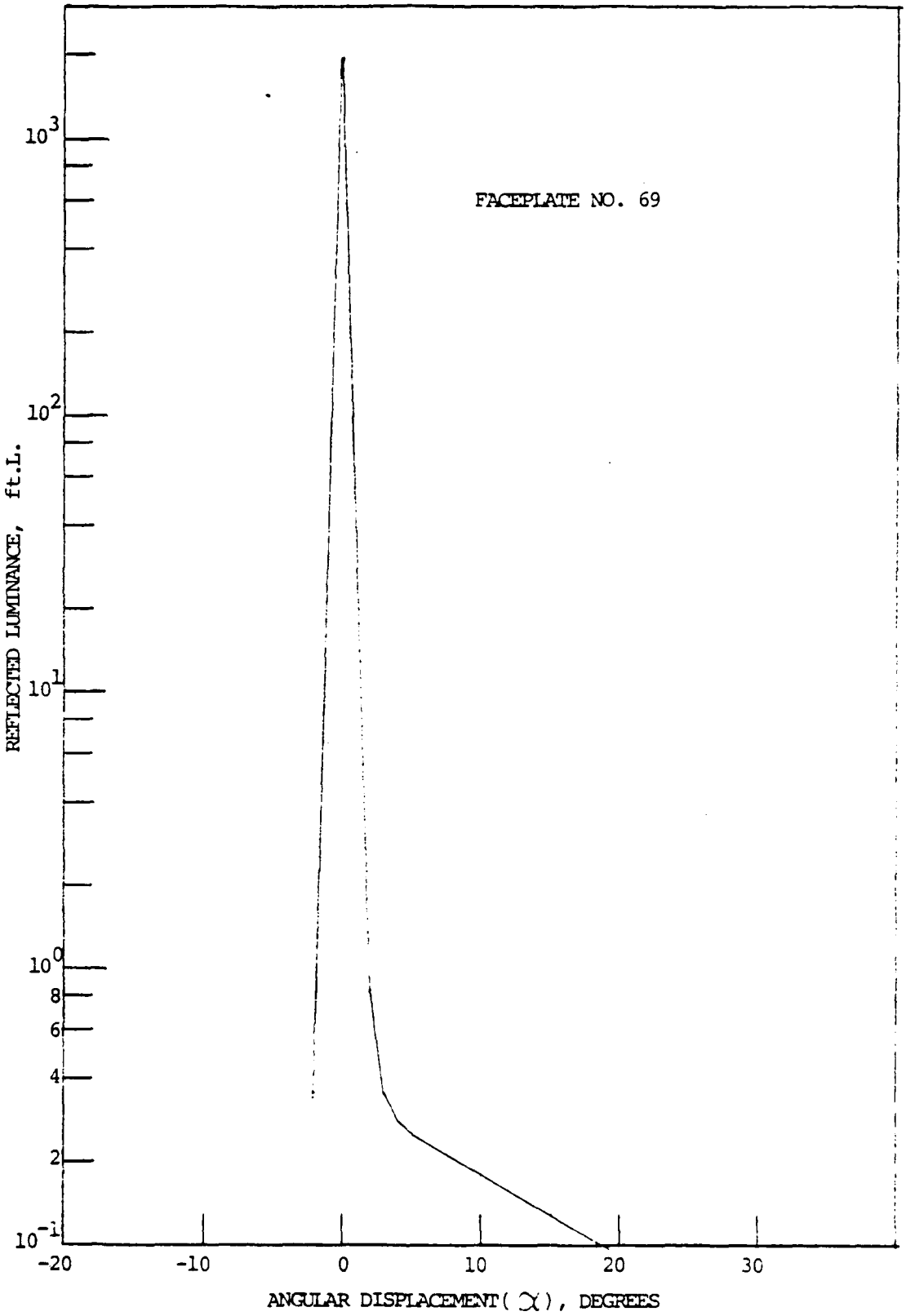

Fig. 57 Reflected Luminance, Faceplate No. 69

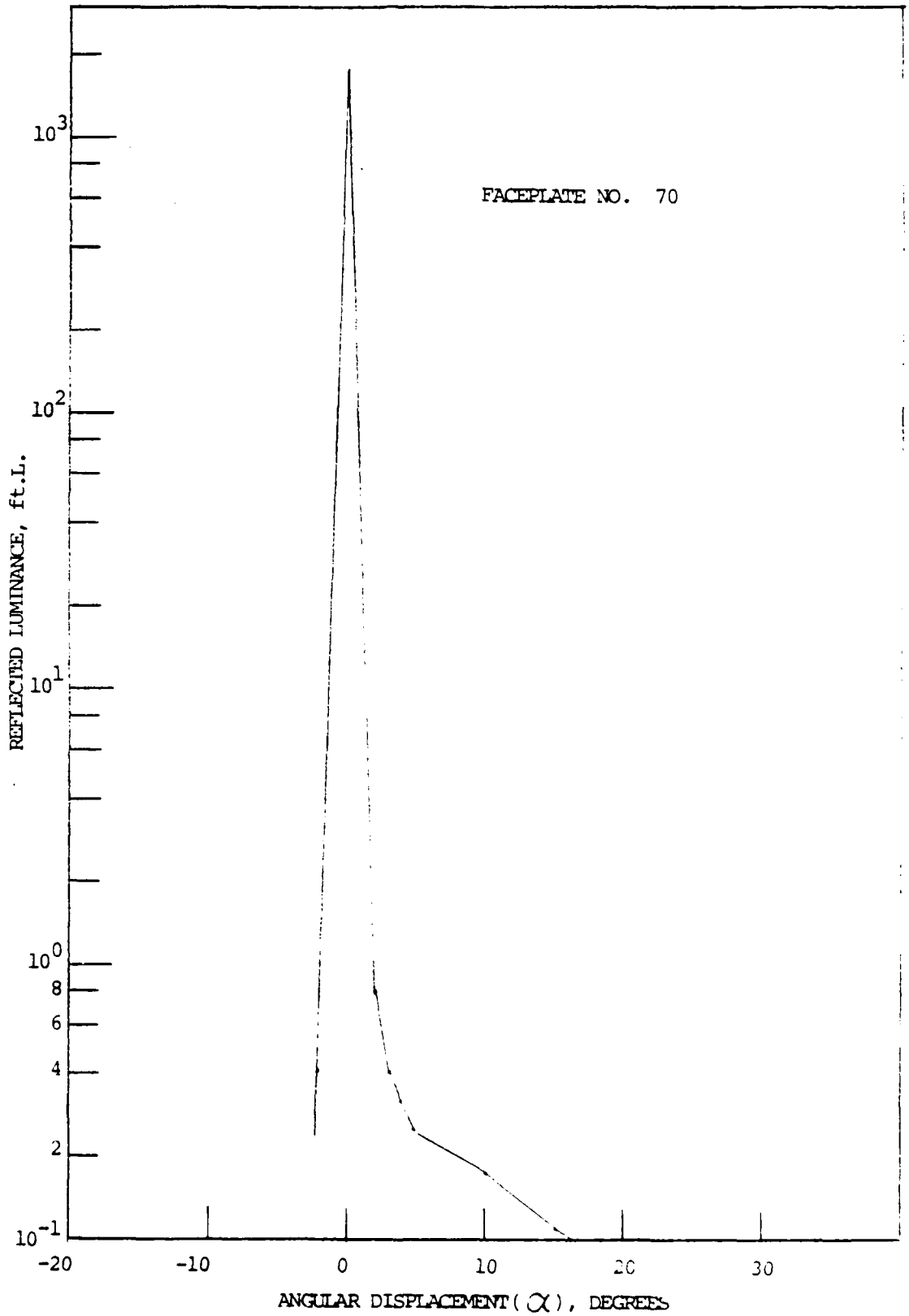

Fig. 58 Reflected Luminance, Faceplate No. 70

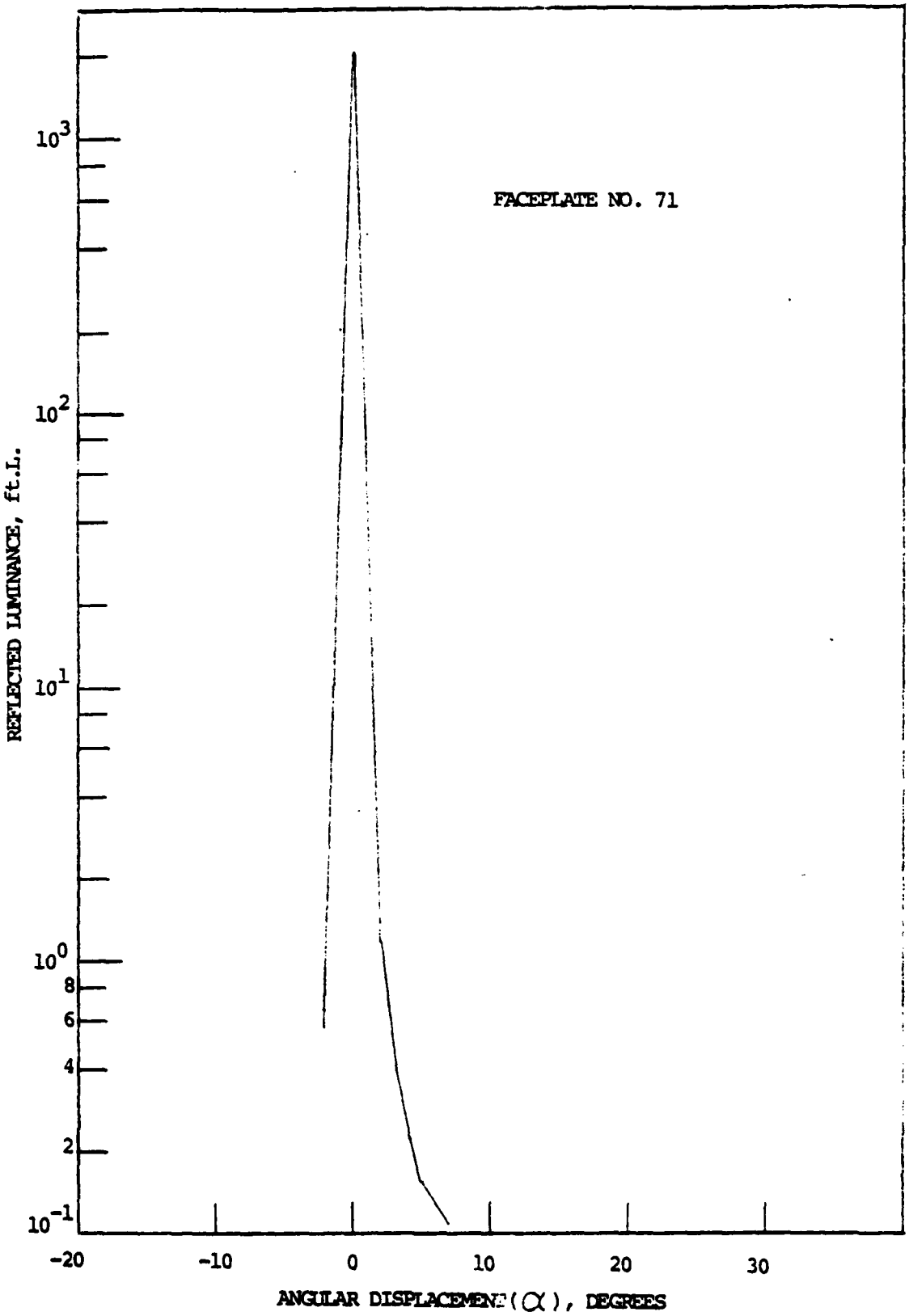

Fig. 59 Reflected Luminance, Faceplate No. 71

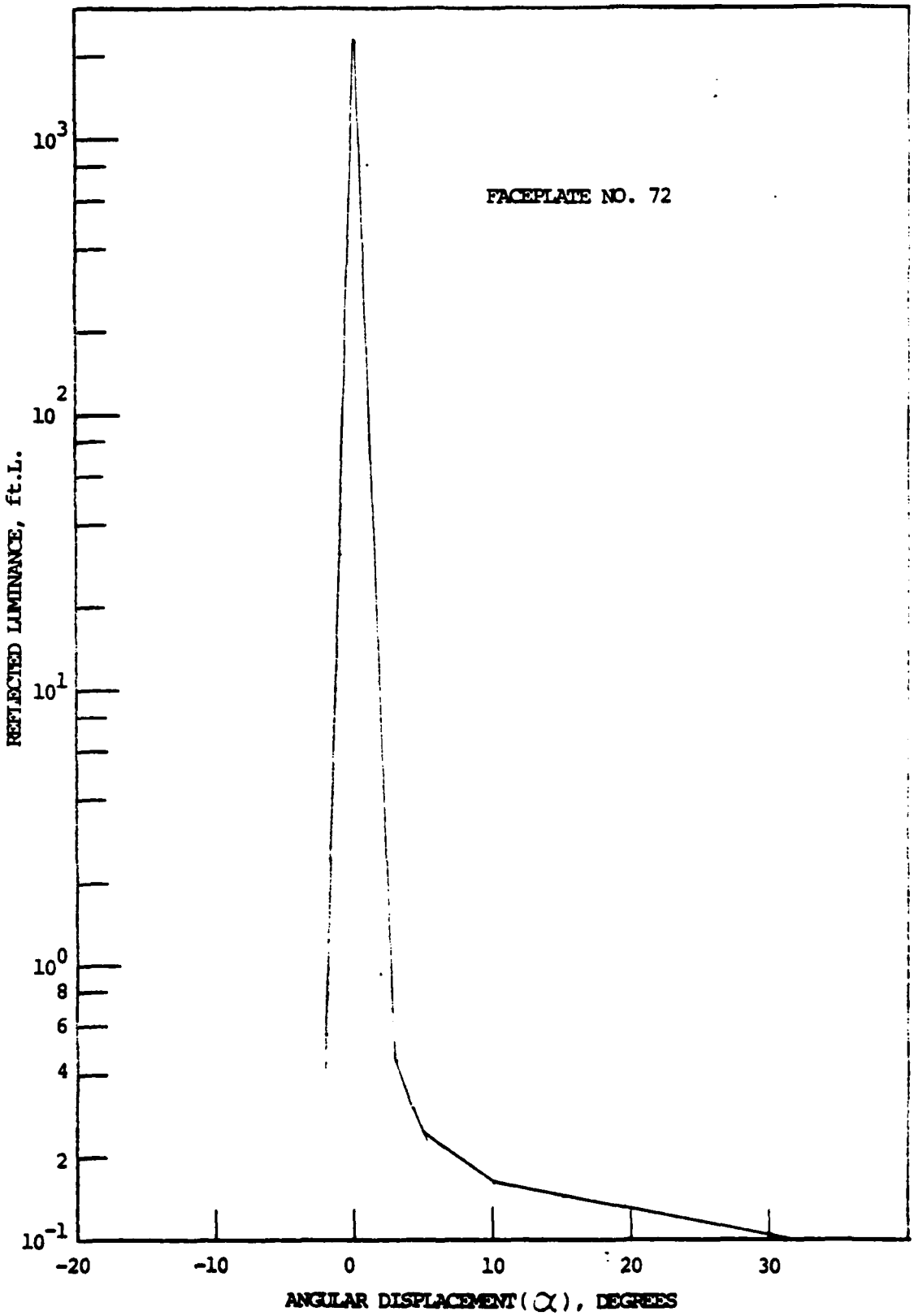

Fig. 60 Reflected Luminance, Faceplate No. 72

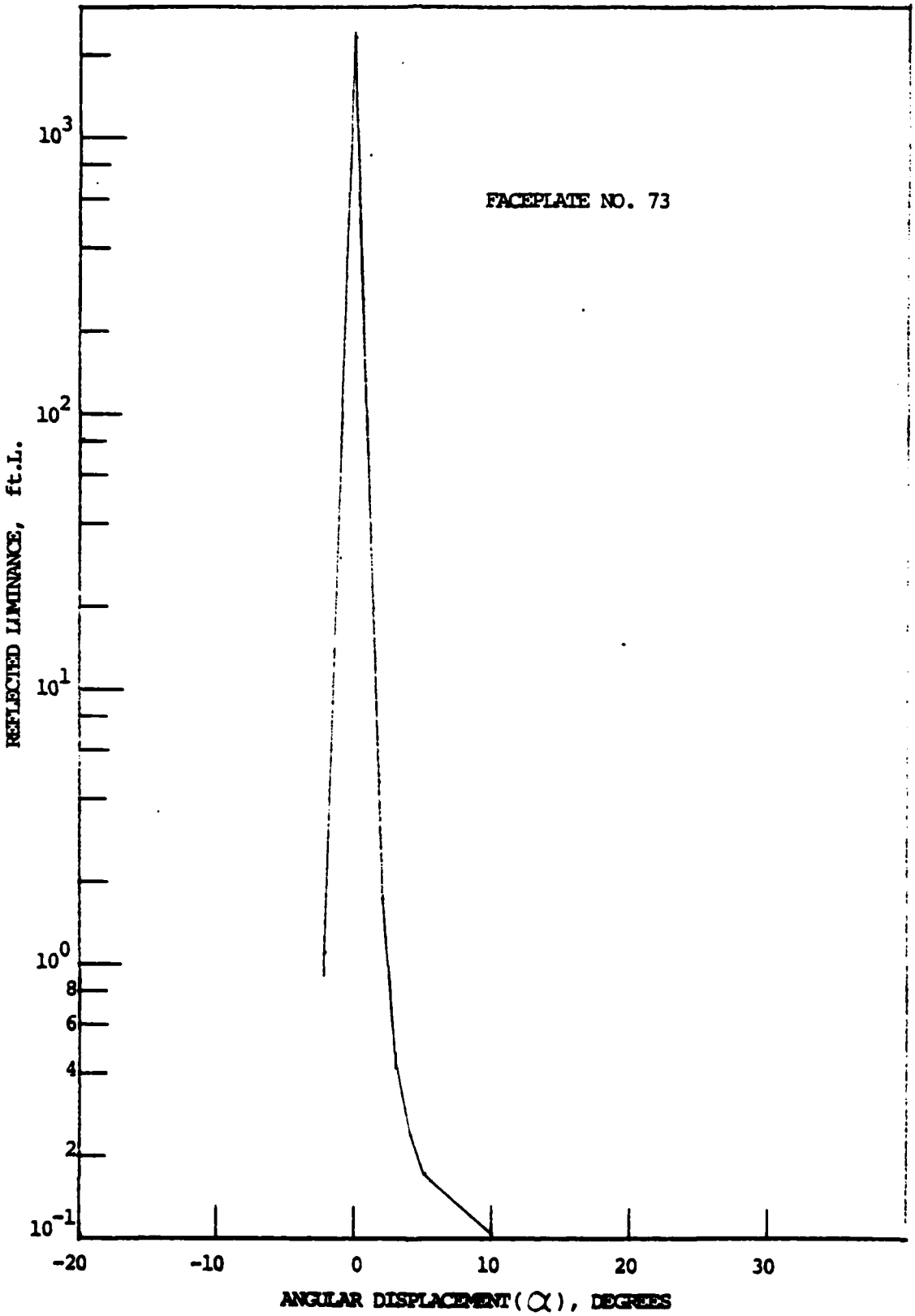

Fig. 61 Reflected Luminance, Faceplate No. 73

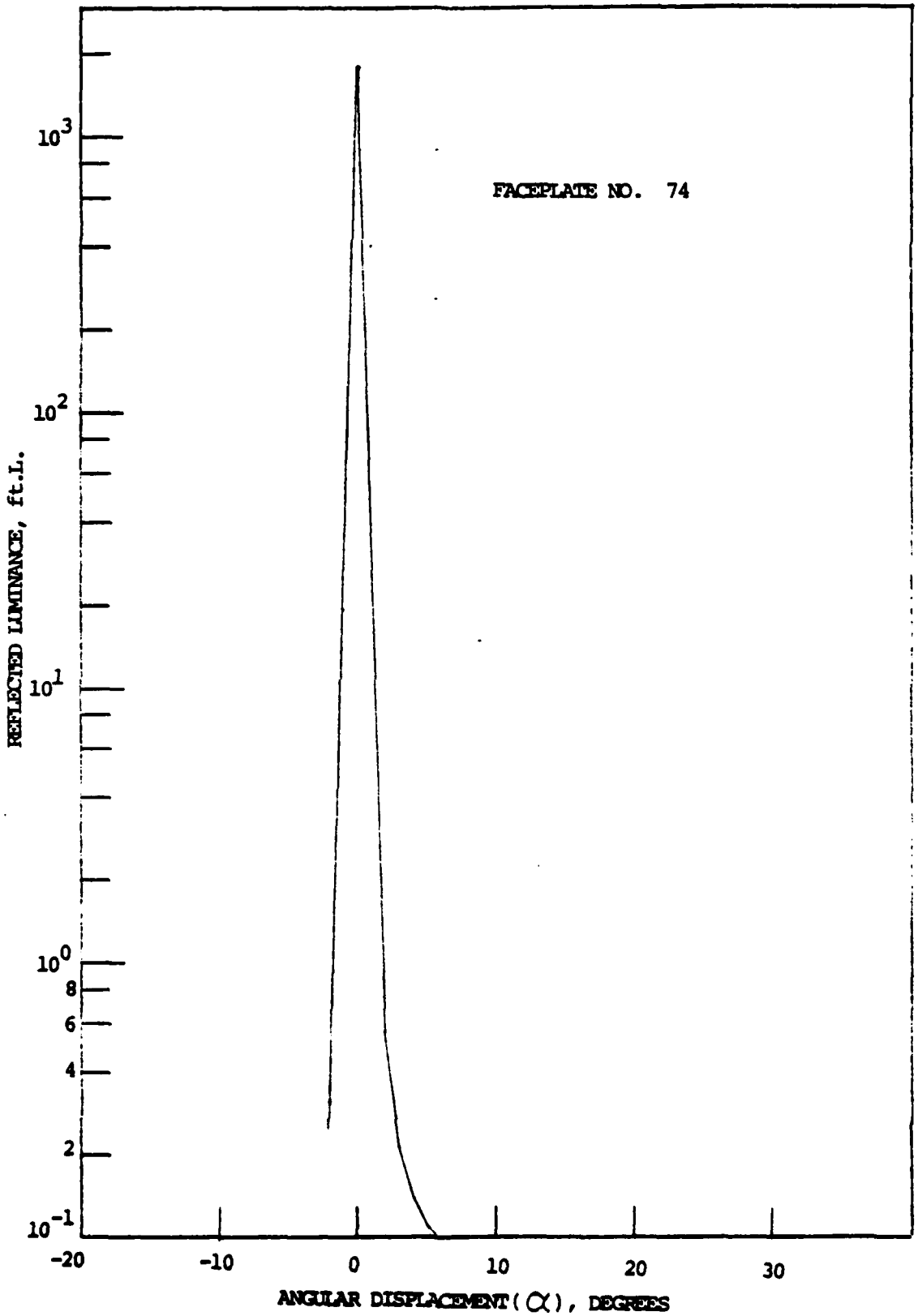

Fig. 62 Reflected Luminance, Faceplate No. 74

degradation of the black film during the sealing process. As a result of the Auger analysis, it was reported that films prepared according to the modified schedule were substantially thicker than those of the original schedule. An increased thickness of the black film implies that a larger amount of electron beam energy would be used in penetrating the black film, leaving reduced energy for exciting the phosphor layer.

Upon being advised of the Auger analysis results, additional films were prepared according to the modified schedule, except that the final no-oxygen deposition time was varied. Thickness of the films was measured by multiple-beam interferometry using a Varian Angstrometer. The results are summarized in Table 12 and graphically in Figure 63. The straight line of Figure 63 is a least squares fit to the experimental points, because, as a first approximation, the thickness would be expected to be linearly proportional to the deposition time. The reason for the rather large scatter in experimental points is not known.

The film thickness is shown to be strongly dependent on the no-oxygen deposition period (comprising the final 3 to 5 minutes of the overall time shown in Table 12). The 25 min. film was observed to be slightly transmitting. All others were completely opaque. It was concluded that a deposition time of 25-1/2 min. should insure opaque films having an average thickness of about 3000Å; this schedule will be used for Lot #3.

Table 11

Oxygen Schedule for Black Back Film

(a) Original Schedule		(b) Modified Schedule	
Time	Vernier	Time	Vernier
0	3.2	0	3.2
2	3.0	2	2.8
4	2.8	4	2.6
6	2.6	6	2.4
8	2.4	8	2.2
10	2.2	10	2.0
12	2.0	12	1.8
14	1.8	14	1.6
16	1.6	16	1.4
18	1.4	18	1.2
20	1.2	20	0.8
22	1.0	22	OFF
24	0.8	27	END
26	OFF		
30	END		

Table 12

NR(V) Film Thickness

Run No.	Time Min.	Thickness Å	
V #9-80	27	3837	Opaque
V #10-80	27	4122	Opaque
V #31-80	25	2714	Transm.
V #32-80	26	3626	Opaque
V #33-80	25-1/2	2854	Opaque
V #34-80	25-1/2	3312	Opaque
V #35-80	25-1/2	2871	Transm.
V #36-80	26	3383	Opaque
V #37-80	25-1/2	2822	V Sl. Transm.

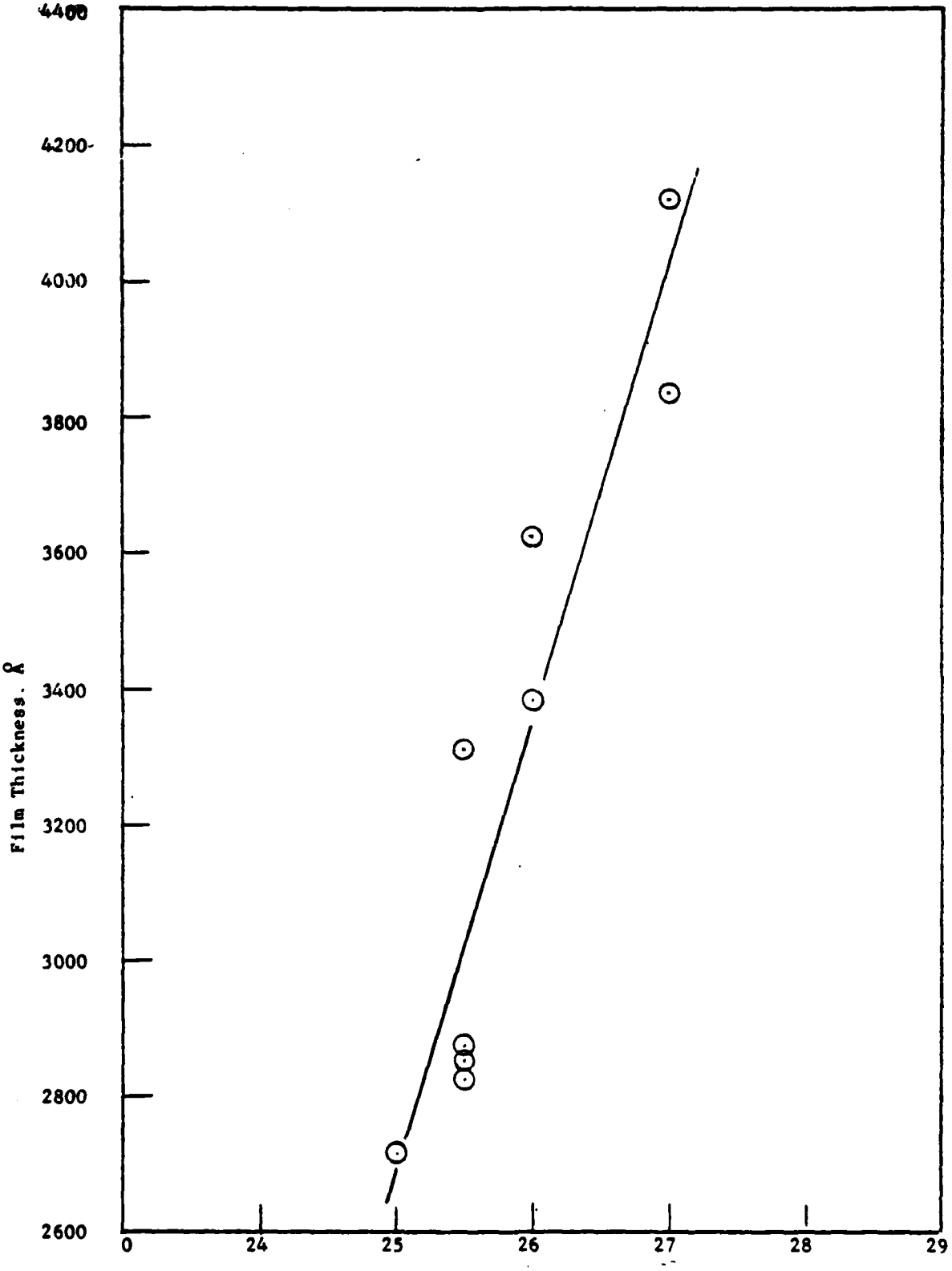

Fig.63 Thickness of Black Film vs. Deposition Time

4.7 Energy Absorption Calculations

Introduction

In our previous calculations, we have used the Feldman range equation (Ref. 4) to estimate the penetration of an electron beam into successive thin film layers as a function of the incident electron beam energy. This has proved useful for determining the appropriate La_2O_2S:Eu and La_2O_2S:Tb phosphor film thicknesses for faceplates intended for use at a maximum screen potential of 20 keV, as required for the present program.

The Feldman equation is

$$R = 250 \frac{A}{\rho} \left(\frac{E}{Z^{1/2}} \right)^n \qquad (1)$$

with

$$n = 1.2/(1 - 0.29 \log_{10} Z),$$

where A is the atomic or molecular weight of the material, Z the atomic number or number of electrons per molecule in the case of compounds, and ρ the density. When the incident energy E is in units of keV, R is the range in Å. The equation has a resemblance to the Thompson-Whiddington square law relation (Ref. 5), except that n is not 2, but instead varies with the material. Feldman found values of n between 1.7 and 3.0 for the materials studied by him. He defined R as a "practical maximum range", lying somewhere between the true maximum range and the extrapolated range that might be obtained from a plot of electron absorption vs. distance. Feldman summarizes several range equations proposed by various investigators, all being similar attempts to fit experimental range values to a Thompson-Whiddington type equation in the form of $R = kE^n$. As pointed out by Casslett and Thomas (Ref. 6), the Thompson-Whiddington law relates only to the energy loss occurring for electrons transiting a material, and was originally given in the form $E_o^2 - E^2 = aX$. It is not an appropriate means for expressing electron range. Moreover, it does not take into account, nor does the Bethe relation, the forward and back scattering which electrons are known to undergo.

It is not surprising, therefore, that when electron energy loss os calculated for electrons transiting a representative faceplate structure, using the Feldman equation, cusp-like curves are obtained as shown in Figure 64, while experimentally measured cathodoluminescence curves are smooth, as shown in Figure 65. (In the absence of saturation effects, cathodoluminescence should be a linear function of absorbed electron energy).

A More Realistic Equation

Kanaya and Okayama (to be referred to hereafter as K & O) have published (Ref. 7) a more realistic treatment of the loss of energy by electronc transiting a solid material. They take into account both elastic and inelastic collisions, diffusion effects due to multiple scattering including backscattering based on Lindhard's ion-beam scattering theory and the Lenard absorption law. The result is a modified Thomson-Whiddington law for which the relatavistically-corrected mass-range ρR is given as

$$\rho R = \frac{2.76 \times 10^{-11} A E_o^{5/3}}{Z^{8/9}} \times \frac{(1 + 0.978 \times 10^{-6} E_o)^{5/3}}{(1 + 1.957 \times 10^{-6} E_o)^{4/3}} . \qquad (2)$$

Since relativistic effects only become significant at energies above 100 keV, the equation can be simplified by disregarding the relativistic correction:

$$\rho R = \frac{2.76 \times 10^{-11} A E^{5/3}}{Z^{8/9}} .$$

With the incident energy E_o in keV, the range in $\mathring{A}$ is

$$R + \frac{276\, A E^{5/3}}{\rho Z^{8/9}} . \qquad (3)$$

Comparison with the Feldman expression (Equation 1) shows a difference in the exponents of E and Z.

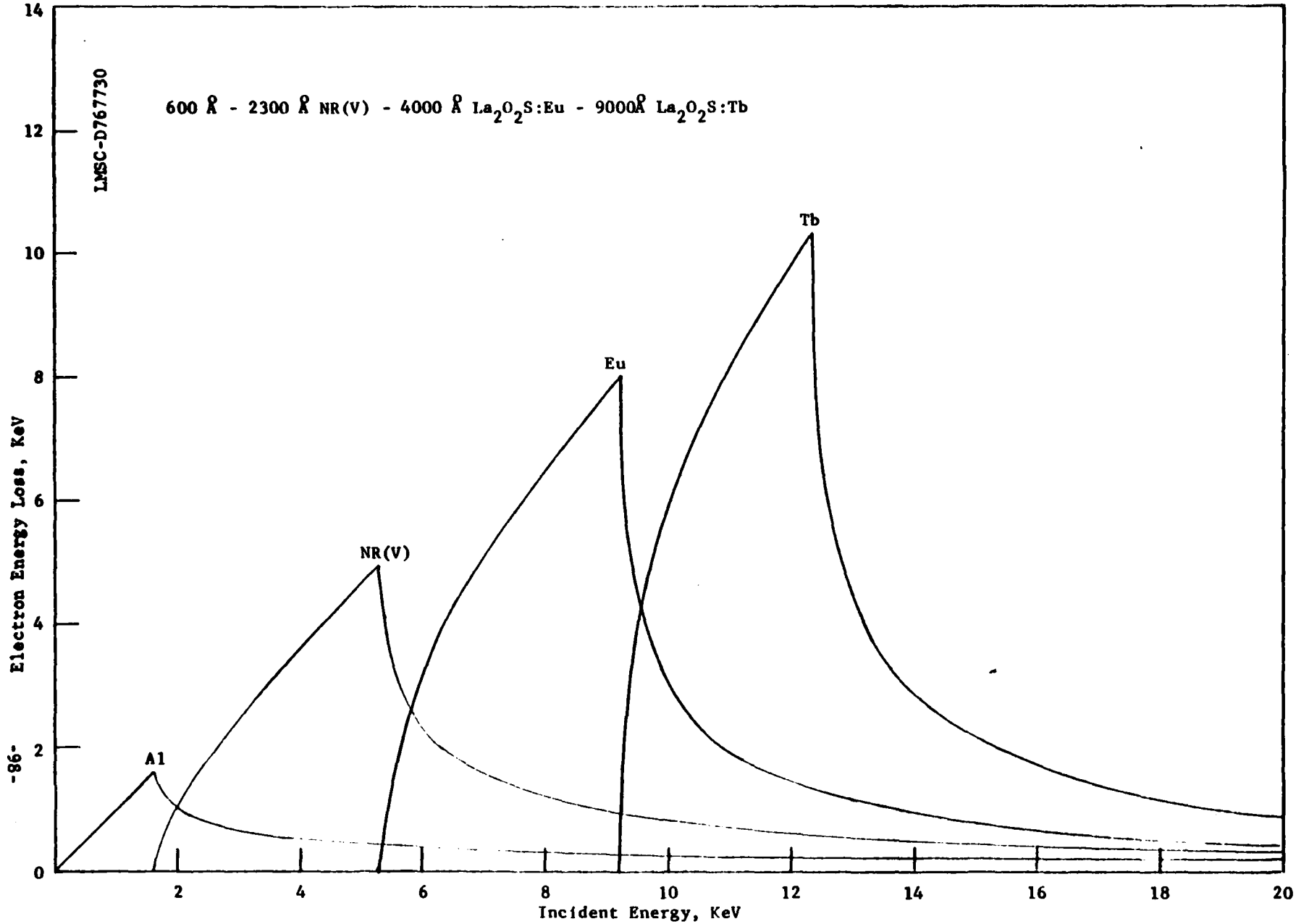

Fig. 64 Energy Loss in Typical Faceplate, Feldman Equation

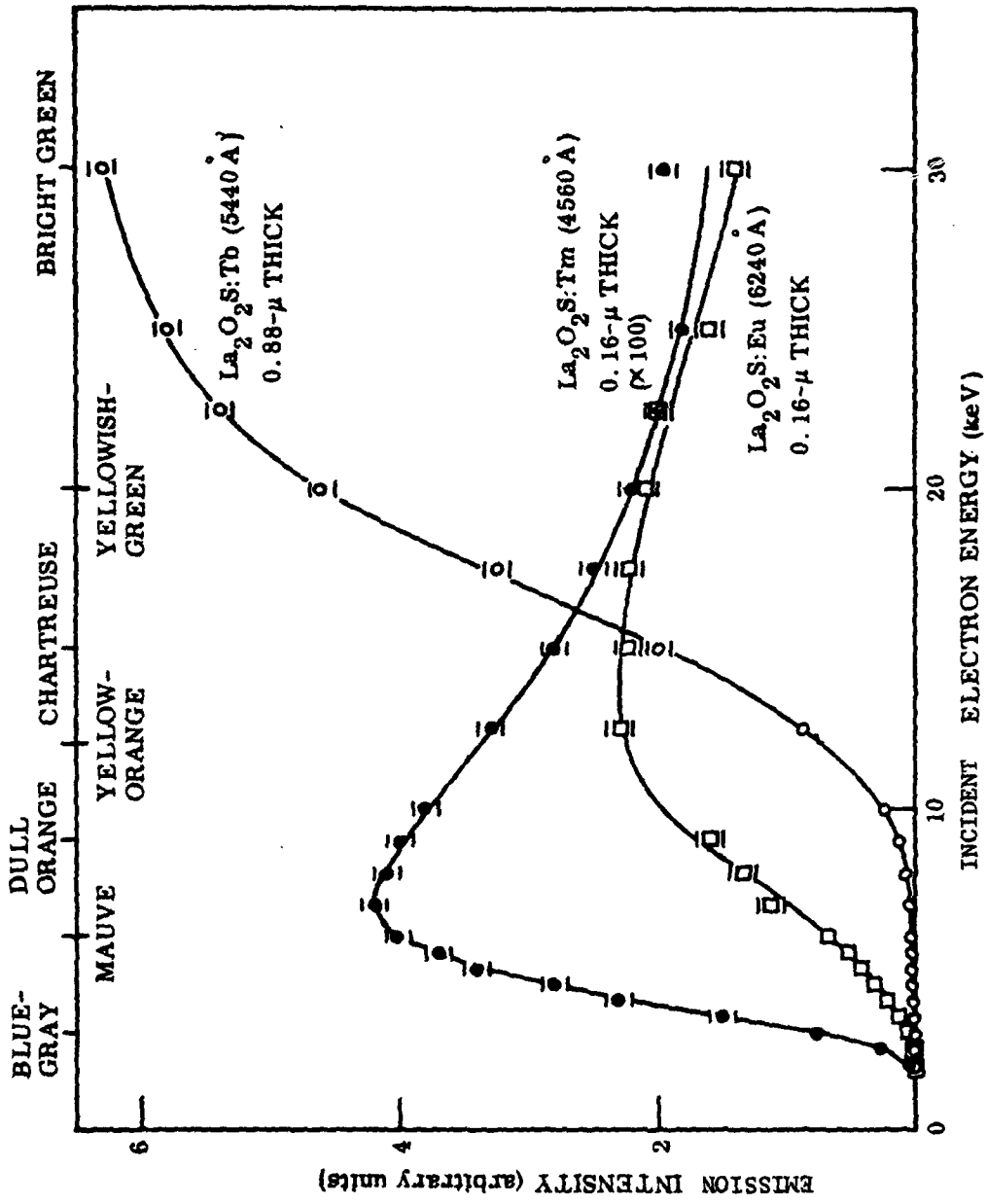

Fig. 65 Intensity Versus Electron Energy for a La_2O_2S:RE Trilayer Film

Denoting the energy absorbed in the material between the surface and depth x by E_a, the fraction of incident energy absorbed is given by K & O as

$$\frac{E_a}{E_o} = 1 - (1 - y)^{3/5} \exp\left(\frac{-\gamma y}{1-y}\right) - \frac{E_B}{E_o}\left[\frac{6 \times 1.9}{5} \int_o^y \frac{\gamma}{(1-y)^{7/6}} \exp\left(\frac{-1.9\gamma y}{1-y}\right) dy \right.$$

$$\left. - \frac{6}{5x2^{5/6}}\left\{1 - \exp\left(\frac{-1.9\gamma y)}{1-y}\right)\right\}\right] \qquad (4)$$

where $y = \frac{x}{R}$ the reduced or normalized depth and E_B/E_o is the mean fractional energy of the backscattered electrons. The second term of Equation (4) is the mean fractional energy transmitted in the forward direction beyond the normalized depth y; the third term (in rectangular brackets) is the fractional loss of energy by back scattering.

K & O describe their equation as semi-empirical, primarily because of the necessity of assuming values for three scattering parameters occurring in relationahips used to derive Equation (4).

K & O present a plot of E_B/E_o vs. Z as measured by several investigators on which they have drawn a curve to best represent the data. No equation is given for the curve, which has only slight curvature. We have, therefore, assumed the curve is adequately represented by an arc of a circle. By reading three points from the plot, the equation of the circle has been determined, and from this a table of E_B/E_o vs. periodic no. Z for all values of Z from 1 to 92 (See Table 13).

It will be noted that Equation (4) contains an integral of a transcendental quantity which cannot be integrated analytically. (By a transformation of variables it can be shown that the integrand has the same form as that of the gamma function, but with only finite limits of integration rather than the limits of 0 to ∞ of the gamma function). Fortunately, we have found that the integral can be evaluated by use of Weddle's rule:

Table 13

E_B/E_o vs. Z

Z	E_B/E_o	Z	E_B/E_o	Z	E_B/E_o
1	.60318	32	.67001	63	.75386
2	.60635	33	.69243	64	.75554
3	.60948	34	.69482	65	.75719
4	.61259	35	.69719	66	.75882
5	.61578	36	.69954	67	.76043
6	.61874	37	.70186	68	.76201
7	.62178	38	.70416	69	.76357
8	.62480	39	.73643	70	.76510
9	.62779	40	.73869	71	.76661
10	.63075	41	.71091	72	.76810
11	.63370	42	.71512	73	.76956
12	.63662	43	.71529	74	.77100
13	.63952	44	.71745	75	.77241
14	.64239	45	.71958	76	.77380
15	.64524	46	.72169	77	.77517
16	.64807	47	.72377	78	.77651
17	.65087	48	.72583	79	.77783
18	.65364	49	.72787	80	.77713
19	.61640	50	.73000	81	.78040
20	.65913	51	.73187	82	.78164
21	.66183	52	.73383	83	.78287
22	.66451	53	.73577	84	.78407
23	.66717	54	.73769	85	.78524
24	.66980	55	.73858	86	.78639
25	.67241	56	.74145	87	.78752
26	.67500	57	.74329	88	.78862
27	.67756	58	.74512	89	.78970
28	.68010	59	.74691	90	.79076
29	.68261	60	.74869	91	.79179
30	.68510	61	.75043	92	.79280
31	.68757	62	.75216		

$$I_W = \int_a^b F(x)dx = \frac{3h}{10}\left[y_o + y_1 + y_2 + 6y_3 + y_4 - 5y_5 + y_6\right] \quad (5)$$

where

$$h = \frac{b-a}{6} = \frac{y}{6}$$

$$y_o = F(0),\ y_1 = F(h),\ y_2 = F(2h),\ \text{etc.}$$

Although it appears difficult to prove analytically, calculations have shown that $y_o = \lim_{y \to 0} F(0) = \gamma$

and $\lim_{y \to 1} F(6) = 0$

when applied to the integrand of Equation (4). This permits us to determine the value of E_A/E_o at the limit $y = 1$ in a simple manner.

A program has therefore been written to calculate E_A/E_o using a TI-59 programmable calculator. (See Appendix). The input data are A_{EFF}, ρ, Z_{Eff}, E_o, X, and E_B/E_o.

The power absorbed in $x(\text{Å})$ of the material is $\frac{E_A}{E_o} \times E_o \times I_o$ where I_o is the incident electron beam current.

Following the suggestion of Prener (Ref. 8) for the case of a phosphor layer coated with a thin aluminum film, we can assume with little error that the electrons penetrating the aluminum film are essentially monoenergetic. The fractional power of the transmitted electrons $\eta_T E_T/E_o$ is given by the second term of Equation 4, where η_T is the fraction of incident current transmitted in the forward direction and E_T is the mean energy of the transmitted electrons. Then the energy of the electrons incident on the phosphor is $(E_T/E_o) \times E_o = E_{o1}$. Using this value of E_{o1} we can again use Equation (4) to calculate the energy absorbed in the phosphor.

A second program has therefore been written for a TI-59 calculator which performs these calculations and gives P_1, P_2, and P_3 as the power absorbed in the aluminum, the La_2O_2S:Eu layer, and the La_2O_2S:Tb layer, respectively.

K & O compared the results of their calculations with experimental data only for various metallic elements. All phosphors, however, are, almost

without exception, compounds; it is thus not clear what values for A and Z are to be used in Equation (3) when the material is a compound. Feldman used the molecular weight for A and the sum of the periodic numbers of the elements in the molecules of the compound for Z. This results in rather large numbers for A and Z. Other authors have weighted the sums of the atomic weights and periodic numbers by the densities for the elements. Z is clearly independent of density, so this second approach is questionable.

We have chosen to determine an effective A and an effective Z on the basis of the mole fraction of elements in the compound. Thus,

$$A_{EFF} = \Sigma\, f_i\, A_i$$
$$Z_{EFF} = \Sigma\, f_i Z_i \qquad (6)$$

Where f_i is the mole fraction of element i in the compound and A_i and Z_i are the atomic weight and periodic number for element i. The values obtained are of reasonable size, and it is believed this procedure is fundamentally sounder than previous approaches.

Results of Calculations

Table 14 presents a comparison of the electron range for aluminum calculated using the Feldman equation with that calculated using the K&O equation (Eqn. 3). Agreement is good only for 0-4 keV. At all higher energies, the Feldman equation predicts ranges increasingly larger than the K&O equation, even though the Feldman range is supposed to be a maximum practical range, less than the maximum range, while the K&O equation is for the maximum range. The Feldman equation is, of course, based on an empirical fit to experimental values in the 1 - 10 KeV range with no consideration of backscattering. On the other hand, the K & O equation provides good agreement with experiments over the much larger range of 1 - 1000 KeV.

Table 14

Electron Range in Al, Å

Incident Energy KeV	Feldman Eqn.	K&O Eqn.
1	257	282
2	879	896
3	1804	1761
4	3004	2845
5	4461	4126
6	6164	5591
7	8101	7229
8	10265	9031
9	12648	10990
10	15245	13100
11	18051	15355
12	21061	17751
13	24222	20285
14	27678	22952
15	31281	25749
16	35072	28673
17	39051	31721
18	43215	34892
19	47562	38182
20	52090	41590

In Table 15 there is presented a comparison between ranges in La_2O_2S calculated using the Feldman equation, the Feldman equation modified by substituting effective A and Z from Equation (6), and the K & O equation. Again, the Feldman equation predicts probably unrealistically large ranges at energies from 10 to 20 KeV. Ranges from the modified Feldman equation lie between these and those of the K & O equation.

The use of a normalized or reduced depth, $y = \frac{x}{R}$, was originally introduced by Seliger (Ref. 9) as a convenient means of representing an entire family of curves by a single curve. K & O present in their paper plots of E_a/E_o vs. y for several elements (C, Al, Cu, Ag, Au, U). We show in Figures 66 and 56 curves calculated for the materials of interest to this program: Al, La_2O_2S, Ta. Ta_2O_5, V and V_2O_5. The curve for La_2O_2S is practically identical to that of Cu, as may be seen from Table 16. Also, the curve for Ta_2O_5 nearly superimposes on that of La_2O_2S as shown in Figure 66. Again, the curve for V_2O_5 is practically identical to that for Al and that for V lies near that of La_2O_2S. (Compare Figures 66 and 67). On the other hand, that for Ta is displaced considerably from that for the others, the limiting value of E_A/E_o as y approaches 1 being considerably less, due to the significantly greater backscattering occurring in Ta and other materials of high atomic number. (Table 16; see also Figure 6 of Ref. 7). This explains clearly why it was found necessary earlier in this work to replace a graded Ta_2O_5-Ta nonreflecting layer with a graded V_2O_5-V layer despite the ease with which Ta_2O_5-Ta films of high quality can be produced. At the time, it was observed that insufficient electron beam energy remained to properly excite the La_2O_2S:Tb layer after transiting the Ta_2O_5-Ta and La_2O_2S:Eu layers.

Next, the power absorbed from an electron beam incident on an 800Å aluminum film has been calculated using the K & O equation for E_a/E_o (Equation 4) for a beam current of 100μA. This current value was chosen merely for convenience; in the absence of phosphor saturation, the emission should scale linearly with incident power density. For simplicity, the terms current and power are used in this section, but should be understood as current density and power density, respectively. The results are shown in Figure 68. The absorbed power has a peak at 2.5 KeV, which is in good agreement with experimental results as will be shown shortly.

Table 15

Electron Range in La_2O_2S, Å

Incident Energy KeV	Feldman Eqn.	Modified Feldman	K&O Eqn.
1	5	88	164
2	45	375	521
3	167	874	1024
4	423	1593	1654
5	868	2537	2399
6	1563	3712	3251
7	2568	5120	4203
8	3949	6765	5251
9	5772	8650	6390
10	8106	10777	7617
11	11020	13149	8928
12	14588	15767	10321
13	18882	18634	11794
14	23975	21750	13345
15	29946	25118	14971
16	36820	28739	16671
17	44825	32615	18444
18	53892	36747	20287
19	64151	41136	22200
20	75683	45784	24181

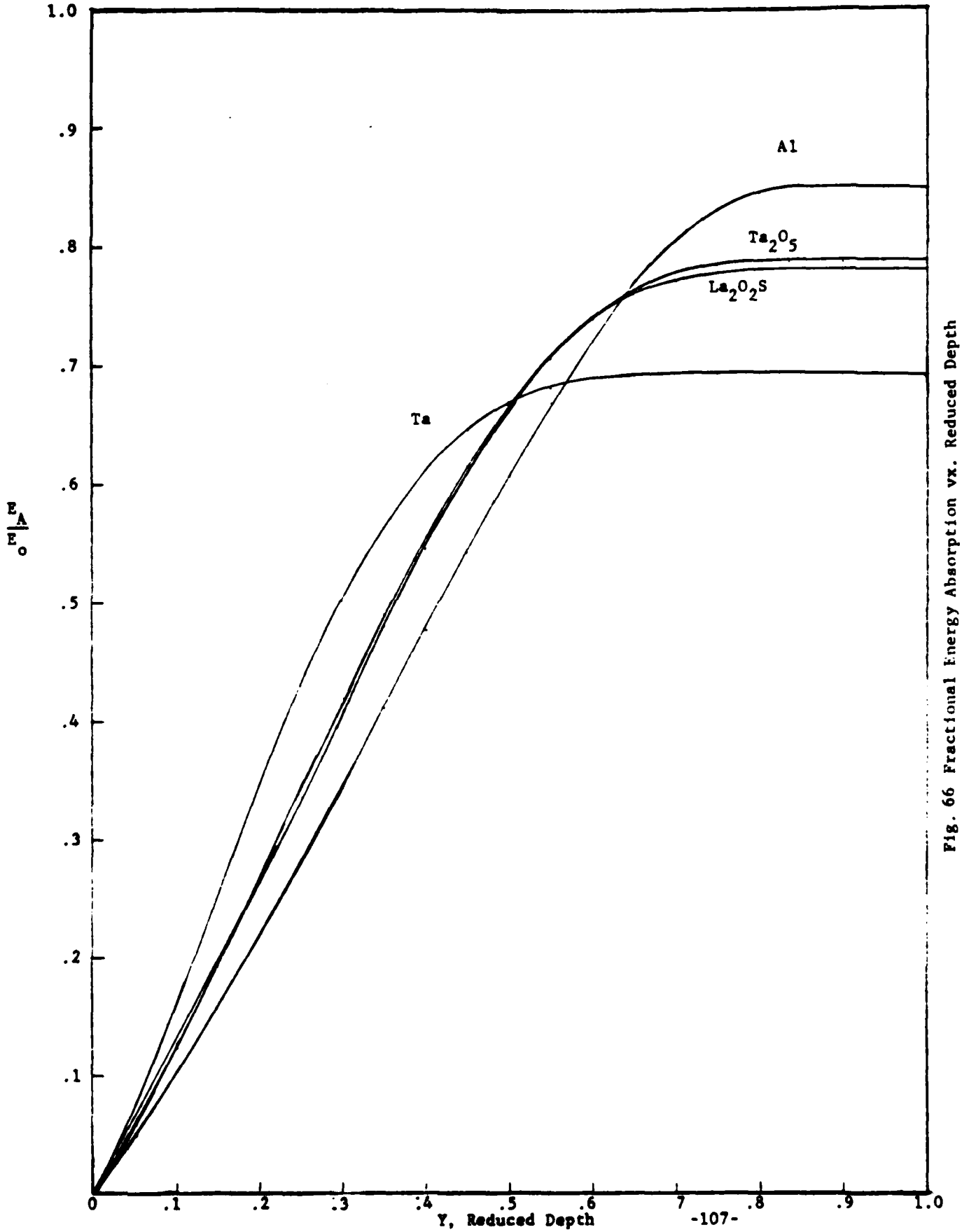

Fig. 66 Fractional Energy Absorption vs. Reduced Depth

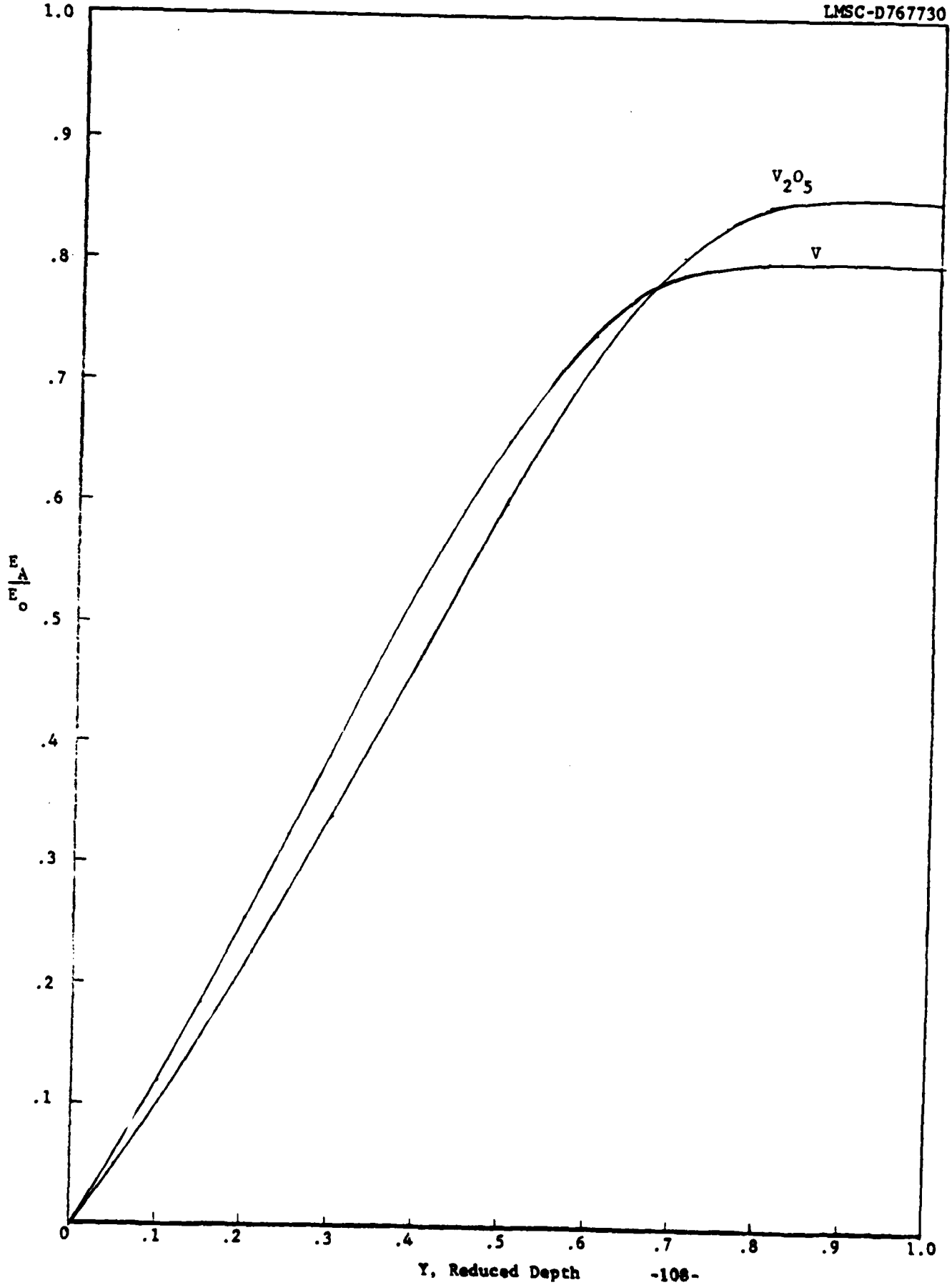

Fig. 67 Fractional Energy Absorbed vs. Reduced Depth

Table 16

E_A/E_o vs. Reduced Depth, Y

Y	Al	Cu	La_2O_2S	V	V_aO_5	Ta	Ta_2O_5
0	0	0	0	0	0	0	0
.05	.05016	.06067	.06102	.05753	.04953	.07574	.05761
.1	.10341	.12658	.12726	.11946	.10203	.16286	.12410
.15	.15967	.19658	.19756	.18513	.15749	.25450	.19253
.2	.21880	.21933	.27056	.25372	.21580	.34461	.26376
.25	.28055	.34323	.34466	.32416	.27673	.42825	.33642
.3	.34449	.41650	.41807	.39517	.33995	.50171	.40895
.35	.41003	.48723	.48884	.46525	.40491	.56265	.47957
.4	.47632	.55338	.55496	.53269	.47086	.61016	.54636
.45	.54224	.61299	.6.446	.59562	.53674	.64466	.60739
.5	.60632	.66428	.66558	.65214	.60118	.66765	.66080
.55	.66677	.70592	.70701	.70048	.66243	.68141	.70506
.6	.72147	.73723	.73810	.73924	.71840	.68858	.73919
.65	.76818	.75844	.75910	.76762	.76677	.69169	.76303
.7	.80481	.77079	.77129	.78594	.80531	.69272	.77749
.75	.83005	.77649	.77689	.79563	.83242	.69295	.78453
.8	.84411	.77825	.77862	.79926	.84798	.69290	.78687
.85	.84931	.77857	.77894	.79985	.85406	.69266	.78723
.9	.84966	.77889	.77926	.79979	.85470	.69222	.78742
.95	.84853	.77958	.77995	.80014	.85354	.69163	.78803
1	.84739	.78051	.78086	.80109	.85216	.69100	.78904
A	26.9815	63.54	68.37656	50.942	25.983	180.948	63.13
ρ	2.699	8.96	5.73	6.0	3.357	16.6	8.2
Z	13	29	29.2	23	12.29	73	26.57

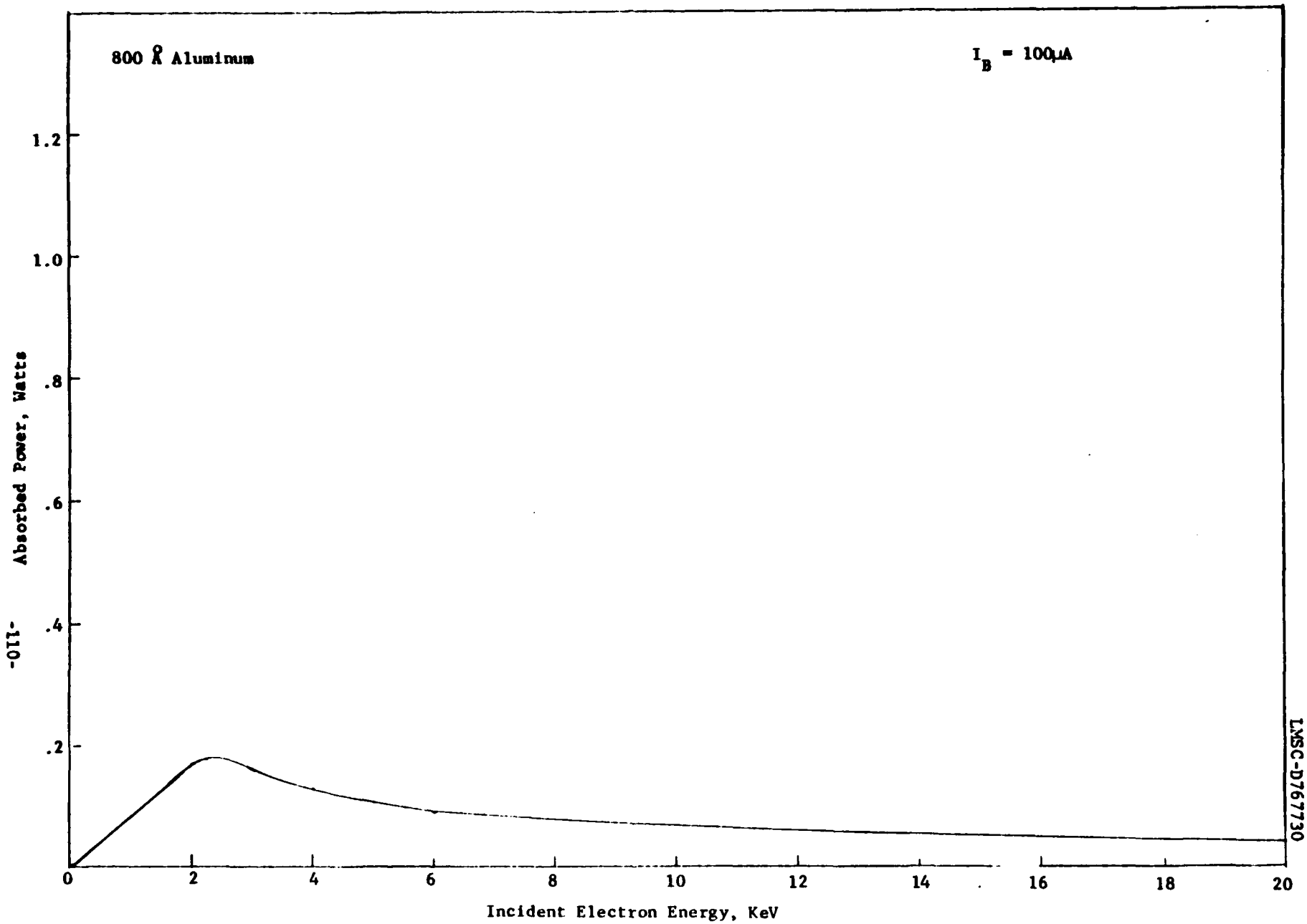

Fig. 68 Calculated Power Absorbed in an Aluminum Film

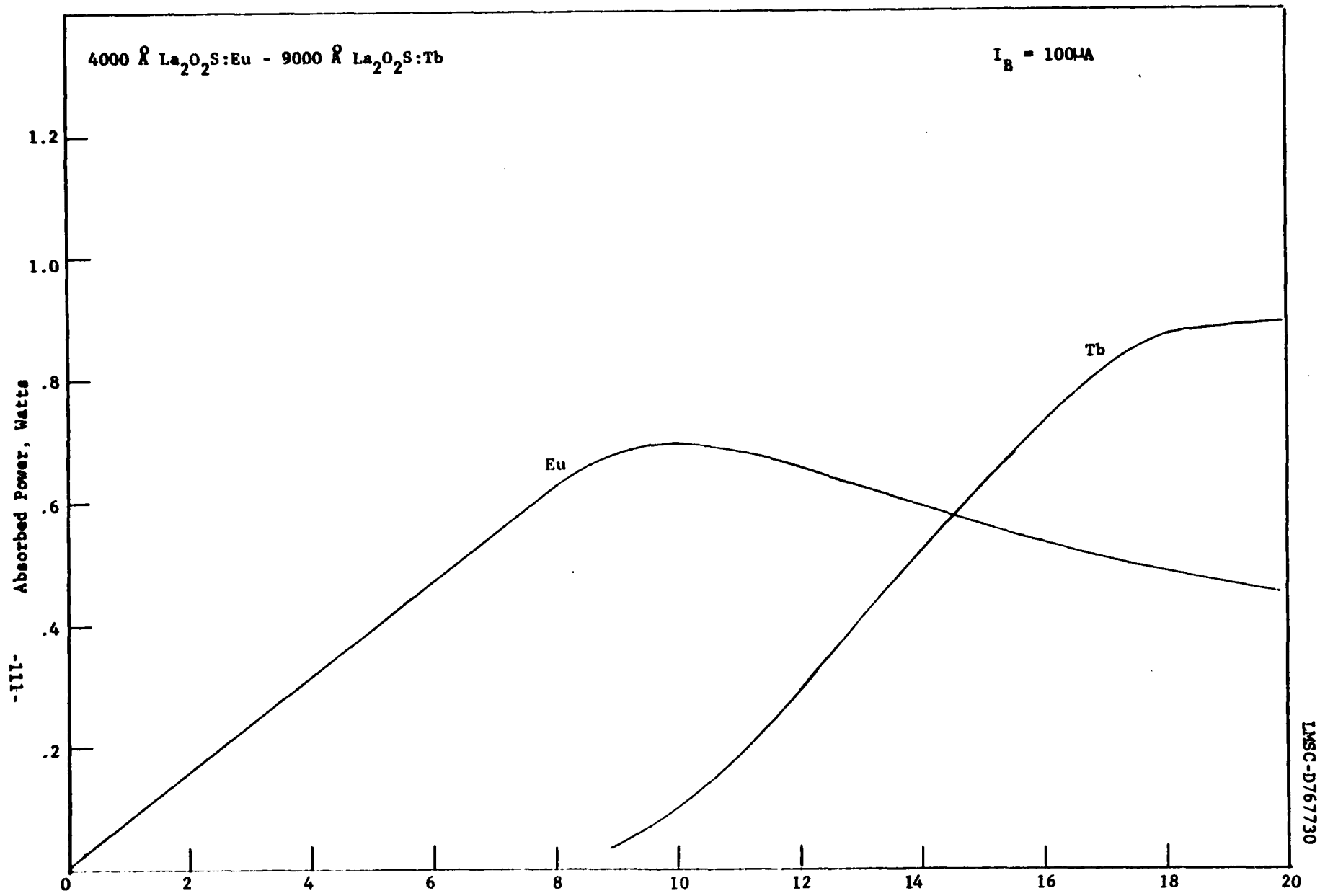

Fig. 69 Calculated Power Absorbed in a Bi-Layer Structure

In the next example, we have used the K&O equation to calculate the power absorbed from a 100μA electron beam in a bi-layer of 4000Å La_2O_2S:Eu over 9000Å La_2O_2S:Tb. The results are shown in Figure 69.

Next, Figure 70 shows the power absorption from a 100μA electron beam incident on a structure consisting of 800Å Al on 4000Å La_2O_2S:Eu on 9000Å La_2O_2S:Tb. These thicknesses are representative of a typical faceplate of this program. Peaks are shown at 2.5 KeV for Al, 10 KeV for the europium-doped layer, and the peak to be expected for the terbium-doped layer is at greater energies than 20 KeV. The calculations are summarized in Table 17.

Finally, there is shown in Figure 71 experimentally determined cathodoluminescence intensities for several La_2O_2S:Tb film thicknesses, (Ref. 18) and in Figure 72 the calculated absorbed power. Results of the calculations for Figure 72 are summarized in Table 18. The figures are strikingly similar. The calculated results for the thicker films differ somewhat from the experimental values; for instance, for the 0.6 micron film, the predicted peak is at 13.5 KeV while the experimettally determined value is at 16 KeV. (Fig. 71). This difference is hardly unexpected because the K & O equation was developed for a single material, rather than a multilayer structure in which the successive interfaces probably modify the scattering. Nevertheless, these nearly quantitative results demonstrate that the K & O equation is a useful tool for the design of multi-layer faceplates.

It is further concluded that use of effective A and Z's calculated according to Equation (6) is a valid approach.

Table 17

I_A = 100 μA

Incident Energy E_b KeV	Incident Power P_o Watts	Range in Al A°	Absorbed in Al P_a Watts	Transmitted Energy E_{o1} KeV	Absorbed in La_2O_2S:Eu P_b Watts	Absorbed in La_2O_2S:Tb P_c Watts	Total Power Absorbed $P_a+P_b+P_c$ Watts
1	0.1	282	.08474	0	0	0	.08474
2	0.2	896	.16948	0.524	.04089	0	.21037
3	0.3	1761	.16433	2.086	.16289	0	.32722
4	0.4	2845	.12810	3.281	.25121	0	.38431
5	0.5	4.26	.10571	4.393	.34307	0	.44878
6	0.6	5591	.09102	5.469	.42706	0	.51808
7	0.7	7229	.08061	6.524	.50946	0	.59007
8	0.8	9431	.07278	7.567	.58938	.00150	.66366
9	0.9	10990	.06665	8.601	.65901	.01261	.73827
10	1.0	13100	.06169	9.629	.68712	.06478	.81359
11	1.1	15355	.05757	10.653	.68043	.15139	.88939
12	1.2	17751	.05410	11.673	.65633	.25514	.96557
13	1.3	10282	.05110	12.690	.62568	.36523	1.04201
14	1.4	27952	.04850	13.705	.59386	.47633	1.11869
15	1.5	25749	.04621	14.719	.56324	.58368	1.19313
16	1.6	78673	.04418	15.731	.53476	.69010	1.26904
17	1.7	31721	.04236	16.741	.50870	.78798	1.33904
18	1.8	34892	.04072	17.751	.48500	.86577	1.39141
19	1.9	38182	.03924	18.760	.46348	.91935	1.42207
20	2.0	41590	.03785	19.768	.44394	.95102	1.43281

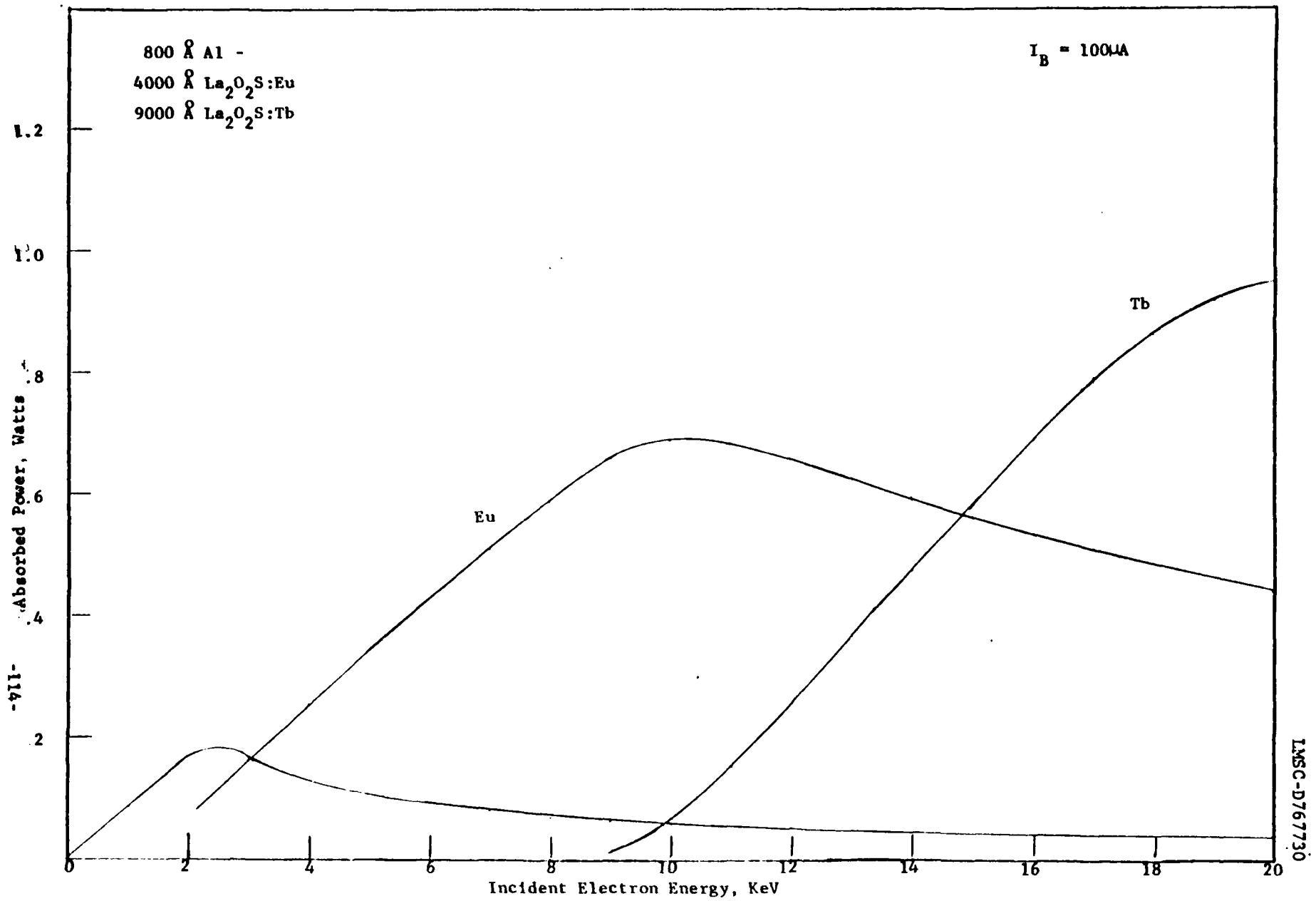

Fig. 70 Calculated Power absorbed in Typical Faceplate

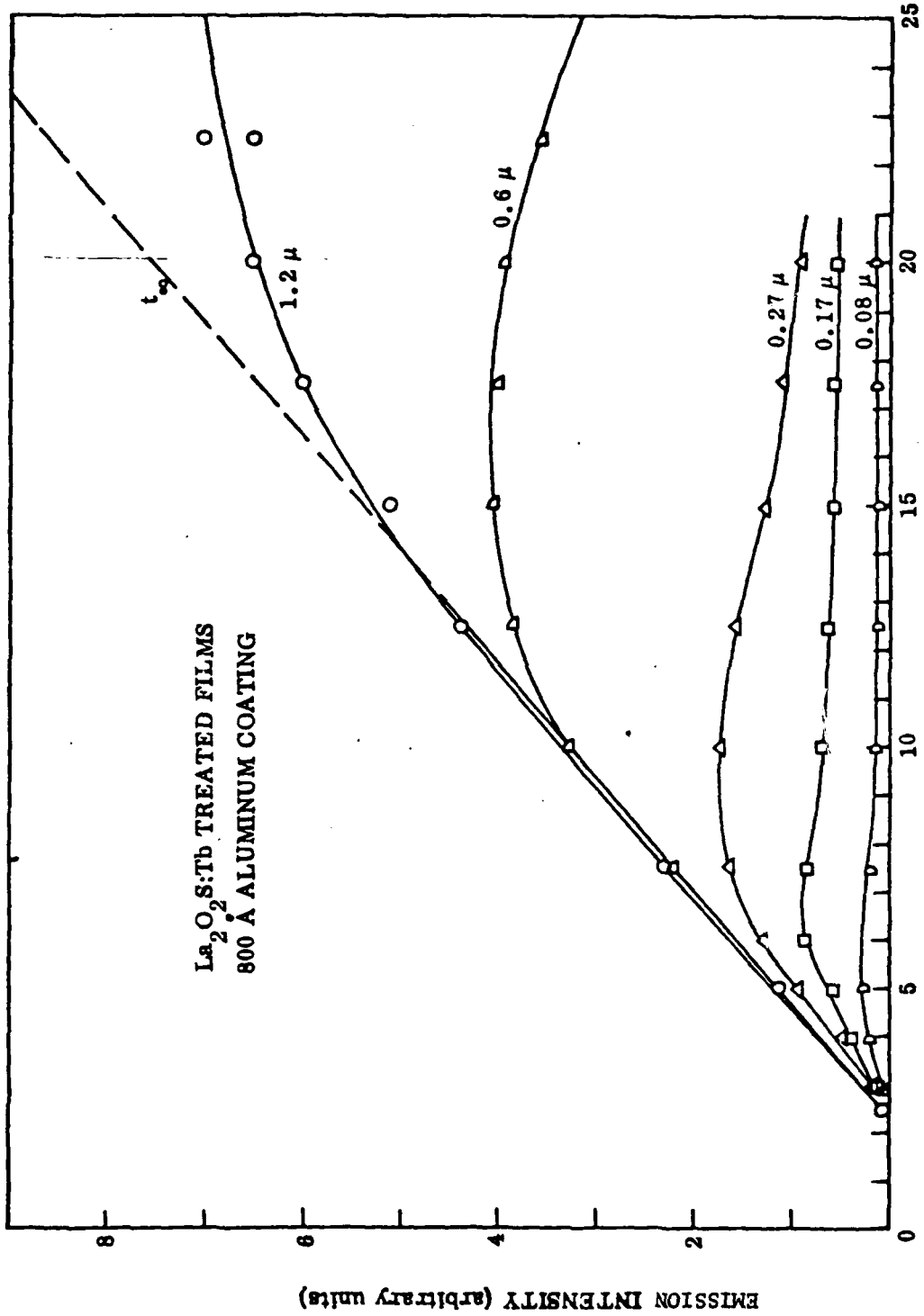

Fig. 71 Experimental Intensity Versus Electron Energy for Several La_2O_2S:Tb Film Thicknesses

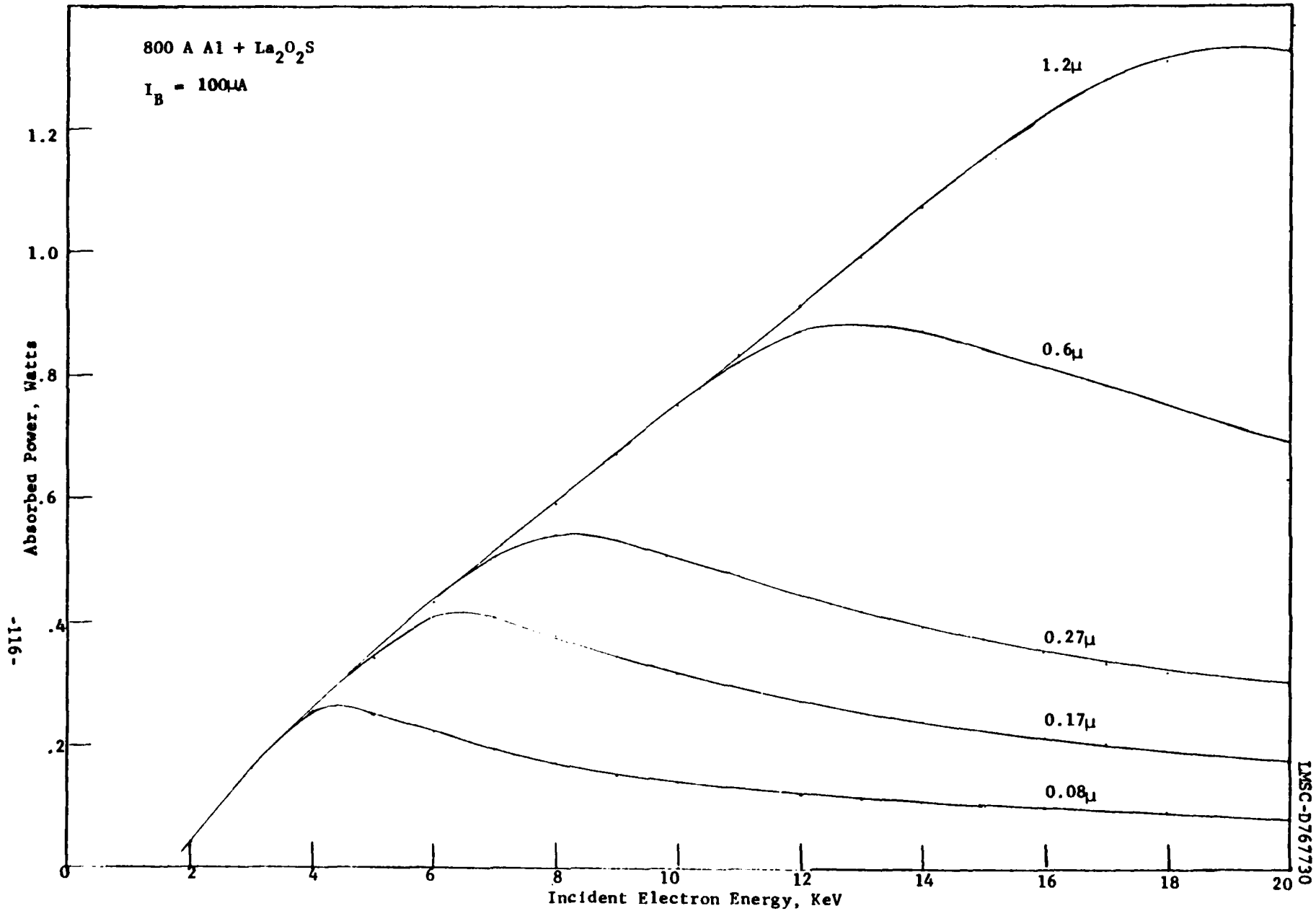

Fig. 72 Calculated Power Absorbed in Several La_2O_2S Film Thicknesses

Table 18

800 Å Al - X Å La_2O_2S $I_B = 100\mu A$

E_o keV	Al 800 Å P_a Watts	800 Å P_b Watts	1700 Å P_b Watts	La_2O_2S 2700 Å P_b Watts	6000Å P_b Watts	12,000 Å P_b Watts
1	.08474	0	0	0	0	0
2	.16948	.04089	.04089	.04089	.04089	.04089
3	.16433	.16289	.16289	.16289	.16289	.16289
4	.12810	.25122	.25621	.25621	.25621	.25621
5	.10571	.25128	.34229	.34307	.34307	.34307
6	.09102	.21843	.40645	.42675	.42706	.42706
7	.08071	.19004	.40432	.50527	.50946	.50946
8	.07278	.16828	.37530	.54245	.59088	.59088
9	.06665	.15151	.34322	.53390	.67162	.67162
10	.06169	.13829	.31433	.50645	.75000	.75189
11	.05757	.12761	.28960	.47450	.82312	.83181
12	.05410	.11878	.26863	.44357	.86666	.91147
13	.05110	.11136	.25081	.41540	.87731	.99091
14	.04850	.10502	.23553	.39033	.86568	1.06854
15	.04622	.09952	.22231	.36816	.84177	1.14635
16	.04418	.09471	.21077	.34856	.81212	1.22102
17	.04236	.09045	.20061	.33118	.78052	1.27948
18	.04072	.08665	.19158	.31570	.74904	1.31506
19	.03924	.08323	.18352	.30183	.71873	1.32921
20	.03785	.08014	.17625	.30183	.69009	1.32658

FOREWORD TO SECTION 4.8

The material in Section 4.8 CRT Contrast Study and 4.9 Reflectance Calculations was originally prepared by LMSC as a subcontractor to the Watkins-Johnson Company under Contract No. DAAB-07-77-C-2639 for inclusion in Research and Development Technical Report DELET-TR-77-2639-F, February 1980. Unfortunately, typographical errors have been found in some of the equations of the two sections which can lead to erroneous results by those attempting to use the equations for calculation. The errors have been corrected here, the text amplified to clarify the relations between the mathematical quantities, and the material supplemented with appropriate references to the literature.

Similar calculations for sapphire faceplates are in progress and the results will be presented in the Final Report of the present contract.

4.8 CRT Contrast Study

We present here a more precise analysis than that previously reported. The contrast ratio C is defined as

$$C = \frac{\text{light emitted and reflected from an excited area}}{\text{light emitted and reflected from an unexcited area}} = \frac{L_{obs} + A_{refl}}{A_{refl}} .$$

Our first task is to develop a rigorous expression for the reflection of ambient light from the CRT faceplate. The interfaces for reflection of ambient light are depicted in Figure 73.

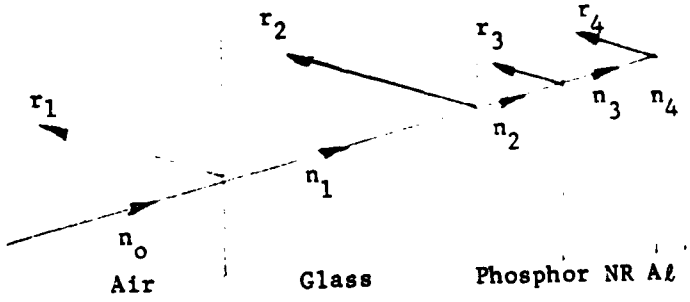

Fig. 73 Cross-Section of CRT Faceplate Showing Interfaces for Reflection of Ambient Light

The refractive indices for air, glass, the phosphor film, the non-reflective (NR) film and the aluminum electrode are represented by n_o, n_1, n_2, n_3, and n_4, respectively. The reflectance at each interface (R_1, R_2. R_3, R_4) is the product of the complex Fresnel coefficient and its complex conjugate, i.e., $R_1 = \tilde{r}_1 \tilde{r}_1^*$, where $\tilde{r}_1 = r_1 e^{i\delta 1}$, r_1 is the amplitude reflectance and δ_1 is the phase shift. The amplitude reflectances are r_1 for the air-glass, r_2 for the glass-phosphor, r_3 for the phosphor-NR film, and r_4 for the NR film-aluminum interfaces.

For convenience, we restrict the analysis to the normal incidence case. This should be adequate for most purposes because the observer will usually view the CRT from a position directly in front of the CRT, and it is known that the non-normal incidence case is satisfactorily represented by the normal incidence treatment for angles of incidence differing from the normal up to about 30 degrees.

For normal incidence, the Fresnel coefficients are

$$r_1 = \frac{n_o - n_1}{n_o + n_1}$$

for a non-absorbing - non-absorbing interface and

$$r_1 = \frac{n_o - n_1 + i\,k_1}{n_o + n_1 - i\,k_1}$$ for a nonabsorbing-absorbing interface.

The corresponding reflections are

$$R_1 = \left(\frac{n_o - n_1}{n_o + n_1}\right)^2 \quad \text{and} \quad R_1 = \frac{(n_o - n_1)^2 + k_1^2}{(n_o + n_1)^2 + k_1^2}, \quad \text{respectively.}$$

The absorption in the phosphor film is negligible for thicknesses of the order of 1 micrometer, so we shall regard the phosphor as a nonabsorbing (or dielectric) medium.

The following treatment is based on the superposition of solutions obtained by resolving the model of Figure 73 into simpler systems.

4.8.1. Glass Plate with Single Nonabsorbing Film on Back. As the first step, we consider a glass plate with a single nonabsorbing film on the back surface (surface furthest from observer) as illustrated in Figure 74.

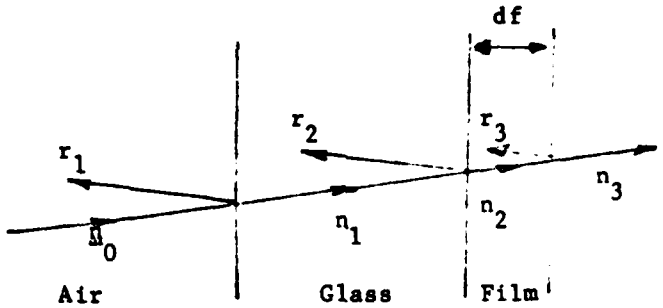

Fig. 74 Nonabsorbing Film on Back of Glass Plate

The reflectivity of a nonabsorbing film of thickness d_f and refractive index n_f sandwiched between semi-infinite media having refractive indices n_a and n_f is (Refs. 10-13):

$$R_f = \frac{r_{1f}^2 + r_{2f}^2 + 2r_{1f}r_{2f}\cos\phi_f}{1 + r_{1f}^2 r_{2f}^2 + 2r_{1f}r_{2f}\cos\phi_f} \tag{1}$$

where

$$\phi_f = \frac{4\pi n_f d_f}{\lambda}$$

$$r_{1f} = \frac{n_f - n_a}{n_f + n_a} = \frac{n_2 - n_1}{n_2 + n_1}$$ in terms of the quantities of Figure 74.

$$r_{2f} = \frac{n_b - n_f}{n_b + n_f} = \frac{n_3 - n_2}{n_3 + n_2} .$$

In a second step, we treat the glass plate as sandwiched between semi-infinite media of air and film material. Thickness of the plate is large compared to the wavelength of visible light, so interference effects do not occur. For infinitely many internal reflections, the reflectivity is (Refs. 14, 15):

$$R_p = \frac{R_1 + R_2 - 2R_1R_2}{1 - R_1R_2} . \tag{2}$$

where R_1 is the reflectivity at the air-glass interface and R_2 is the reflectivity at the glass-film interface. Clearly, $R_2 = R_f$ while R_1 is given by

$$R_1 = \left(\frac{n_1 - n_o}{n_1 + n_o}\right)^2$$

so that

$$R_p = \frac{R_1 + R_f - 2R_1R_f}{1 - R_1R_f} . \tag{3}$$

Thus, if the film thickness and refractive indices are known, a value for R_p can be calculated.

4.8.2 Glass Plate with Phosphor Film and Ideal NR Film ($r_3 = 0$).

Now, if the NR film of Figure 73 is a perfect absorber, this implies that the refractive index of the NR material at the phosphor film-NR film interface is identical to that for the phosphor film. In this ideal case, the reflectivity at the phosphor film-NR film is zero. The reflectivity at the glass-phosphor film interface will then be the same as if the phosphor-NR film combination were replaced with a semi-infinite media of phosphor material. The reflectivity is now given by Equation (2) with R_1 and R_2 simply

$$R_1 = \left(\frac{n_1 - n_o}{n_1 + n_o}\right)^2$$

$$R_2 = \left(\frac{n_2 - n_1}{n_2 + n_1}\right)^2 .$$

4.8.3 Glass Plate with Phosphor Film and Non-Ideal NR Film ($r_3 \neq 0$)

If the NR film is not ideal, there may be (a) reflectance at the phosphor film-NR film interface due to mismatch of refractive indices, or also (b) reflection from the NR film-aluminum interface if the NR film is not a perfect absorber. We shall not attempt a solution for case (b) because the NR films to be employed are inhomogeneous films for which the refractive index is variable through the film and exact solutions are possible only for certain unique index gradients. Also, ambient light must traverse the film twice in order to contribute appreciable reflectance at the phosphor film-NR film interface, and since only films having considerable absorption are of interest for CRT applications, the intensity of ambient light reflected from the NR film-aluminum interface will be negligibly small on arriving again at the phosphor film-NR film interface.

Even were such reflected ambient to make an appreciable contribution, the effect would be nearly the same as though there were an additional degree of mismatch between the interface indices for the phosphor and NR films.

(a) Mismatch of Indices for Phosphor and NR Films

Here it is assumed that the NR film is a perfect absorber, but a mismatch of refractive indices occurs at the phosphor film-NR film interface. In this case, $r_3 \neq 0$ (Figure 73). The reflectivity is given by Equation (2) with R_f of Equation (1) substituted for R_2, as in Section 4.8.1 The thickness of the phosphor film must be known in order to calculate the reflectivity. Depending upon the film thickness and the associated phase shift, the overall reflectivity may be greater or less than when there is no mismatch.

4.8.4 Contrast Calculations

To calculate the contrast ratio C, we shall simplify the treatment by considering the NR film to be ideal, so that no emitted light is reflected at the phosphor-NR film interface. Only the emitted light directly transmitted through the glass plate from a point in the phosphor reaches the observer. For nonabsorbing materials, the transmittance is

$$T = 1-R.$$

Here the reflectivity R is that for a plate sandwiched between semi-infinite media of air and phosphor:

$$R_p = \frac{R_1 + R_2 - 2R_1R_2}{1-R_1R_2}$$

where the reflectivity at the glass-air interface

$$R_1 = \left(\frac{n_1 - n_o}{n_1 + n_o}\right)^2$$

and the reflectivity at the phosphor-glass interface

$$R_2 + \left(\frac{n_3 - n_2}{n_3 + n_2}\right)^2 .$$

Then,

$$T_p = 1 - R_p$$

so that if L is the luminance of the phosphor,

$$L_{obs} = T_p L = (1 - R_p)L.$$

For ambient light of incident intensity A, the light reflected to the observer is

$$A_{refl} = A R_p$$

Thus

$$C = \frac{L_{obs} + A_{refl}}{A_{refl}}$$

becomes

$$C = \frac{(1 - R_p)L + R_p A}{R_p A} \quad .$$

Taking the solar illuminance constant as 13.67 lumens/cm^2, the ambient illumination of a CRT faceplate in direct sunlight is 1.27×10^4 f.c. (Ref. 16).

For a faceplate of Corning #1720 aluminosilicate glass and La_2O_2S phosphor film, $n_o = 1$, $n_1 = 1.53$, $n_2 = 2.20$. Then, $R_1 = 0.043884$ and $R_2 = 0.032265$. Hence, $R_p = 0.073422$, so that the ambient light reflected to the observer is $A_{refl} = 932.4$ fL. Of this amount, 557.3 fL is the result of reflection at the front surface.

By coating the front surface with an antireflection coating, the reflected ambient light could be reduced to 375 fL, which is the result of the mismatch between the glass and the phosphor film.

Substituting the above value of R_p, the contrast equation becomes

$$C = \frac{(1-0.073422)L + (0.073422)A}{0.073422A}$$

$$= 12.61990 \frac{L}{A} + 1 \quad .$$

For direct sunlight, $A = 1.27 \times 10^4$ fL, so we have

$$C = 9.937 \times 10^{-4} L + 1.$$

Table 19 presents the contrast ratio for various values of L, when no front surface AR coating is used.

With an AR coating on the front surface, R_p becomes simply the reflectivity of the glass-phosphor interface, or

$$R_p = 0.032265 \ .$$

Then,

$$C = \frac{(1 - 0.032265)L + 0.032265A}{0.032265A}$$

$$= 29.993 \frac{L}{A} + 1 \quad .$$

Table 19

No AR - 1720 - La_2O_2S - IDEAL NR

L	C
100	1.099
200	1.199
300	1.298
400	1.398
500	1.497
600	1.596
700	1.696
800	1.795
900	1.894
1000	1.994

For direct sunlight

$$C = 2.362 \times 10^{-3} L + 1.$$

Table 20 presents the contrast ratio for various values of L attainable with use of a front surface AR coating.

Figure 75 provides a graphical comparison of the two cases.

Table 20

AR - 1720 - La_2O_2S - IDEAL NR

L fL	C
100	1.236
200	1.472
300	1.709
400	1.945
500	2.181
600	2.417
700	2.653
800	2.889
900	3.126
1000	3.362
2000	5.723
3000	8.056
4000	10.466
5000	12.808

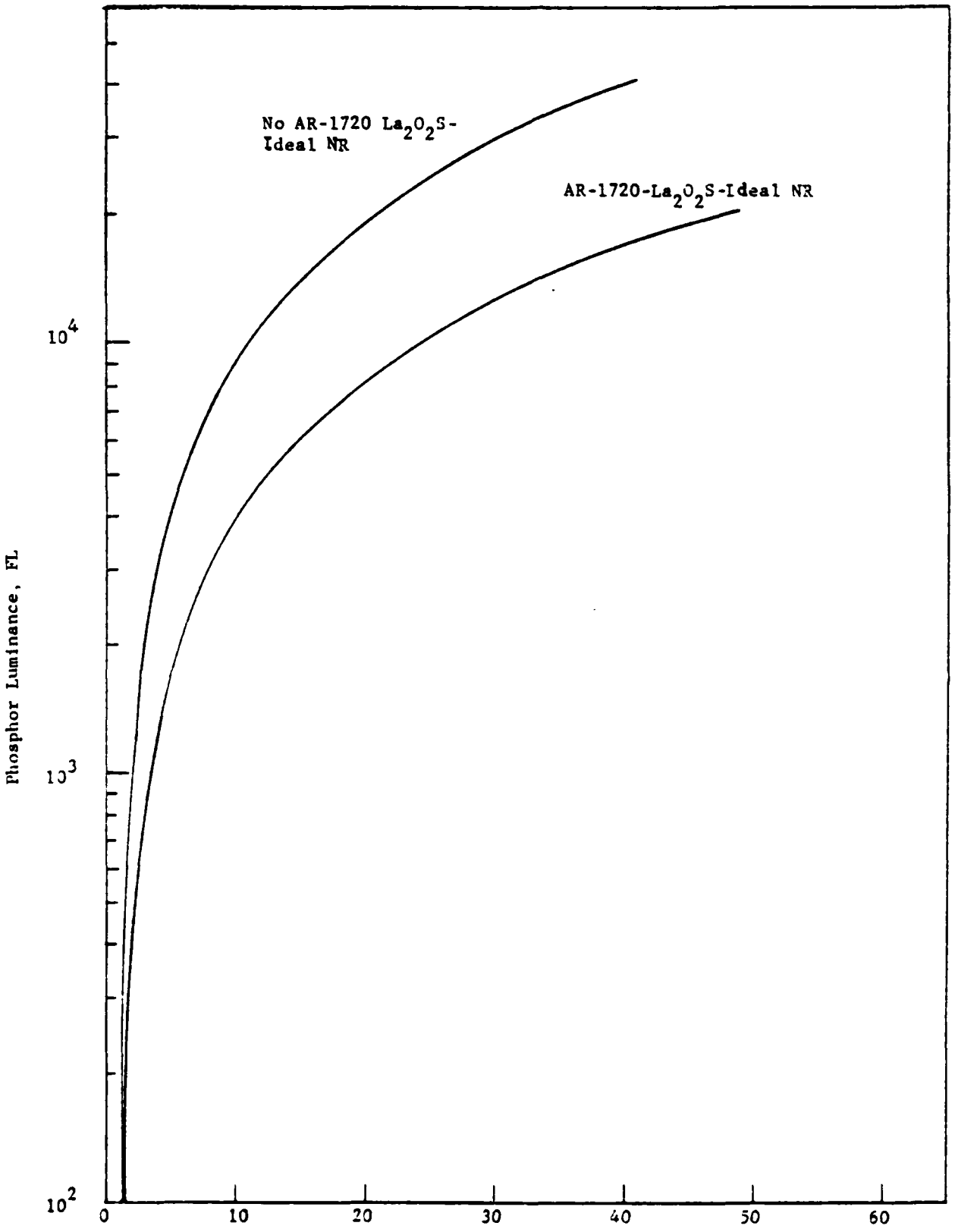

Fig. 75 Contrast Ratio in Direct Sunlight

If the mismatch between the glass and the phosphor could be eliminated by using a phosphor having an index the same as the glass, the effect on contrast would be as follows:

Assuming no AR coating and an ideal NR film, the reflectivity becomes simply that of the front surface. That is,

$$R_p = 0.043884 \quad .$$

Then,

$$C = \frac{(1 - 0.043884) - L + 1}{0.043884A}$$

$$= 21.787 \frac{L}{A} + 1.$$

For direct sunlight

$$C = 1.716 \times 10^{-3} L + 1.$$

The curve is intermediate between the two previous curves.

If the NR film is not ideal, then the reflectivity must be calculated using Equations (1) and (3). In addition to the refractive indices, the thickness of the phosphor film and the reflectivity at the phosphor-NR film interface must be known.

For a 1720 glass - La_2O_2S - Non-ideal NR film assembly, we have $n_o = 1$, $n_1 = 1.53$ and $n_2 = 2.20$.

Assuming a La_2O_2S thickness of 12,000 A^o and a reflectivity at the La_2O_2S-NR interface of 0.5%, then at a wavelength of 5400 A^o

$$r_{2f} = (.005)^{\frac{1}{2}} = .0707107$$

$$r_{1f} = \frac{2.20 - 1.53}{1.53 - 1.53} = - 0.17962$$

$$R_1 = \left(\frac{1.53 - 1}{1.53 + 1}\right)^2 = .043884$$

$$\phi_f = \frac{4\pi(2.20)(12,000)}{5400} = 61.43559 \text{ radians}$$

$$20\pi - \phi_f = 1.396263 \text{ radians}$$

$\text{Cos } \phi_f = 0.173648$

$2r_{1f}r_{2f}\text{Cos } \phi_f = -4.41114 \times 10^{-3}$

$R_f = 0.032994 = P_2$

$R_p = 0.074090$

Then

$C = \frac{(1 - .074090)}{.074090A} L + 1 = 12.50 \frac{L}{A} + 1$ for which the factor 12.5 differs only slightly from the factor 12.699 of our first curve.

4.9 Reflectivity Calculations

In Section 4.8, the results of calculating the reflectivity of normally incident light (i.e., perpendicular to the plane of the faceplate) were presented for (1) a glass plate with a nonabsorbing film on its back surface, (2) a glass plate with a phosphor film and an ideal NR film, and (3) a glass plate with phosphor film and non-ideal film. The results of calculating the reflectivity for oblique incidence are presented in this section.

The reflectivity of a nonabsorbing film between semi-infinite medie for oblique incidence is given, as before, by the equation

$$R_f = \frac{r_{1f}^2 + r_{2f}^2 + 2r_{1f}r_{2f}\cos \phi_f}{1 + r_{1f}^2 r_{2f}^2 + 2r_{1f}r_{2f}\cos \phi_f}$$

Here, however, ϕ_f is given as

$$\phi_f = \frac{4\pi n_f d_f \cos \theta_f}{\lambda}$$

where θ_f is the angle at which light is refracted in the film. If θ_o is the angle at which light is incident upon the film, by Snell's law

$$n_o \sin \theta_o = n_f \sin \theta_f \ .$$

Also, for oblique incidence, it is necessary to distinguish between the parallel and perpendicular polarization components of light, for which the Fresnel coefficients are

$$r_{1p} = \frac{n_f \cos \theta_a - n_a \cos \theta_f}{n_f \cos \theta_a + n_a \cos \theta_f}$$

$$r_{2p} = \frac{n_2 \cos \theta_f - n_f \cos \theta_2}{n_2 \cos \theta_f + n_f \cos \theta_2}$$

and

$$r_{1s} = \frac{n_a \cos \theta_a - n_f \cos \theta_f}{n_a \cos \theta_a + n_f \cos \theta_f}$$

$$r_{2s} = \frac{n_f \cos \theta_f - n_b \cos \theta_b}{n_f \cos \theta_f + n_b \cos \theta_b}$$

Denoting the reflectance intensity for the p-component by I_p^r and for the s-component by I_s^r, the overall reflectivity is

$$R_f = \frac{I_p^s + I_s^r}{2} .$$

The calculated reflectivities of this section are the specular reflectivities. The models for the calculations have been selected to represent ambient light incident on the external surface of a cathode ray tube. It is assumed that the light is incoherent, so that interference does not occur between light reflected from the front surface and rear surface of the glass, although infinitely many reflections occur between the glass surfaces. The phosphor film, of the order of 1 micron thickness, is, however, a thin film, so that interference does occur for reflections from the two surfaces of the film.

Thin film optical calculations for oblique incidence are relatively tedious, and particularly so in the case of absorbing materials. Extensive thin film calculations are ordinarily performed with the aid of a computer. For many purposes, however, a limited number of points, say 20 or so, permit construction of a reflectivity curve with satisfactory definition. It has been found that a programmable calculator, such as the TI-59, is well suited for such calculations, and several programs have been written by us for the purpose.

The calculated results are presented in Table 21, 22, 23, and 24 for a glass plate, a glass plate with an La_2O_2S film of 12,886Å thickness, a glass plate with an La_2O_2S film of 12,272Å thickness, and a glass plate with an La_2O_2S film and ideal NR film, respectively.

Calculations were made for these two La_2O_2S film thicknesses because maximum reflectivity at normal incidence occurs for an La_2O_2S film thickness of 12,886Å, and minimum reflectivity for 12,272Å. When an ideal NR film is present, the thickness of the La_2O_2S film is immaterial.

The calculated overall reflectivities are shown graphically in Figure 76. The curve labeled "Plate + La_2O_2S Film" is for a 12,272Å thickness. The hump in this curve peaking at 45° is the result of interference in the film.

It is seen from Figure 76 that the reflectivity is nearly constant from 0° to 40° for both the plate and the plate + La_2O_2S + NR film. For angles greater than 40°, the reflectivities increase rapidly. It is also seen from the figure that the reflectivity for the plate + La_2O_2S + NR film is less than for the plate alone. This is because the plate has two glass-air interfaces, each having a reflectivity of 0.04388, while the plate + La_2O_2S + NR combination has one glass-air interface (reflectivity = 0.04388) and one glass-phosphor interface (reflectivity = 0.03227). The overall reflectivity is given by the equation

$$R = \frac{R_1 + R_2 - 2R_1R_2}{1 - R_1R_2} \quad .$$

Table 21 GLASS PLATE

Oblique Incidence

Media	Index	θ_o, Deg.	I_p^r	I_s^r	R
Air n_o	1	0	.08408	.08408	.08408
1720 Glass n_1	1.53	5	.08328	.08488	.08408
Air n_2	1	10	.08086	.08735	.08410
		15	.07680	.09161	.08421
		20	.07106	.09793	.08449
		25	.06362	.10667	.08515
		30	.05449	.11840	.08645
		35	.04379	.13385	.08882
		40	.03185	.15405	.09295
		45	.01945	.18031	.09988
		50	.00809	.21438	.11123
		55	.00073	.25838	.12956
		60	.00279	.31484	.15881
		65	.02371	.38643	.20407
		70	.07884	.47555	.27720
		75	.18997	.58356	.38676
		80	.38036	.70978	.54507
		85	.65914	.85073	.75493
		90	1.00000	1.00000	1.00000

Table 22
GLASS PLATE OVER La_2O_2S FILM
Oblique Incidence

Media	Index	θ_o, Deg.	I_p^r	I_s^r	R
Air n_o	1	0	.29367	.29367	.29367
1720 Plate n_1	1.53	5	.29195	.29518	.29357
La_2O_2S n_2	2.20	10	.28550	.29843	.29197
Air n_3	1	15	.27074	.29979	.28527
		20	.24289	.29367	.26828
Film Thickness	12886.4Å	25	.19819	.27393	.23611
(Max. for $\theta_o = 0$)		30	.13887	.23702	.18794
Wavelength	5400Å	35	.07729	.18967	.13348
		40	.03489	.16026	.09757
		45	.02421	.19247	.10834
		50	.03421	.29656	.16538
		55	.04264	.42818	.23541
		60	.03786	.54392	.29089
		65	.02814	.63301	.33057
		70	.04149	.70365	.37257
		75	.11981	.76829	.44405
		80	.30417	.83713	.57065
		85	.60971	.91504	.76238
		90	1.00000	1.00000	1.00000

Table 23
GLASS PLATE OVER La_2O_2S FILM
Oblique Incidence

Media	Index	θ_o, Deg.	I_p^r	I_s^r	R
Air n_o	1	0	.08404	.08408	.08404
1720 Plate n_1	1.53	5	.08344	.08505	.08425
La_2O_2S n_2	2.20	10	.08340	.09000	.08670
Air n_3	1	15	.08877	.10476	.09676
		20	.10438	.13713	.12075
Film Thickness	12272.7Å	25	.13035	.19173	.16104
(Min. for θ_o = 0)		30	.15916	.26379	.21147
Wavelength	5400Å	35	.17825	.33908	.25867
		40	.17633	.40175	.28904
		45	.14860	.44161	.29510
		50	.10042	.45571	.27807
		55	.04890	.44802	.24846
		60	.01749	.43198	.22474
		65	.02426	.43375	.22900
		70	.07822	.48241	.28032
		75	.18981	.58437	.38709
		80	.37784	.71794	.54789
		85	.65554	.85952	.75752
		90	1.00000	1.00000	1.00000

Table 24

GLASS PLATE OVER La_2O_2S FILM OVER IDEAL NR FILM
Oblique Incidence

Media	Index	θ_0, Deg.	I_p^r	I_s^r	R
Air n_o	1	0	.07342	.07342	.07342
1720 Glass n_1	1.53	5	.07288	.07397	.07342
La_2O_2S	2.20	10	.07124	.07563	.07344
		15	.06851	.07850	.07350
		20	.06468	.08270	.07369
		25	.05976	.08846	.07411
		30	.05376	.08846	.07493
		35	.04685	.10600	.07643
		40	.03919	.11884	.07901
		45	.03121	.13548	.08337
		50	.02373	.15703	.09038
		55	01822	.18530	.10176
		60	.01734	.22271	.12003
		65	.02593	.27283	.14938
		70	.05280	.34081	.19680
		75	.11424	.43413	.27418
		80	.24112	.56364	.40328
		85	.49421	.74490	.61956
		90	1.00000	1.00000	1.00000

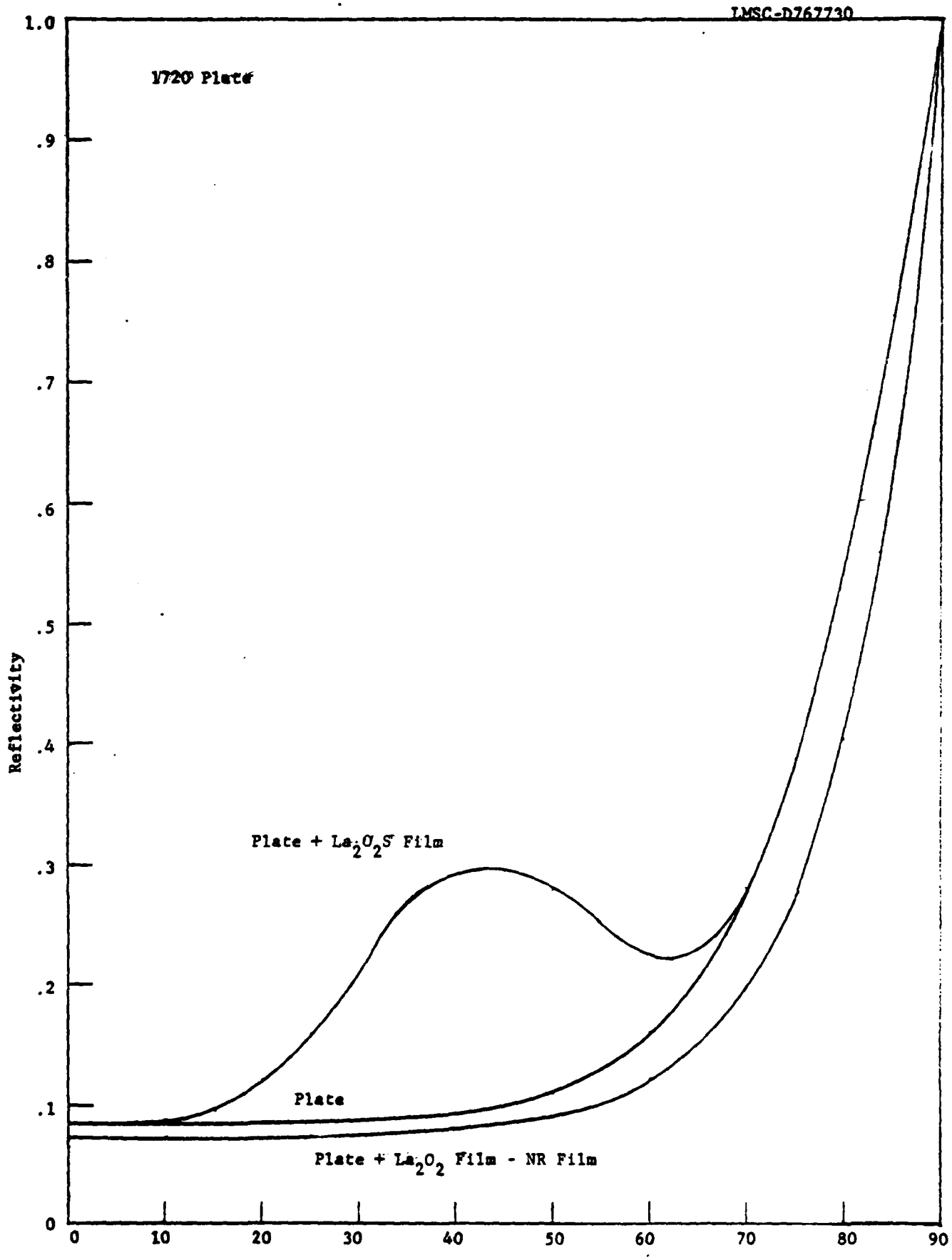

Fig. 76 Angle of Incidence

4.10 Delivery of Faceplates

Lot #1 was shipped to ERADCOM via Federal Air Express on February 4, 1980.

Lot #2 was shipped to ERADCOM via Federal Air Express on May 15, 1980.

Lot #3 was expected to be shipped before the end of May.

5.0 CONCLUSIONS

Adequate pre-heating of the faceplate prior to the $H_2 + SO_2$ treatment eliminates the distortion previously encountered as the result of stresses arising from the expansion coefficient mismatch between the phosphor films and the alumino-silicate glass substrate coupled with temperature gradients due to inadequate pre-heating.

Despite a number of modifications, the cathodoluminescent measuring system remains limited by the 5UP1 gun to screen currents of 120 microamperes at a writing speed of 5,000 in./sec. and a 60 Hz refresh rate.Under these conditions the brightness of the 1710 faceplate at 10 Kev is only 1 foot-lambert. To achieve adequate contrast under strong ambient illumination, substantial increase in current density is necessary, which requires replacement of the 5UP1 gun by one capable of providing screen current of the order of 500 - 1000 microamperes and a narrower line width (0.016 in. or less).

A study of the black film thickness as a function of deposition conditions indicates that a simple adjustment of the deposition schedule will assure opaque NR films at a thickness not exceeding 3300Å; this will avoid too great a loss of incident beam energy in penetrating the black film.

An equation developed by Kanaya and Okayama permits calculation of the energy absorption by phosphors from a penetrating electron beam which is in semi-quantitative agreement with experiemntal results; by contrast, calculations using the Feldman equation yielded a curve of unrealistic shape. Appropriate values of effective molecular weight and effective periodic number of a compound for use with the K & O equation can be calculated from those of the component elements as mole function summations. The calculations show that Rutherford backscattering is responsible for the excess electron beam energy loss that was observed with tantalum-based black films.

6.0 PROGRAM FOR NEXT INTERIM PERIOD

The cathodoluminescence measurements on Lot #3 will be completed and the faceplates shipped to ERADCOM.

The cathodoluminescence measuring system will be modified to permit replacement of the 5UP1 gun by a magnetically deflected gun capable of delivering screen currents of 300-500 microamperes.

Faceplates Lots #4 and #5, totaling nineteen faceplates, will be fabricated on 3 in. dia. sapphire substrates. The faceplates will be characterized by cathodoluminescence and optical reflectance measurements before shipment to ERADCOM.

7.0 REFERENCES

1. L. Ozawa and P. M. Jaffe, "The Mechanism of the Emission Color Shift with Activator Concentration in Eu^{+3} Activated Phosphors", J. Electro Chem, Soc. 118, 1678-9 (1971)
2. H. Forest, "Emission Color of Y_2O_2S:Eu Phosphor", J. Electrochem. Soc. 120, 693 (1973)
3. L. Ozawa, H. Forest, P. M. Jaffe, and G. Ban, "The Effect of Exciting Wavelength on Optimum Actuator Concentration", J. Electrochem. Soc., 118, 484 (1971)
4. C. Feldman, "Range of 1-10 KeV Electrons in Solids", Phys. Rev. 117, 455 (1960)
5. R. Whiddington, Proc. Roy. Soc. (London) A86, 360 (1912)
6. V. E. Cosslett and R. N. Thomas, "Multiple Scattering of 5-30 KeV Electrons in Evaporated Metal Films II: Range-Energy Relations", Brit. J. Appl. Phys. 15, 1283 (1964)
7. K. Kanaya and S. Okayama, "Penetration and Energy-Loss Theory of Electrons Solid Targets", J. Phys. D: Appl. Phys. 5, 43 (1972)
8. J. S. Prener, "Electron Penetration and Power Dissipation in Thin Films of La_2O_3:Eu", J. Electrochem. Soc. 122, 1516 (1975)
9. H. H. Seliger, Phys. Rev. 100, 1029 (1955)
10. O. S. Heavens, Optical Properties of Thin Solid Films, Academic Press, Inc., New York, 1955, p. 81
11. A. Vasicek, Optics of Thin Films, North-Holland Publ. Co., Amsterdam, 1960, p. 108
12. H. Anders, Thin Films in Optics, The Focal Press, London, 1965, p. 27
13. M. Born and E. Wolf, Principles of Optics, Fifth Edition, Perganum Press, Oxford, 1975, p. 62
14. Reference 2, p. 64, Equation (3-23).
15. P. H. Berning, Physics of Thin Films 1, 54 (1963), Equation (53)
16. American Institute of Physics Handbook, Second Edition, McGraw-Hill Book Company, Inc., New York, 1963, p. 2-141

17. M. Born and E. Wolf, Principles of Optics, Fifth Ed., Perganum Press, N.Y., 1975, p. 182

18. R. V. Alves, et al., Luminescent Applications of Rare Earth Materials Annual Report, Jan. 1971, ARPA Contract No. DAHC-15-70-C-0164

8.0 APPENDIX

8.1 Electron Beam Energy Absorption Calculator Program

This program has been developed for use with a Texas Instruments TI-59 Programmable calculator to facilitate the electron beam energy absorption calculations described in Section 4.7. The program is applicable to a multilayer thin film phosphor screen comprising a metallic conductor layer on a bi-layer phosphor, each layer of the phosphor consisting of the same host compound, but having different activators.

The program employs several subroutines and also logical-decision steps. Some annotation has been provided as an aid to understanding the program. Modification is practically certain to result in error and is therefore not recommended.

ELECTRON BEAM ENERGY ABSORPTION

1.	Enter Magnetic Card:	1 INV 2nd Write		
		2 INV 2nd Write		
2.	Enter Data:	Index I_o	STO 00	Amperes
		Index A_a	STO 01	Effective Atomic Wt.
		Index ρ_a	STO 02	Density, Gm/cm^3
		Index Z_a	STO 03	Effective Periodic No.
		Index E_o	STO 04	KeV
		Index X_a	STO 05	Å, Layer a
		Index $(E_B/E_o)_a$	STO 06	From table
		Index A_b	STO 07	Effective Atomic Wt.
		Index ρ_b	STO 08	Density, Gm/cm^3
		Index Z_b	STO 09	Effective Periodic No.
		Index X_b	STO 11	Å, Layer b
		Index X_c	STO 12	Å, Layer c
		Index $(E_B/E_o)_b$	STO 13	From table

3. Press R/S Read P_a
4. Press R/S Read P_b
f. Press R/S Read P_c

By substituting R/S for the NOP instructions, the following additional values may be read; in sequence shown:

R/S for NOP at STEP	READ
321	R_o
335	y_a
288	E_A/E_o for a
343	E_{o1}
---	P_a
288	E_A/E_o for b
---	P_b
288	E_A/E_o for c
---	P_c

Whenever data is changed, for example, entering a new value for E_o, press RST before initial R/S.

$$\frac{\gamma}{(1-y)^{7/6}} \exp\left[-1.9y/(1-y)\right]$$

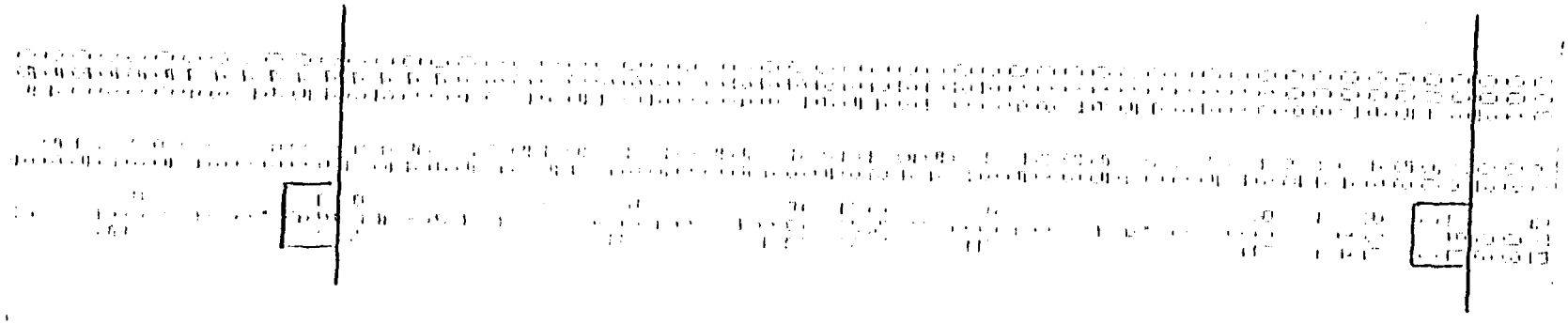

$(1-y)^{3/5}$

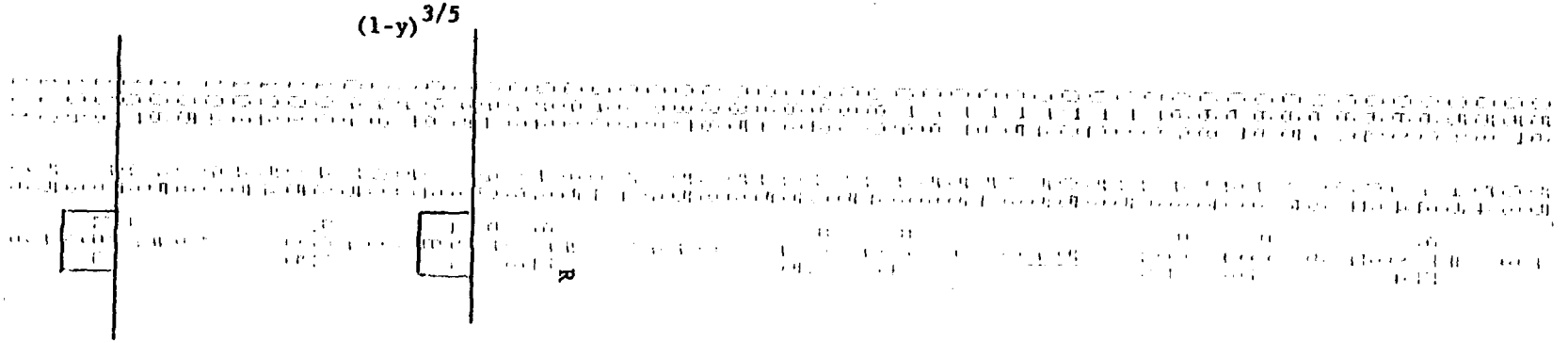

R

Numerical Integration

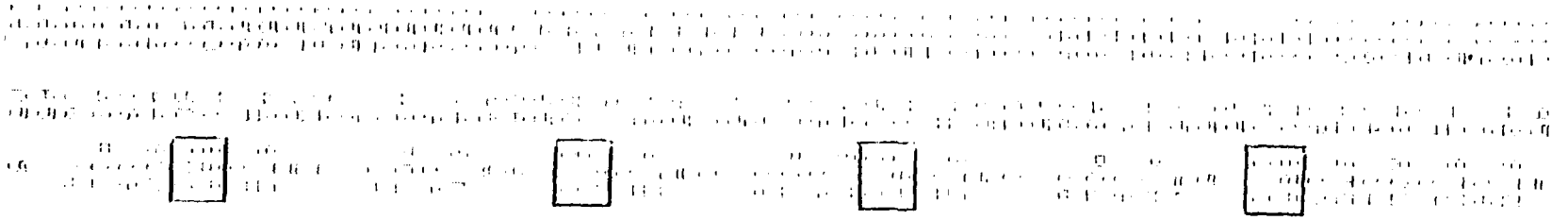

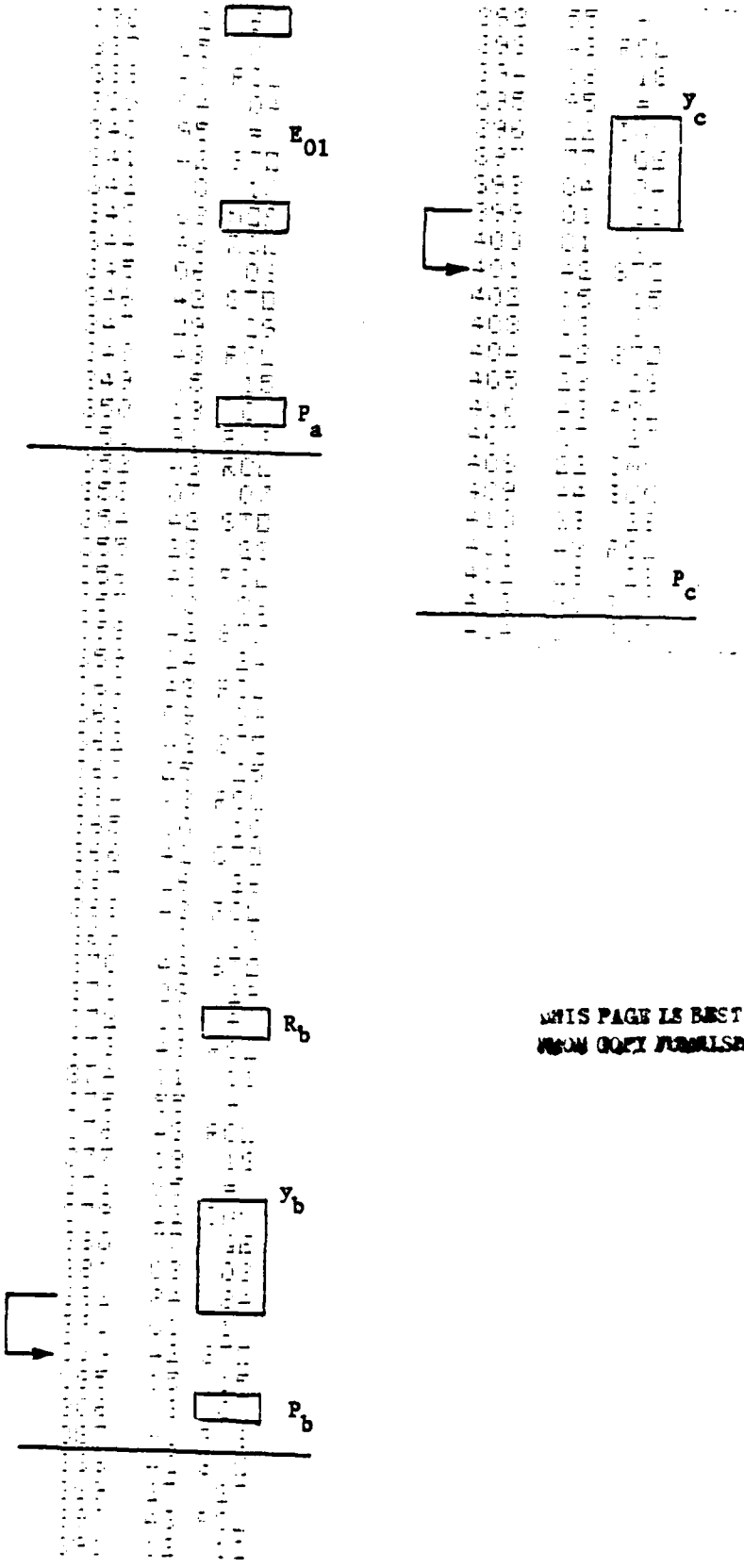

8.2 RANGE AND FRACTIONAL ENERGY ABSORPTION CALCULATOR PROGRAM

This program has been developed to facilitate compiling a list of range R vs. incident energy E_o, and fractional absorbed energy E_a/E_o vs. reduced depth y for a given material using the relationship developed by Kanaya and Okayama (Ref. 4). By entering various values of x, the corresponding values for y and E_A/E_o can be obtained. By entering new values of y, the corresponding E_A/E_o values can be obtained for constructing a curve of E_A/E_o vs. y.

The limiting value of E_A/E_o for y= 1 is readily obtained. y = 1 corresponds to the maximum range of electrons in the material. When the material thickness exceeds the range (y> 1), the value of y = 1 is automatically substituted in calculating the fractional absorbed energy.

ELECTRON BEAM ENERGY ABSORPTION

1.	Enter magnetic card:		1 INV 2nd Write
			2 INV 2nd Write
2.	Enter data:		
	Index A	STO 01	
	Index ρ	STO 02	Gm/cm^3
	Index Z	STO 03	
	Index E_o	STO 04	KeV
	Index x	STO 05	Å
	Index E_B/E_o	STO 06	
3.	Press R/S	READ	R in Å
4.	Press R/S	READ	y
5.	Press R/S	READ	E_A/E_o
6.	Enter new value of x		STO 05
	Press R/S	READ	y
	Press R/S	READ	E_A/E_o
7.	Enter a value of y		
	Press A	READ	y just entered
	Press R/S	READ	E_A/E_o

Whenever E_o is changed, store new value in 04, press RST, then press R/S as for Step 3.

Step	Code	Key
000	61	GTO
001	00	00
002	44	44
003	76	LBL
004	50	IxI
005	53	(
006	43	RCL
007	07	07
008	94	+/-
009	65	×
010	43	RCL
011	11	11
012	65	×
013	01	1
014	93	.
015	09	9
016	55	÷
017	53	(
018	01	1
019	75	-
020	43	RCL
021	11	11
022	54	)
023	54	)
024	22	INV
025	23	LNX
026	65	×
027	43	RCL
028	07	07
029–055	[illegible]	[illegible]

Step	Code	Key
056	55	÷
057	03	3
058	54	)
059	95	= y
060	42	STO
061	07	07
062	03	3
063	07	7
064	06	6
065	65	×
066	43	RCL
067	01	01
068	55	÷
069	43	RCL
070	04	04
071	45	Yˣ
072	53	(
073	05	5
074	55	÷
075	03	3
076	54	)
077	55	÷
078	53	(
079	43	RCL
080	02	02
081	65	×
082	43	RCL
083–111	[illegible]	[illegible] (= R, = y)

Step	Code	Key
112	[illegible]	[illegible]
113	55	÷
114	06	6
115	95	=
116	42	STO
117	10	10
118	42	STO
119	11	11
120	[illegible]	SBR
121	50	IxI
122	55	÷
123	05	5
124	95	=
125	44	SUM
126	06	06
127	43	RCL
128	10	10
129	65	×
130	02	2
131	95	=
132	42	STO
133	11	11
134	[illegible]	SBR
135	50	IxI
136	44	SUM
137	06	06
138	43	RCL
139	10	10
140–167	[illegible]	[illegible]

THIS PAGE IS BEST QUALITY PRACTICABLE FROM COPY FURNISHED TO DDC

8.3 Faceplate Processing Equipment

8.3.1 RF Sputtering System

The RF Sputtering System used to deposit the phosphor and NR films of the contract is shown in Figure 66. This system consists of an NRC 6 in. diffusion pump vacuum system, an MRC Model SM-8500 RF/DC sputtering module and a Lepel 5KW RF power supply with impedance matching network.

A Spectra Physics one-half milliwatt He-Ne laser is used to monitor thickness of the phosphor film, the reflected beam being detected with a UDT p-i-n diode; the signal is fed to an Op-Amp, then to a recorder.

8.3.2 Sulfurization Furnace

The tube furnace used for the high temperature sulfurization treatment for improving the phosphor film luminescent brightness is shown in Figure 67. This consists of a three-zone furnace with 4 in. o.d. quartz tube, supplies of hydrogen, argon, and sulfur dioxide gases, with flowmeters provided with micrometer valves, a chamber for burning off the hydrogen-rich exit gases, and an exhaust system for disposing of the spent gases.

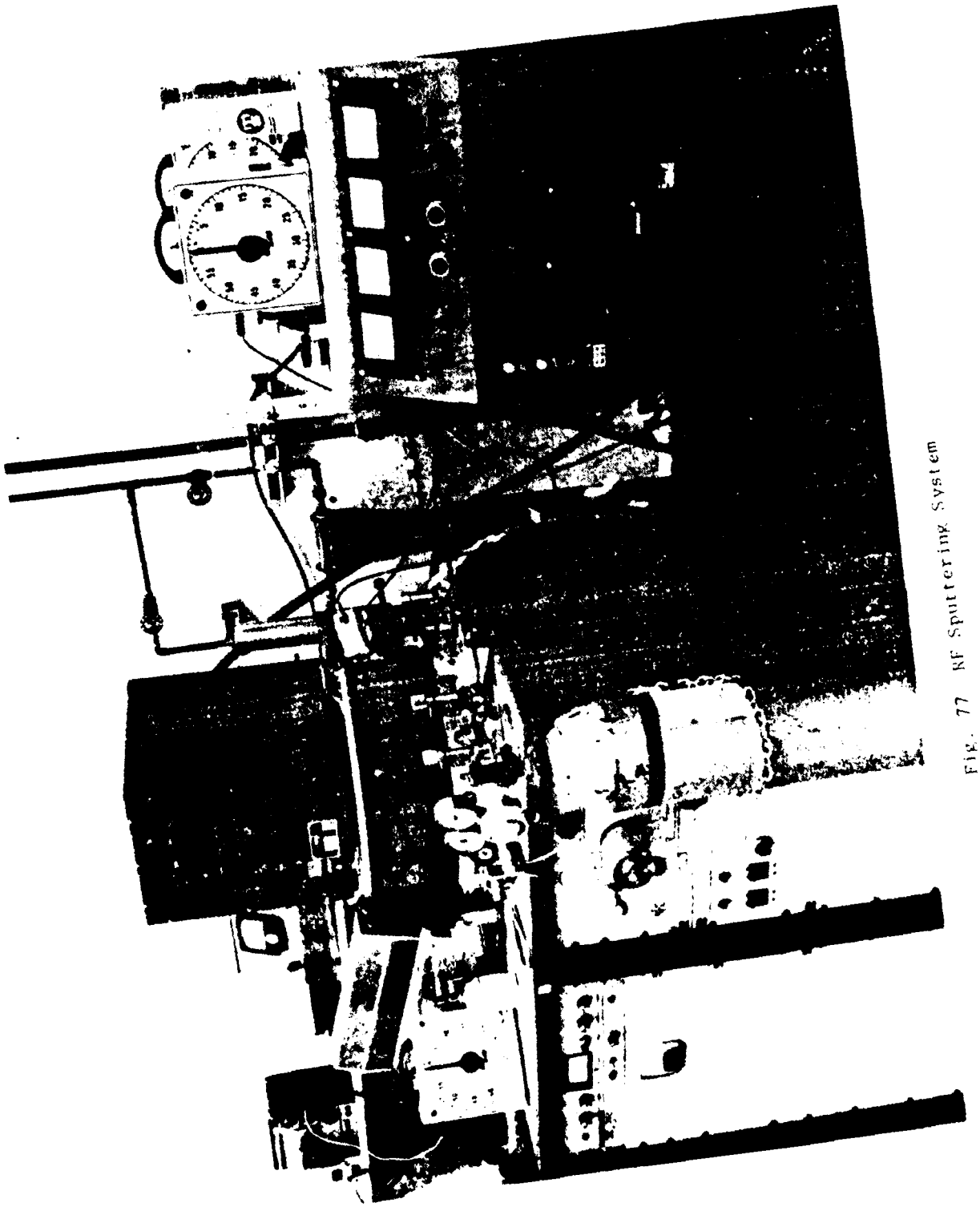

Fig. 77 RF Sputtering System

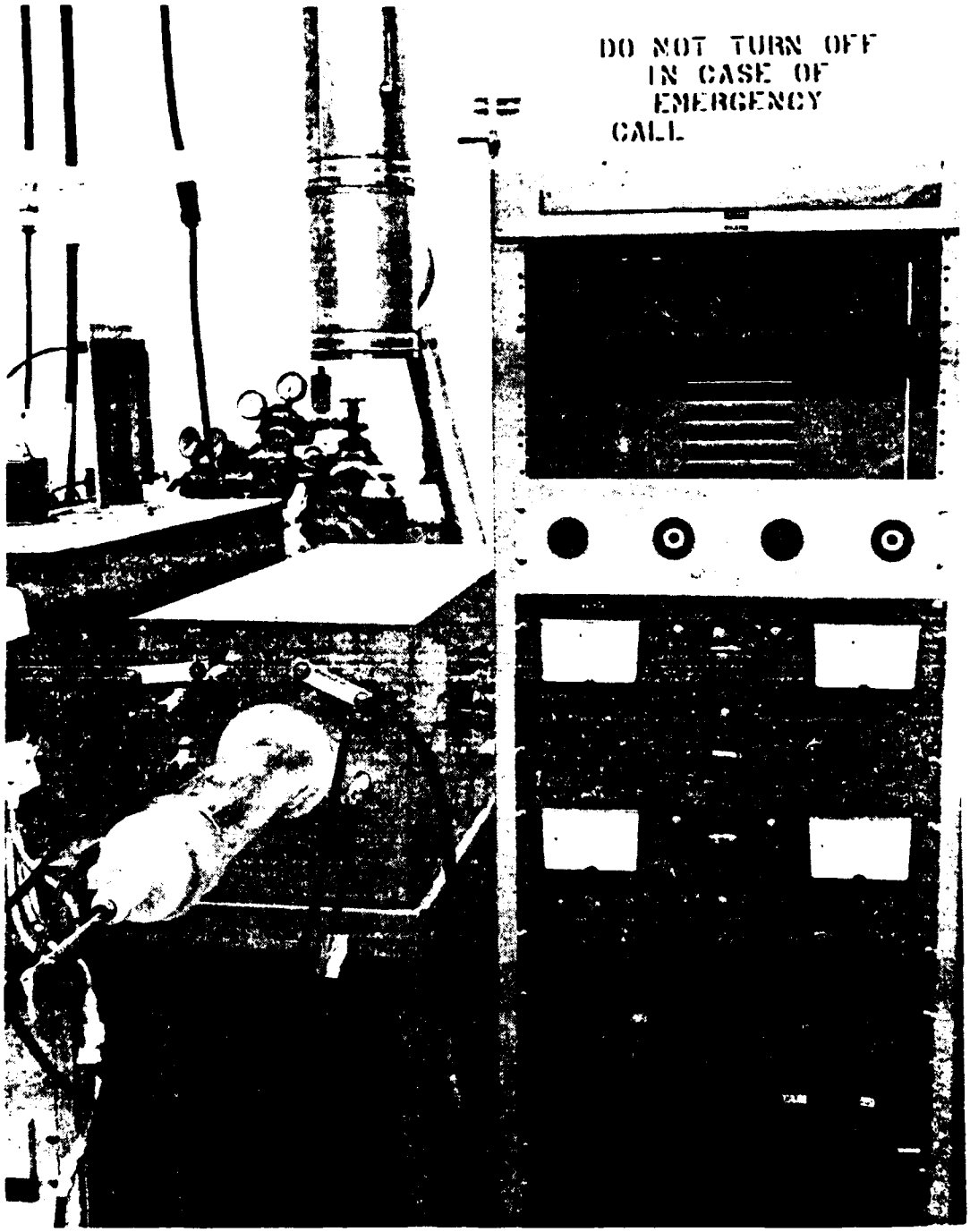

Fig. 78 Sulfurization Furnace

DISTRIBUTION:

101 Defense Technical Information Center
Attn: DTIC-TCA
Cameron Station (Bldg. 5)
012 Alexandria, Va. 22314

203 GIDEP Engineering & Support Dept.
TE Section
P.O. Box 398
001 NORCO, Ca. 91760

205 Director
Naval Research Laboratory
Attn: Code 2627
001 Washington, D.C. 20375

301 Rome Air Development Center
Attn: Documents Library (TILD)
001 Griffiss AFB, N.Y. 13441

437 Deputy for Science & Technology
Office, Ass't Sec. Army (R&D)
001 Washington, D.C. 20310

438 HQDA (DAMA-ARZ-D/Dr. F.D. Verderame)
001 Washington, D.C. 20310

482 Director
U.S. Army Mat'l Systems Analy. Actv
Attn: DRXSY-T
001 Aberdeen Proving Ground, Md. 21005

563 Commander, DARCOM
Attn: DRCDE
5001 Eisenhower Ave.
001 Alexandria, Va. 22333

564 Crd. U.S. Army Signals Wrfre Lab
Attn: DELSW-OS
Vint Hill Farms Station
001 Warrenton, Va. 22185

579 Crd. PM Concept Analysis Ctrs.
Attn: DRCPM-CAC
Arlington Hall Station
001 Arlington, Va. 22212

602 Cdr. Night Vision & Electro-Optics
ERADCOM
Attn: DELMV-D
001 Fort Belvoir, Va. 22060

603 Cdr. Atmospheric Sciences Lab
ERADCOM
Attn: DELAS-SY-S
001 White Sands Missile Range,
N.M. 88002

607 Cdr. Harry Diamond Labs
Attn: DELHD-CO, TD (In Turn)
2800 Powder Mill Road
001 Adelphi, Md. 20783

609 Cdr. ERADCOM
Attn: DRDEL-CG, CD, CS (In Turn)
2800 Powder Mill Road
001 Adelphi, Md. 20783

612 Cdr. ERADCOM
Attn: DRDEL-CT
2800 Powder Mill Road
001 Adelphi, Md. 20783

680 Commander
U.S. Army Electr R&D Command
000 Fort Monmouth, N.J. 07703

1 DELEW-D
1 DELET-DD
1 DELSD-L (Tech Library)
2 DELSD-L-S (STINFO)
4 Originating Office

681 Commander
U.S. Army Communictns R&D Command
Attn: USMC-LNO
001 Fort Monmouth, N.J. 07703

705 Advisory Group on Electron Devices
201 Varick Street, 9th Floor
002 New York, New York 10014

103 Code R123, Tech Library
DCA Defense Comm Engrg Ctr
1800 Hienle Ave.
001 Resten, Va. 22090

104 Defense Communications Agency
Technical Library Center
Code 205 (P. A. Tolovi)
001 Washington, D.C. 20305

206 Commander
Naval Electronics Lab Center
Attn: Library
001 San Diego, Ca. 92152

406 Commandant
U.S. Army Aviation Center
Attn: ATZQ-D-MA
001 Fort Rucker, Al. 36362

475 Cdr. Harry Diamond Laboratories
Attn: Library
2800 Powder Mill Road
001 Adelphi, Md. 20783

507 Cdr. AVRADCOM
Attn: DRSAV-E
P.O. Box 209
001 St. Louis, Mo. 63166

604 Chief
Office of Missile Electron Warfare
Electronic Warfare Lab, ERADCOM
001 White Sands Missile Range, N.M. 88002

701 MIT Lincoln Laboratory
Attn: Library (RM A-082)
P.O. Box 73
002 Lexington, Ma. 02173

703 NASA Scientific & Tech Info Facility
Baltimore/Washington Intl Airport
P.O. Box 8757
001 Md. 21240

Dr. Robert Trimmier
Sperry Flight Systems
Mail Station 109B
21111 N. 19th Ave.
001 Phoenix, Ariz. 55027

Mr. Robert Parutz
LORAL Electronics System
999 Central Park Ave.
001 Yonkers, N.Y. 10704

Applied Physics Laboratory
John Hopkins University
John Hopkins Road
Attn: Mr. Charles Feldman
001 Laurel, Md. 20810

General Electric Company
50 Fordham Road
Attn: Mr. Richard L. Skovhalt
001 Wilmington, Ma. 01887

Naval Research Laboratory
4555 Overlook Ave. S.W.
Code 5333
Attn: Mr. Paul Thibaud
001 Washington, D.C. 20375

General Electric Company
P.O. Box 5000
Mail Drop 120
Attn: Mr. Sam S. Jobes
001 Birmingham, N.Y. 13902

Westinghouse Electric Corp.
Industrial and Government
Tube Division
Westinghouse Circle
Attn: Mr. N. J. Taylor
001 Horseheads, N.Y. 14545

XEROX Corporation
Attn: Dr. Benjamin Kazan
Palo Alto Research Center
3333 Coyote Hill Road
001 Palo Alto, Ca. 94304

Thomas Electronics, Inc.
Attn: Mr. Peter Seats
100 Riverview Drive
001 Wayne, N.J. 07470

Dumont Electron Tubes and Devices Corp.
Attn: Mr. E. W. Swenarton
750 Bloomfield Ave.
001 Clifton, N.J. 07015

Northrop Corporation
Attn: Mr. Walter Goede
Electronics Division
1 Research Park
001 Palos Verdes, Ca. 90274

Watkins-Johnson Co.
Attn: Mr. Norman Lehrer
442 Mount Herman Road
001 Scotts Valley, Ca. 95066